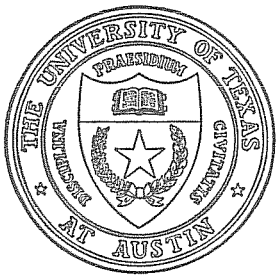

PMFSEL REPORT NO. 88-2
DECEMBER 1988

STUDY OF REINFORCED CONCRETE BEAM-COLUMN JOINTS UNDER UNIAXIAL AND BIAXIAL LOADING

By

Yukinobu Kurose
Gilson N. Guimaraes
Zuhua Liu
Michael E. Kreger
James O. Jirsa

Partially Supported by
National Science Foundation
Grant No. ECE-8320398

PHIL M. FERGUSON STRUCTURAL ENGINEERING LABORATORY
Department of Civil Engineering / Bureau of Engineering Research
The University of Texas at Austin

PMFSEL Report No. 88-2

DECEMBER 1988

STUDY OF REINFORCED CONCRETE BEAM-COLUMN JOINTS UNDER UNIAXIAL AND BIAXIAL LOADING

by

Yukinobu Kurose
Gilson N. Guimaraes
Zuhua Liu
Michael E. Kreger
James O. Jirsa

Partially Supported by
National Science Foundation
Grant No. ECE-8320398

PHIL M. FERGUSON STRUCTURAL ENGINEERING LABORATORY
Department of Civil Engineering/Bureau of Engineering Research
The University of Texas at Austin

Any opinions, findings, conclusions, or recommendations expressed in this publication are those of the author and do not necessarily reflect the views of the National Science Foundation.

ABSTRACT

Three reinforced concrete beam-column joints were tested under the U.S.-New Zealand-Japan-China Cooperative Project on Design of Reinforced Concrete Beam- Column Joints and are described in detail. The specimens were tested under bi- directional loading. All three included a floor slab. The test results were evaluated using data from other programs to critically examine current design guidelines. Using a larger data base, it was possible to propose some modifications to existing design provisions.

ACKNOWLEDGEMENTS

The research was supported by the National Science Foundation under Grant ECE-8320398. Mr. Kurose was a research scholar at The University of Texas on assignment from Shimizu Construction Co. of Japan. Mr. Liu was a research Scholar from Tongji University in Shanghai, China. The support of NSF, Shimizu Construction Co., and Tongji University is gratefully acknowledged.

TABLE OF CONTENTS

LIST OF FIGURES

LIST OF TABLES

1. INTRODUCTION

A series of seismic tests on reinforced concrete slab-beam-column connections were conducted as part of a cooperative program developed by researchers from Japan, New Zealand, the United States, and China. The program was conducted primarily at the Universities of Tokyo, Canterbury and Texas, and discussed by the research teams in meetings held in Monterey, California in 1984[1] and in Tokyo in 1985[2]. Guidelines for test specimens and test procedures were established at the meetings.

The objective of the program was to evaluate the behavior of slab-beam-column connections designed following the code requirements or guidelines in each country. However, it should be noted that there are considerable differences in the design approaches for beam-column joints among these countries. In the United States, ACI committees have recommended that joint shear should be carried entirely by concrete[3,4]. Joint lateral reinforcement is provided to maintain the integrity of the joint. On the contrary, the New Zealand code[5] expects lateral reinforcement to carry a large amount of joint shear. Concrete is considered much less effective in resisting shear than expected in the U.S. codes. In Japan, there are no code provisions for reinforced concrete joints but usual design approaches for the joint are relatively close to U.S. codes except that lateral reinforcement is considered to carry a small amount of joint shear. The cooperative program is aimed at explaining these differences by collaborating on seismic tests of reinforced concrete beam-column joints.

Three full-scale slab-beam-column connections were tested at the University of Texas as part of the program. The specimens were designed using the recommendations of ACI Committee 352[3] and Appendix A of ACI 318-83[4]. One of the three specimens was tested uni-directionally and others bi-directionally following test procedures established for the cooperative program. All specimens failed in joint shear after developing beam flexural yielding. The specimens, procedures and results of the tests are described. In this report, the joint shear strength is examined from various viewpoints using not only test results reported here, but also tests reported in Japan and the United States.

2. TEST PROGRAM

2.1 Specimens

Three reinforced concrete beam-column subassemblies, shown in Fig. 2.1, were tested under seismic load conditions. The specimens were full-scale models with a 5-in. thick floor slab. Specimen J1 had beams in only one direction and was tested unidirectionally. Specimen J2 and J3 had beams in both directions and were subjected to bidirectional loading. Specimen J2 was an interior joint and J3 was an exterior joint. Beam and column dimensions were the same in the specimens. Slab corners were removed to permit transport of the specimen through the lab.

Details of the specimens are shown in Figs. 2.2-2.4. The beam section was 16- in wide and 20-in. deep. Top and bottom beam bars were varied in each specimen to produce forces which were expected to reach the recommended joint shear strength[3]. Note that all the beams had heavier reinforcement at the top than at the bottom. The column had a 20-in. wide square section and was designed to have a capacity greater than the capacity of the beams even under bidirectional loading. Although ACI 318 Appendix A does not specify a limit on the beam or column depth to bar diameter ratio, ACI 352 specifies a value of 20. Therefore, #8 or smaller beam or column bars meet the ACI limit. Hooked bars in Specimen J3 met the anchorage requirements of ACI 318, Eq. A-5. The beam-column joint was laterally reinforced with five sets of #4 bars. Each set consisted of one closed hoop and two single-leg crossties (one in each direction). The hoop was closed with 135° hooks. The crosstie had a 135° hook at one end and a 90° hook at the other end. All hooks terminated in a six-bar- diameter extension. Three layers of lateral reinforcement were placed between the top and bottom beam bars.

The slab was 5-in. thick and reinforced with double layers of #3 bars in both directions, as shown in Fig. 2.5. Specimen J1 had heavy top reinforcement in the transverse direction to prevent overstressing reinforcement in the cantilever slab under dead load. The bottom slab reinforcement was continuous over the beams in J1 and J2, and was anchored with hooks into the spandrel beams in J3. The bar position of the beam, column and slab reinforcement is given in Appendix A.

As shown in Fig. 2.6, the specimen was fabricated on a shored platform. Plywood forms were built on the platform and coated with lacquer. Beam and column bar cages were dropped into the forms and slab bars were placed as shown in Fig. 2.7. Ready-mixed concrete was used to cast the specimen in two stages. The lower column, beams and slab were cast in one operation. Several days after the first placement, the specimen was transported from the platform to the testing floor and the upper column was cast. In both stages, concrete was placed with a bucket and consolidated with vibrators. A construction joint in the column was formed several inches above the top of the slab.

Normal weight concrete with a design strength of 4000 psi and deformed grade 60 bars were used in the specimens. The concrete compressive strength and the tensile properties of the reinforcement are given in Table 2.1. The concrete strength used in various calculations is 3500 psi for 31, 3700 psi for J2 and 4700 psi for J3, respectively.

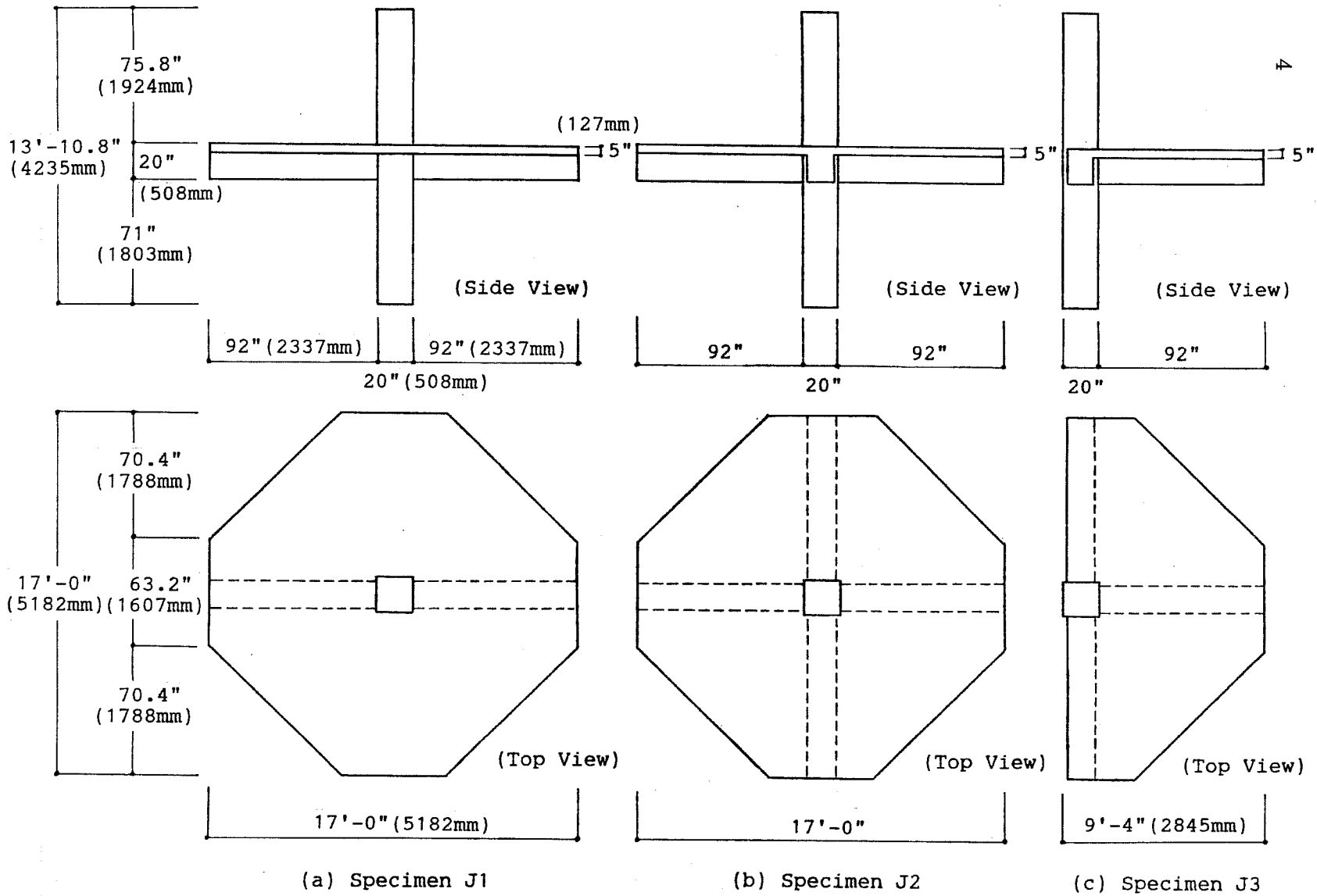

Figure 2.1 Specimen Configurations

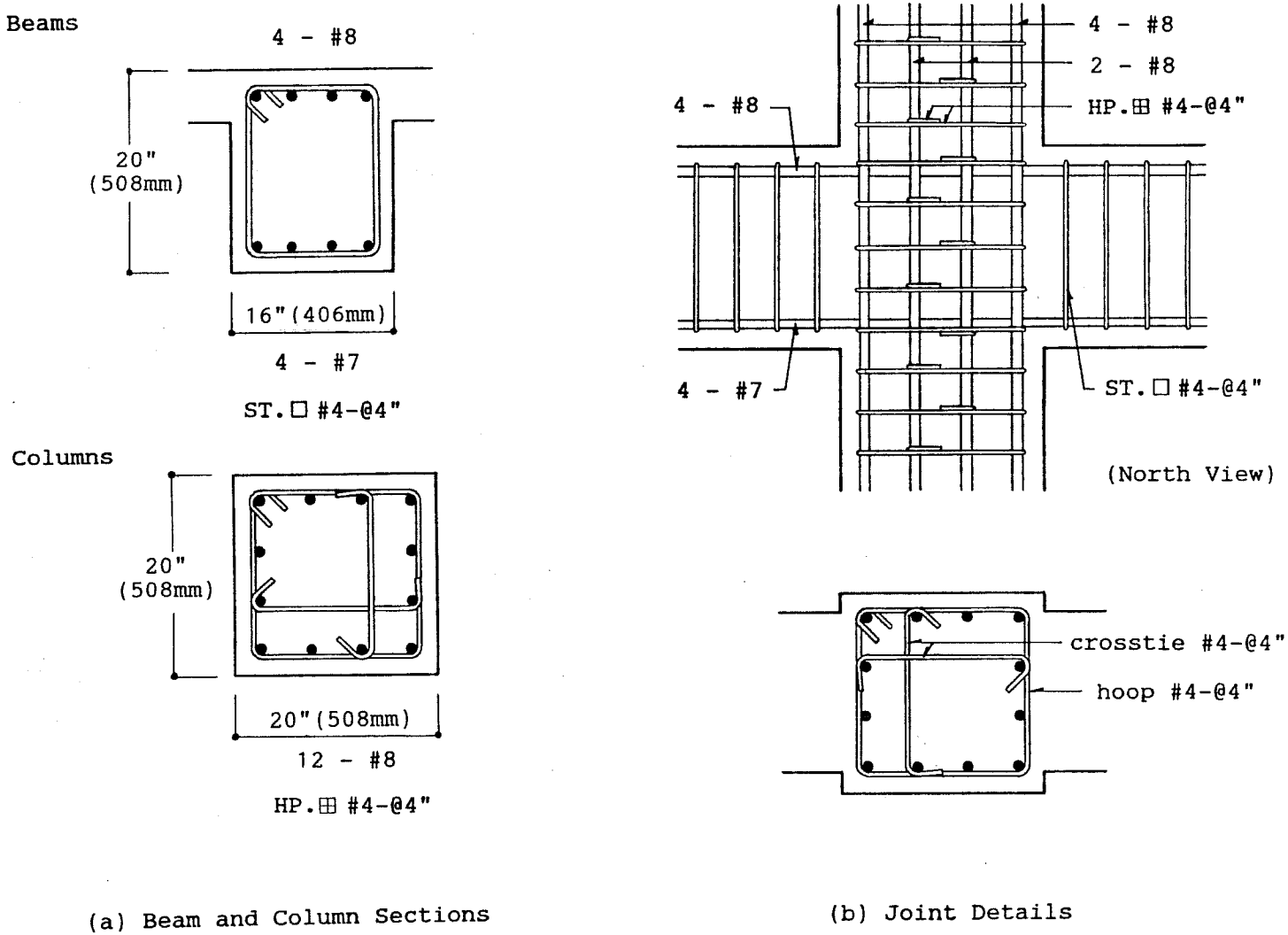

Figure 2.2 Details of Specimen J1

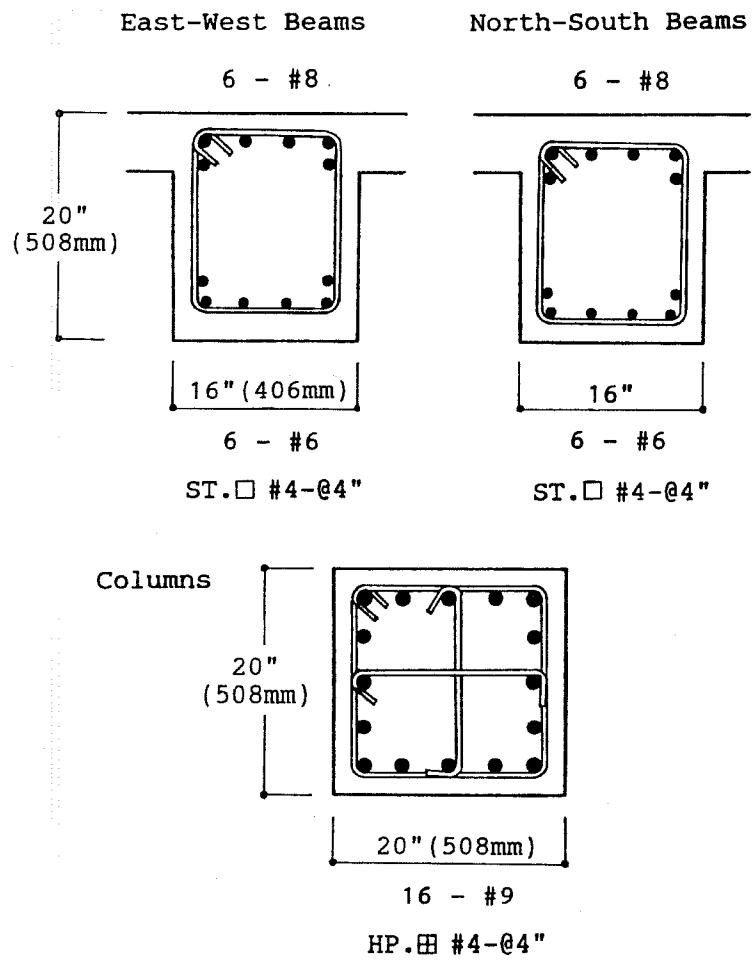

(a) Beam and Column Sections

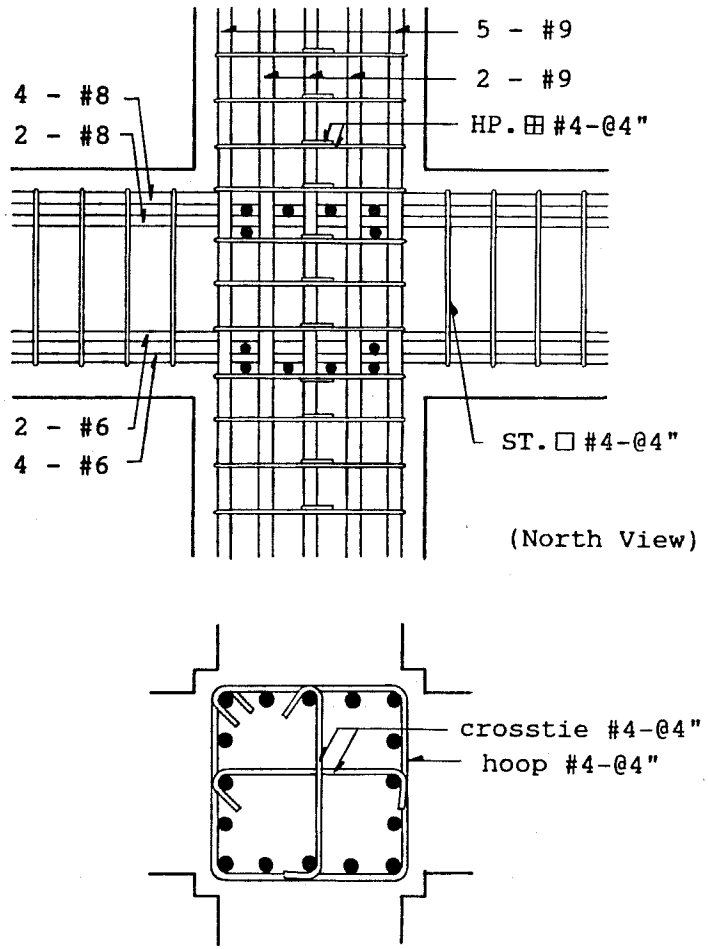

(b) Joint Details

Figure 2.3 Details of Specimen J2

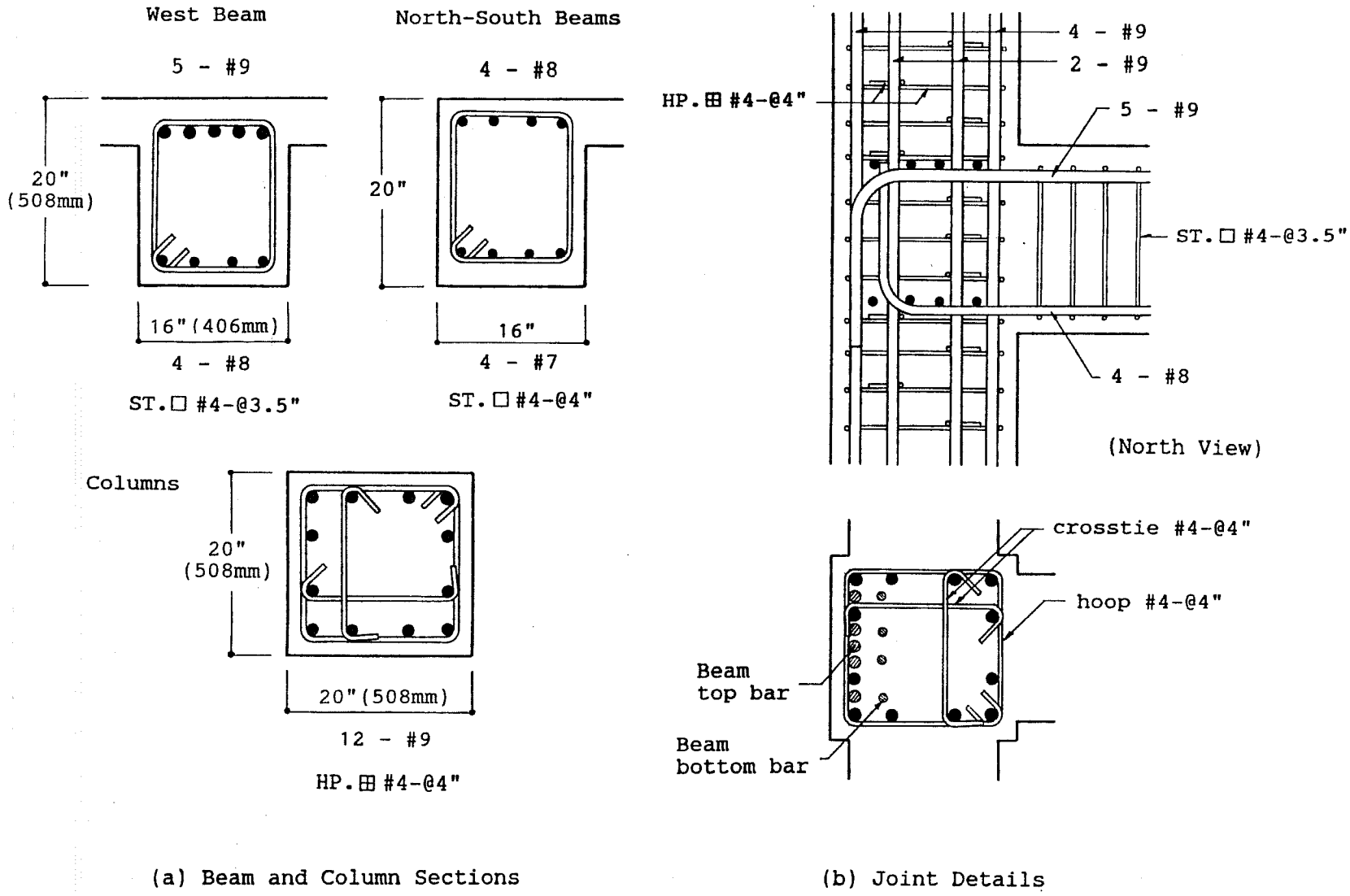

Figure 2.4 Details of Specimen J3

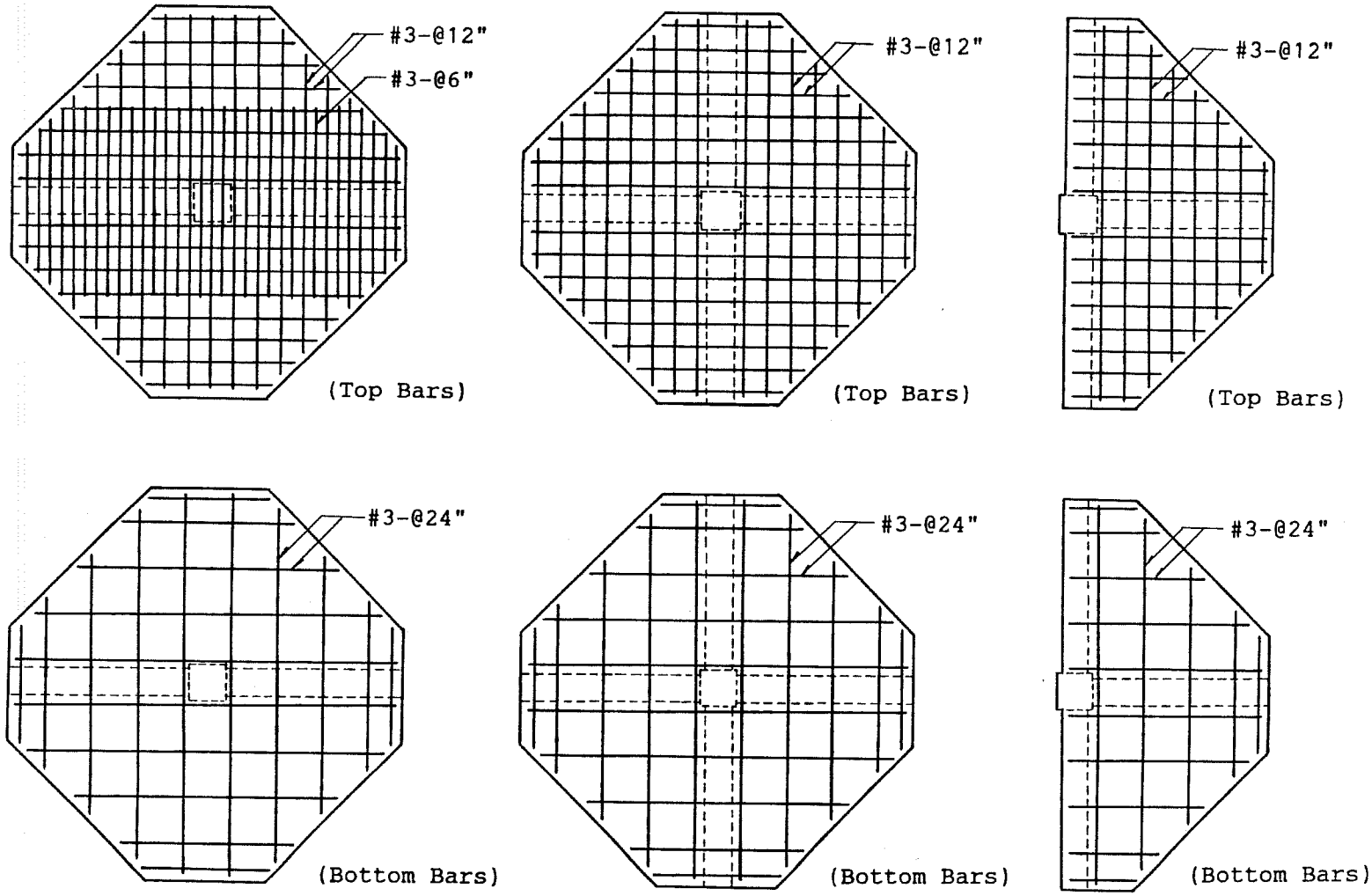

Figure 2.5 Slab Reinforcement

Table 2.1 Material Properties

(a) 28-day Compressive Strength of Concrete (psi)

POSITION	SPECIMEN J1	SPECIMEN J2	SPECIMEN J3
Slab, Beam, Joint and Lower Column	3240 (3500)	3700 (4010)	4700
Upper Column	3520	3780	3250

(): strength at the time of testing

(b) Rebar Strength

Bar Size	Bar Diameter (mm)	Yield Strength (ksi)	Ultimate Strength (ksi)
#3	10	80.8	118.2
#4	13	79.7	111.9
#6	19	74.2	108.9
#7	22	65.6	101.4
#8	25	67.2	106.0
#9	29	66.6	106.1

1 ksi = 70.3 kgf/cm^2 = 6.89 MPa

2.2 Loading Program

The loading apparatus is illustrated in Fig. 2.8 and the specimen in the test setup is shown in Figs. 2.9-2.11. The bottom of the column rested on a pin connection that allowed rotations in all directions. The top of the column was attached to the reaction wall with struts that were tensioned to prevent horizontal translation of the column and rotations about the vertical column axis. Although the struts were rigid enough to prevent movement of the specimen in the EW direction (perpendicular to the reaction wall), the top of the column was found to move slightly in the NS direction (parallel to the reaction wall) under biaxial loading. Therefore, the story drift measured in the NS direction had to be corrected by eliminating the column movement.

Hydraulic rams were used to load the specimen. Each ram was installed at the beam tip, as shown in Fig. 2.12, and was controlled manually by a hydraulic pump. During biaxial loading cycles, the loading direction was changed alternately at every quarter cycle. After completion of the quarter cycle in one direction, hydraulic valves in the completed direction were closed to maintain the ram displacements and the valves in the other direction were opened to execute the succeeding quarter cycle. The two jacks in one direction (one jack in the EW direction for J3) were operated to produce a racking load on the specimen (one ram up and the other ram down in equal displacements). Although no axial load was applied to the column, unbalanced beam shear imposed a compressive axial force on the lower column, except for specimen J3. Upward loading on J3 in the EW direction

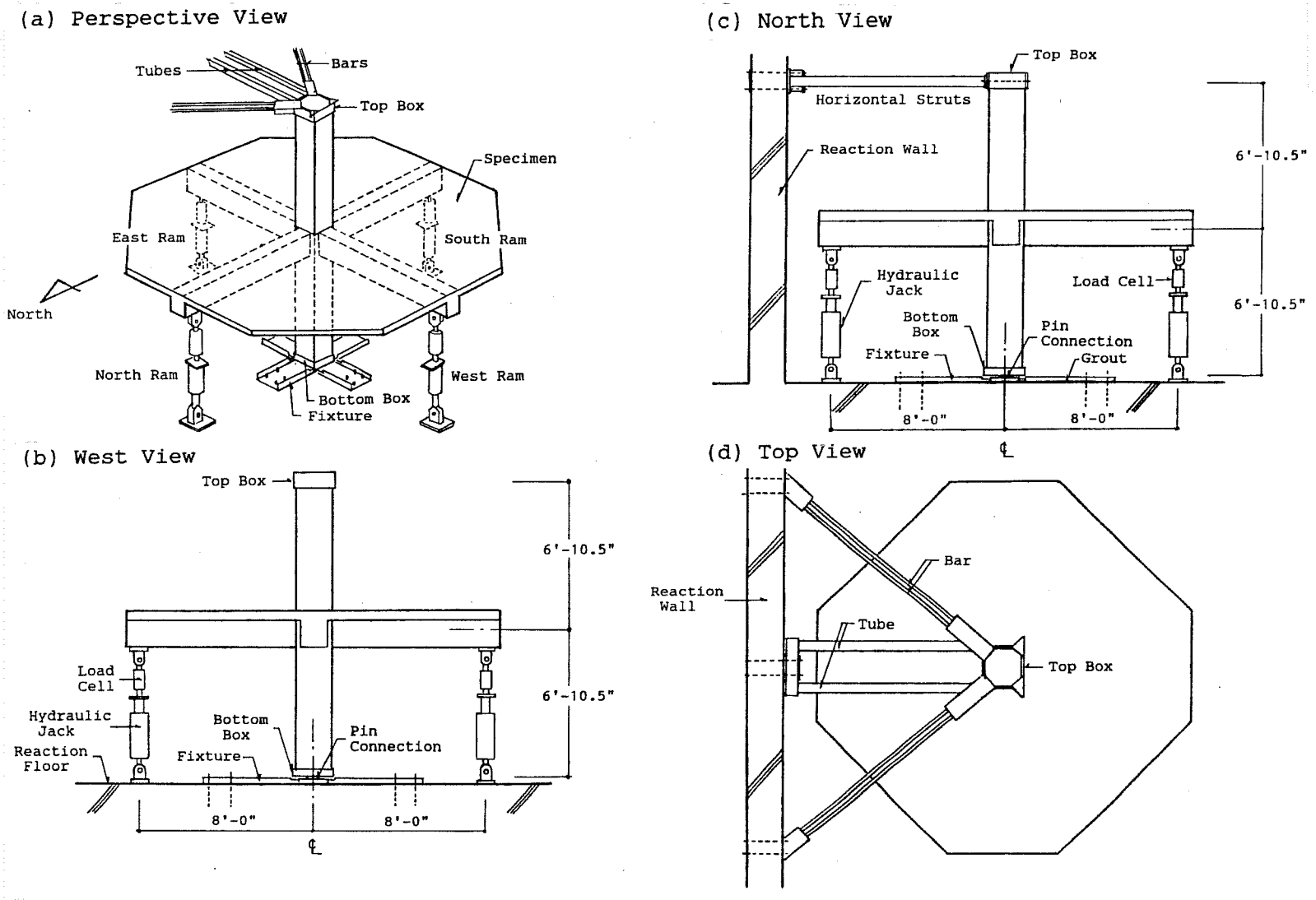

Figure 2.8 Loading Setup for Specimen J2

produced uplift at the column base. As shown in Fig. 11, a special steel rod was used to carry the axial tensile force to the reaction floor.

The loading histories for the three specimens are shown in Fig. 2.13. Specimen J1 was loaded in the EW direction only. specimens J2 and J3 were loaded in both directions but mainly in the EW direction. For east loading (positive loading) in the EW direction, the east beam was deflected upward and the west beam downward and for west loading (negative loading) the beams were deflected in the opposite sense. The loading histories followed the displacement paths which were agreed on at the Tokyo meeting in 1985[2]. However, some revisions were made in the histories because the specimens were so flexible that the yield deflection exceeded a drift angle of 1%. Therefore, peak displacements in the histories were defined as multiples of 1% drift instead of the yield deflection.

2.3 Instrumentation

Strain gages were placed on reinforcing bars at critical sections of the slab, beam, column and joint. The heaviest concentration of gages was in the joint region. Load cells, displacement transducers and dial gages were mounted on the hydraulic rams to measure loads and displacements, as shown previously in Fig. 2.12. The output from load cells and transducers were plotted on X-Y recorders to monitor progress of the test. Dial gage readings were taken to operate the two hydraulic rams equally but in the opposite directions.

Instrumentation for deformations in and at the joint is shown in Fig. 2.14. A pocket-size digital inclinometer was used to measure joint shear distortion and beam rotations for Specimen J1. The inclinometer readings were taken manually at every load stage, as shown in Fig. 2.15. For Specimens J2 and J3, the deformations were measured mainly with displacement transducers and supplemented with inclinometer readings. Transducers were mounted on a steel reference frame (attached near the joint to the reaction floor) to measure joint shear distortion. Transducers were also mounted on the specimen to measure beam and column end rotations, as shown in Fig. 2.16.

As shown in Fig. 2.17, the story drift angle was defined as the sum of beam tip displacements divided by the overall beam length, L (16-ft.), but was corrected by eliminating the overturning movement of the specimen (lateral deflection at top of column). An additional set of displacement transducers were mounted on the top of the specimen to monitor the overturning movement due to flexibility of the diagonal steel struts. The movement was found negligible in the EW direction, but was as much as 20% of the story drift in the NS direction during biaxial cycles. This was reduced in later tests by pretensioning the struts. Therefore, story drift was corrected using the horizontal displacement measured at the top of the column. The joint shear distortion, γ, was defined as the difference between the joint rotation measured along a vertical side, α, and that along a horizontal side, β. Rotations α and β were measured with the inclinometer for J1 and with transducers for J2 and J3.

The story shear was calculated from the load cell measurements using the following equation:

$$V = \frac{L}{2H} (P_1 + P_2)$$

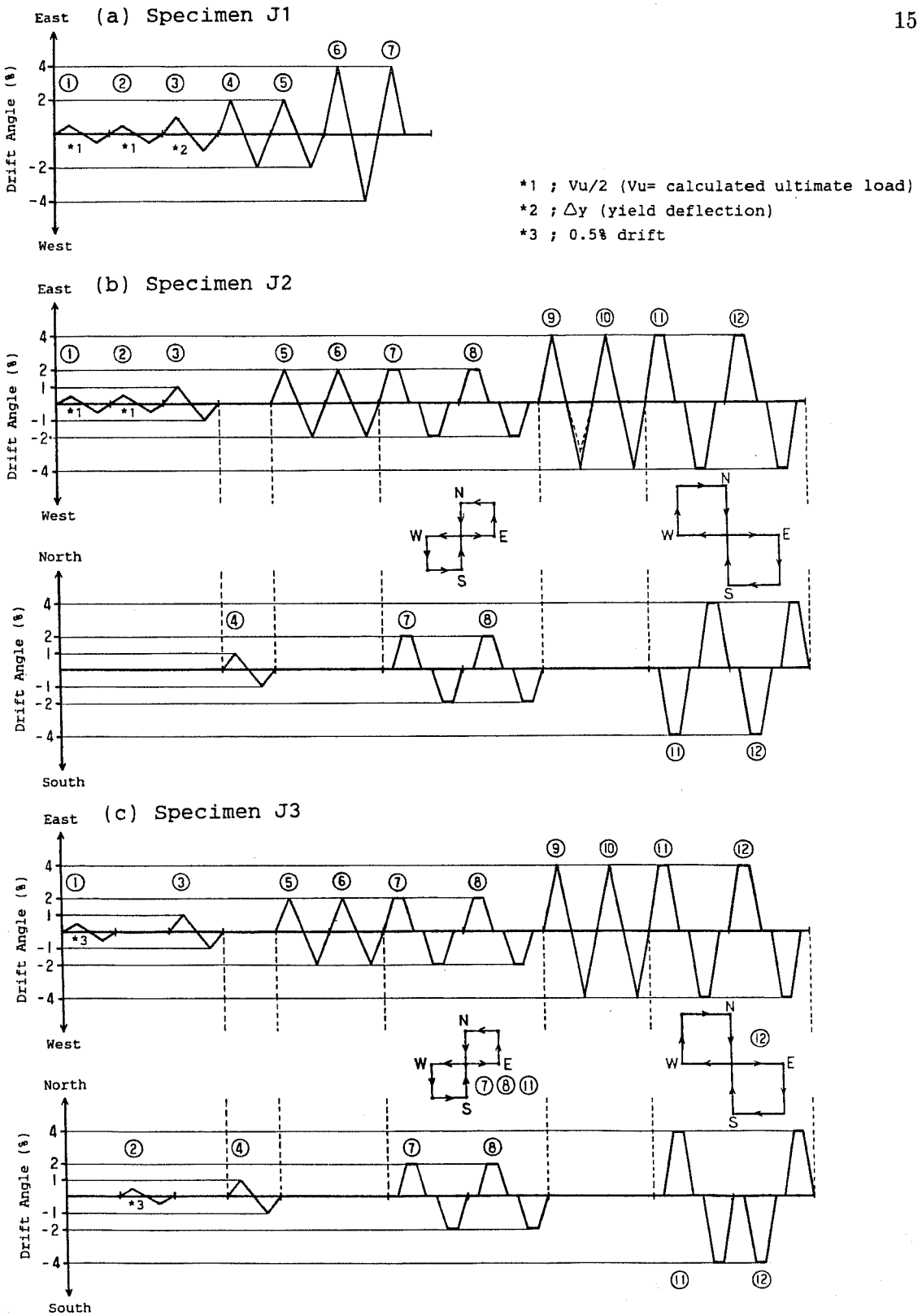

Figure 2.13 Loading Histories

where

L = overall beam length (16 ft)

H = overall column height (13 ft - 9 in)

P_1, P_2 = load cell measurements in one direction

3. TEST RESULTS

3.1 Overall Behavior of Specimens

3.1.1 Crack patterns. Specimen J1 (Figs. 3.1-3.3) developed flexural cracks in the slab, beam, and column and shear cracks in the joint. Some of the slab flexural cracks propagated into the beam and were inclined to the beam axis (flexural-shear cracks). The joint shear cracks propagated vertically into the lower column but did not extend into the upper column, probably because the top of the joint was confined by the slab. The cover concrete in the joint crushed and spalled under loading to 4% drift. The beams and columns suffered less damage than in the other specimens, because joint shear distortion dominated the overall deformation of the specimen (see Section 3.2).

Specimen J2 (Figs. 3.4-3.6) developed flexural cracks in the slab, beam and column and flexural-shear cracks in the beam. Although the beams on all four sides of the joint made it difficult to monitor joint shear cracks visually, a few cracks were observed in the corner of the joint at 1% drift. Some torsional cracks, inclined to the beam axis, formed near the column at 1% drift in the EW direction and in the east and west beams at 2% drift in the NS direction. Horizontal cracks were also observed in the beam at the interface between the beam and the bottom of the slab. Inclined cracks (shear cracks) formed in the columns and short vertical cracks formed in the lower column at the junction to the beam. During biaxial cycles to 2% drift, concrete started crushing in and near the joint. Crushing and spalling of the concrete progressed with additional load cycles. Most of the corner concrete in the joint was lost during biaxial cycles to 4% drift. The bottom concrete at beam ends spalled considerably during the final stages of loading. Spalling exposed some reinforcing bars in the joint region.

Specimen J3 (Figs. 3.7-3.9) developed flexural cracks in the slab, beam and column and flexural-shear cracks in the beam. Torsional cracks occurred in the beams in both directions. Shear cracks were observed on the east side of the joint. Concrete started crushing in and near the joint during biaxial cycles to 2% drift. The cover concrete on the east side of the joint spalled gradually during cycles to 4% drift and reinforcing bars, including column bars and vertical extensions of hooked top beam bars, were exposed.

3.1.2 Story shear - drift angle relations are shown in Figs. 3.10 (a) through 3.10 (c). The load stages at which first yielding of reinforcement was observed is indicated by the notation. The broken line, labeled V_u, shows the ultimate load calculated assuming beam hinges form. It should be noted that all the specimens reached higher strength than the calculated ultimate load. The story shear and drift angle measured at loading peaks are tabulated in Appendix B.

Specimen J1 showed pinching in the story shear-drift angle relation, as seen in Fig. 3.10(a). First yielding of slab, beam and column bars occurred under loading to 2% drift (cycle 4). The second cycle at 2% drift exhibited a narrow and slip-shaped hysteresis loop. A large drop in the story shear was observed at 4% drift because the specimen failed in joint shear.

Specimen J2 was subjected to biaxial loading which produced the vertical segments in the story shear-drift angle relations, as shown in Fig. 3.10(b). The loss of stiffness and strength in the second load cycles at 2 and 4% drift levels is quite apparent. Particularly in biaxial cycles at 4% drift, considerable deterioration occurred in the story shear, indicating failure of the specimen. First

(i) South View

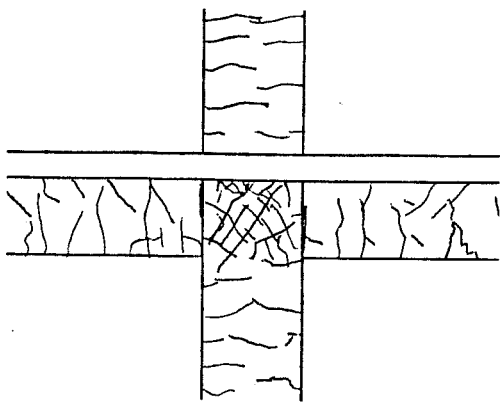

after 1% drift loading (cycle 3)

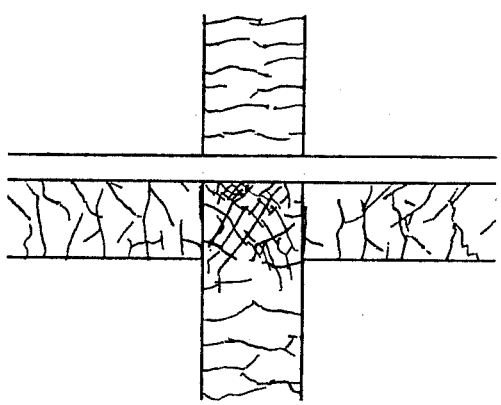

after 2% drift loading (cycle 5)

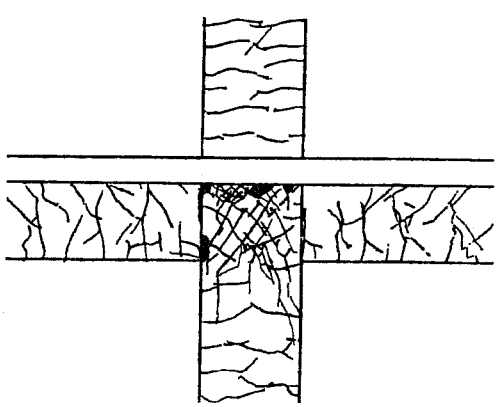

after 4% drift loading (cycle 7)

Figure 3.1 Crack Patterns for Specimen J1 at Various Loading Stages

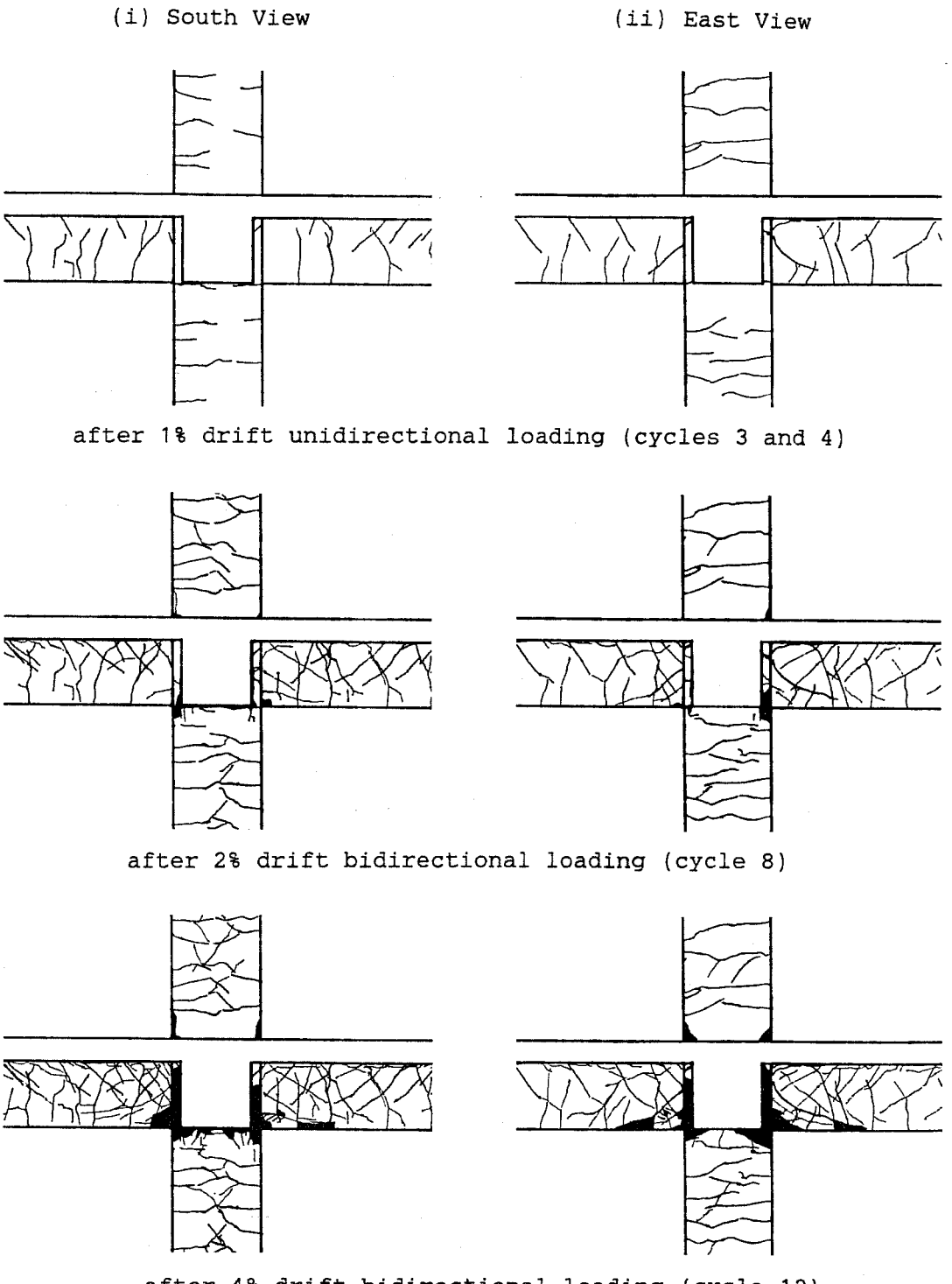

Figure 3.4(a) Crack Patterns for Specimen J2 at Various Loading Stages

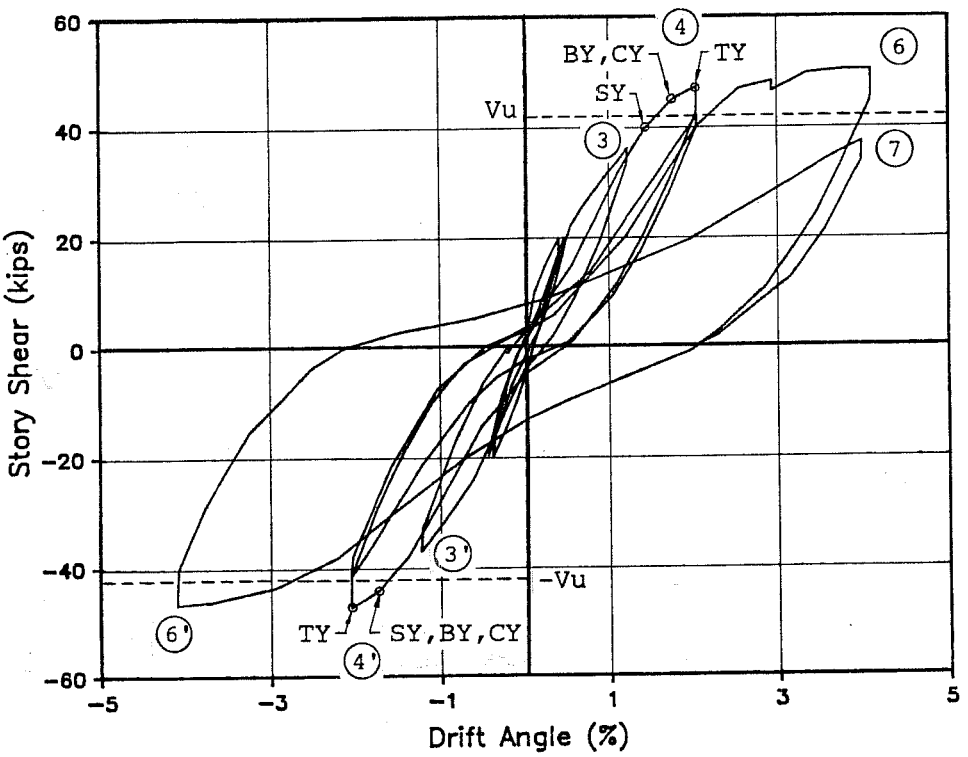

where

BY : bottom bar yielding (beam)
CY : column bar yielding
SY : slab bar yielding
TY : top bar yielding (beam)
Vu : calculated ultimate load
(beam hinge mechanism)
○ : loading cycle

Figure 3.10(a) Story Shear-Drift Angle Relation for Specimen J1

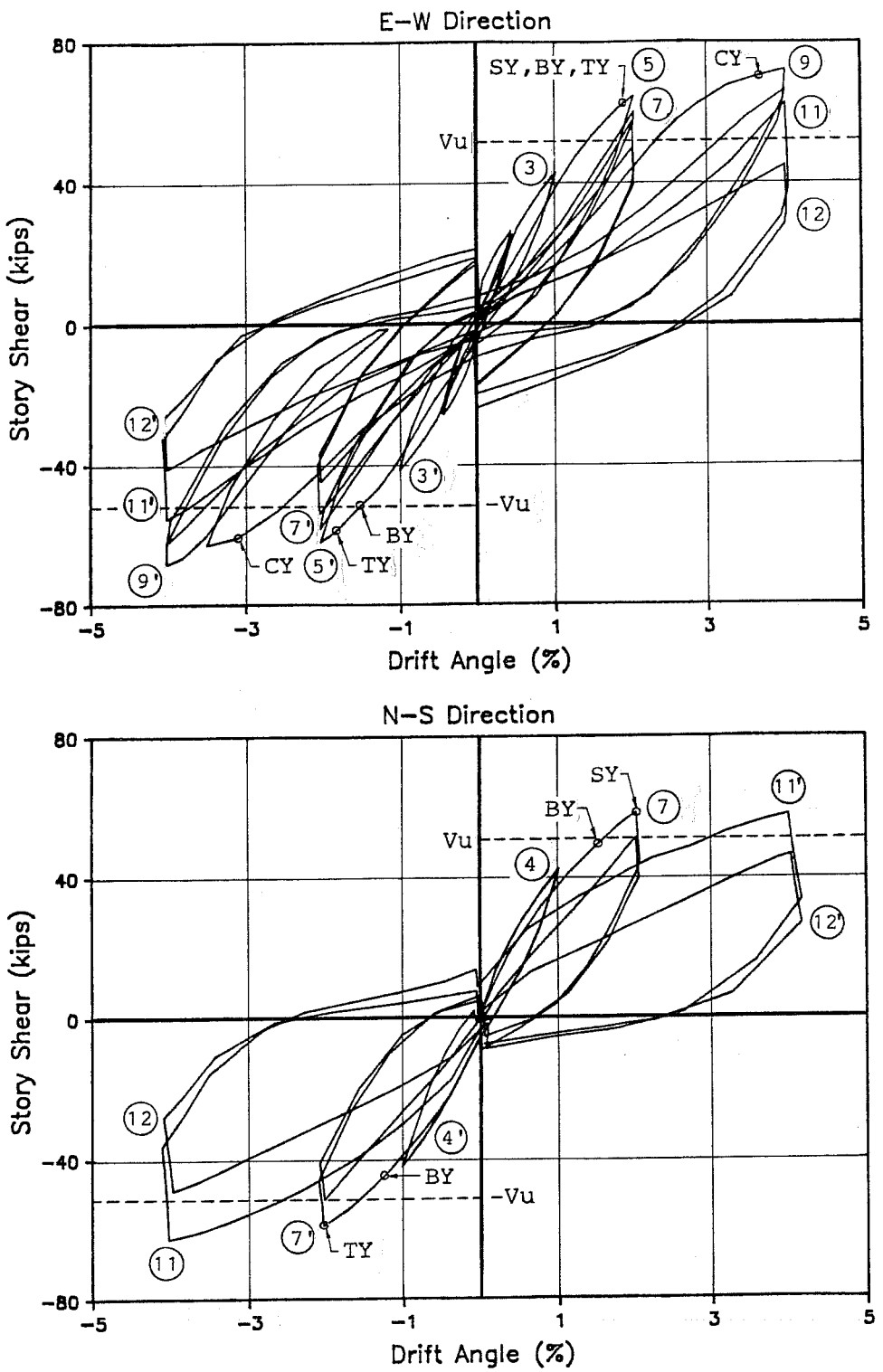

Figure 3.10(b) Story Shear-Drift Angle Relations for Specimen J2

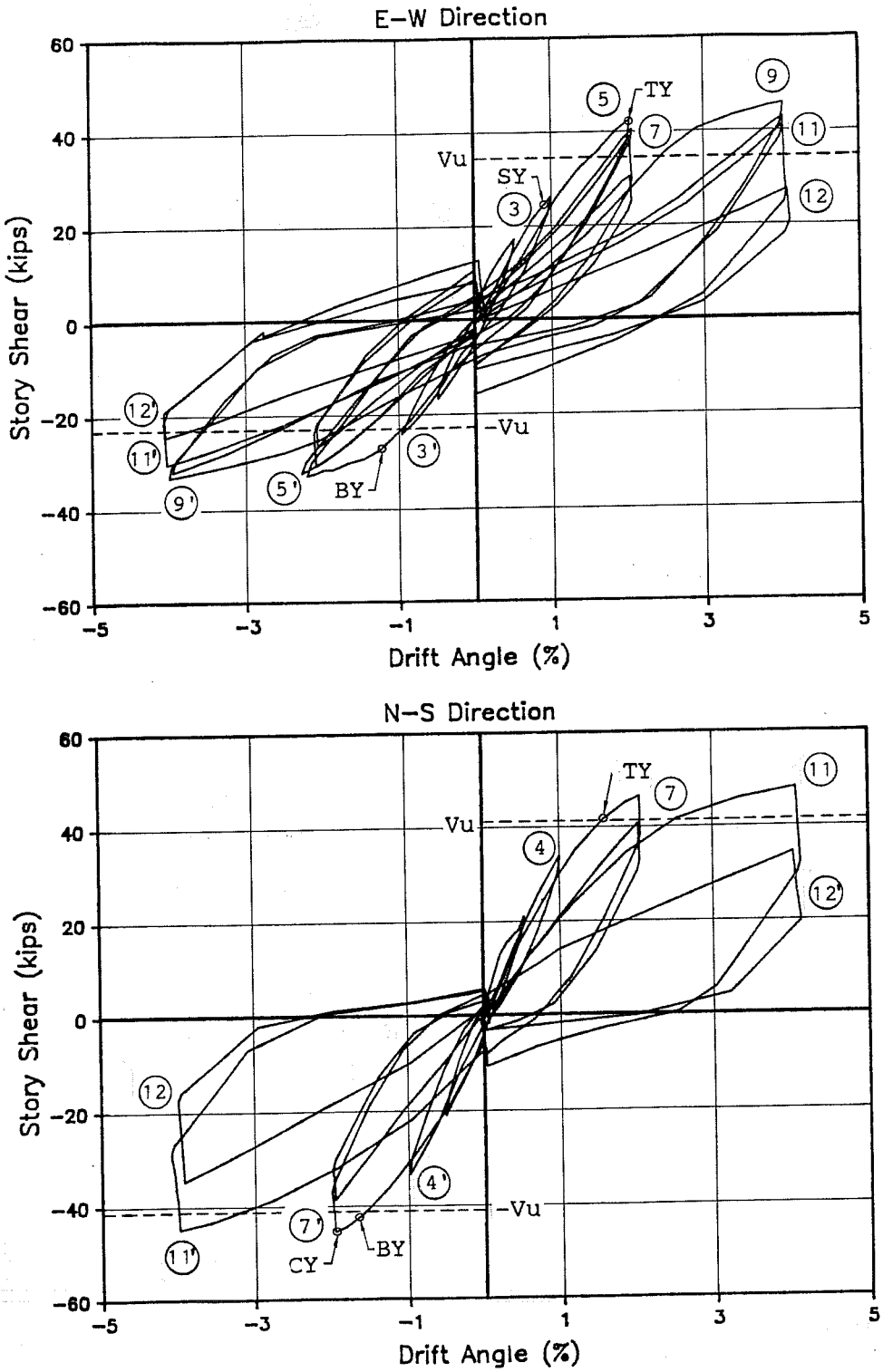

Figure 3.10(c) Story Shear-Drift Angle Relations for Specimen J3

yielding of slab and beam bars occurred under loading to 2% drift (cycle 5 in the EW direction and cycle 7 in the NS direction). Column bars yielded under uniaxial loading to 4% drift (cycle 9). During negative loading in cycle 9, the pin connection of the east ram fractured suddenly so that the hydraulic pressure had to be released to zero load. The ram was removed and the test was delayed for nine days until a new pin was obtained. The specimen was unloaded during this period, however, gravity loads increased some strains particularly in the slab and beam bars. After the pin was replaced, the test was resumed. The pin failure required an extra loading cycle (see cycle 9 in the EW direction). The curves in the NS direction were nearly identical except at 4% drift levels. It should be noted that the stiffness of the specimen measured in the NS direction at the initial stage of cycle 4 was reduced to 40% of the initial stiffness in cycle 1 by the preceding load cycles in the EW direction.

Specimen J3, subjected to biaxial loading, also showed vertical segments in the story shear-drift angle relations, as seen in Fig. 3.10(c). The vertical segments indicate the biaxial interaction of story shears in which loading in one direction lowered the shear in the other direction. In the EW direction, the specimen reached higher shear under downward loading (+ drift) than under upward loading (- drift) because heavy top beam reinforcement and large participation of slab reinforcement developed a greater moment in the west beam under the downward loading than under the upward loading. As a result, the story shear-drift angle relation showed more pronounced pinching in the downward loading than in the upward loading. Large tensile forces at the top of the beam forced the bottom concrete to close cracks and carry compressive forces. The participation of the bottom concrete stiffened the beam section and led to pinching in the load-deflection curve. The large loss of strength under the downward loading at 4% drift level was the result of anchorage distress in #9 top bars in the west beam. The hysteretic behavior in the NS direction is quite similar to that for Specimen J2. First yielding of slab bars occurred under loading to 1% drift (cycle 3). Beam bars yielded in cycles to 2% drift (cycle 5 in the EW direction and cycle 7 in the NS direction). Column bars yielded under biaxial loading at 2% drift (cycle 7).

Equivalent viscous damping factors in the EW direction were calculated from the story shear-drift angle relations, as shown in Fig. 3.11. The equivalent damping factors were quite low ranging from around 0.05 to 0.1 in the first several half cycles and increasing to values of 0.08 to 0.2 in the half cycles at 4% drift levels. The low values indicate low energy dissipating capacity and reflect pinching of the hysteresis loops. Pinching was caused by shear distress in the joint (shear pinching) and flexural distress in the slab, beam and column (flexural pinching). The flexural pinching was likely due to the following sources:

(1) heavy top reinforcement in the beam

(2) participation of concrete and reinforcement of the slab

(3) crushing of concrete in the column under biaxial loading.

Some bond deterioration probably occurred along beam and column bars within the joint and led to more pinching. These phenomena are discussed in Sections 3.2 through 3.4.

3.1.3 Drift angle and story shear orbits are shown in Figs. 3.12 and 3.13. The drift angle in one direction was kept constant during loading in the other direction as shown in the drift angle orbits. However, the interaction between loading directions is quite apparent in the skewed nature of

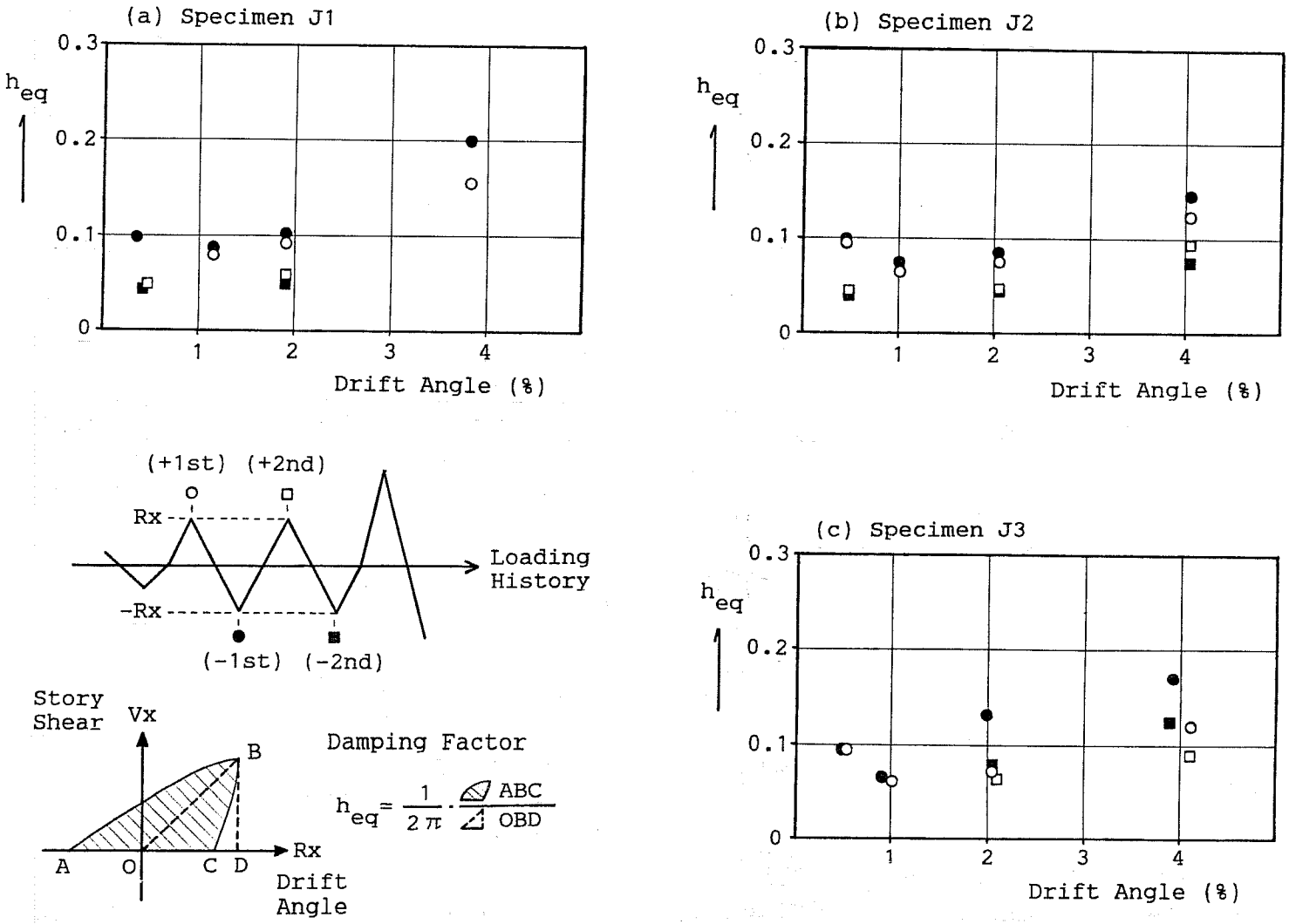

Figure 3.11 Equivalent Viscous Damping Factors in East-West Direction

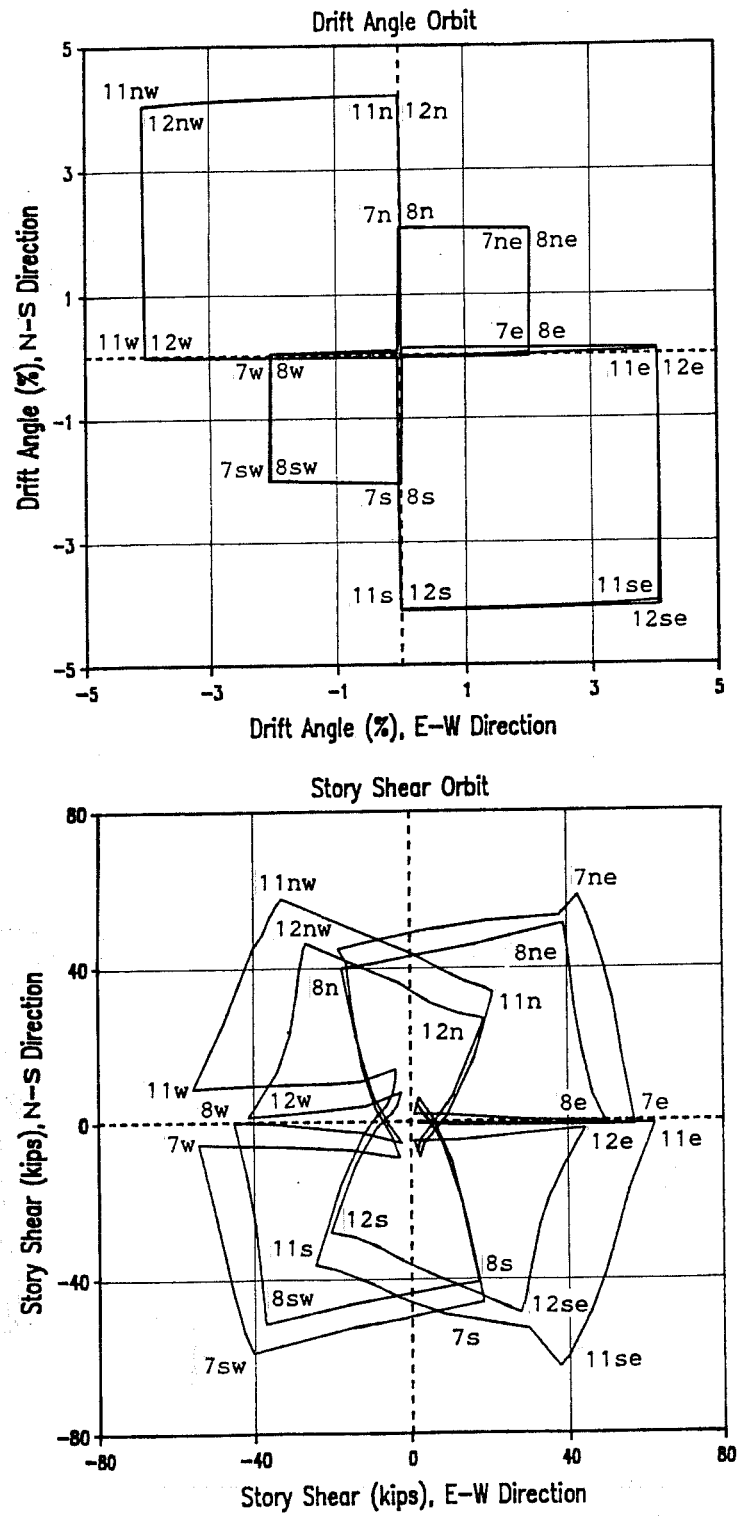

Figure 3.12 Drift Angle and Story Shear Orbits for Specimen J2

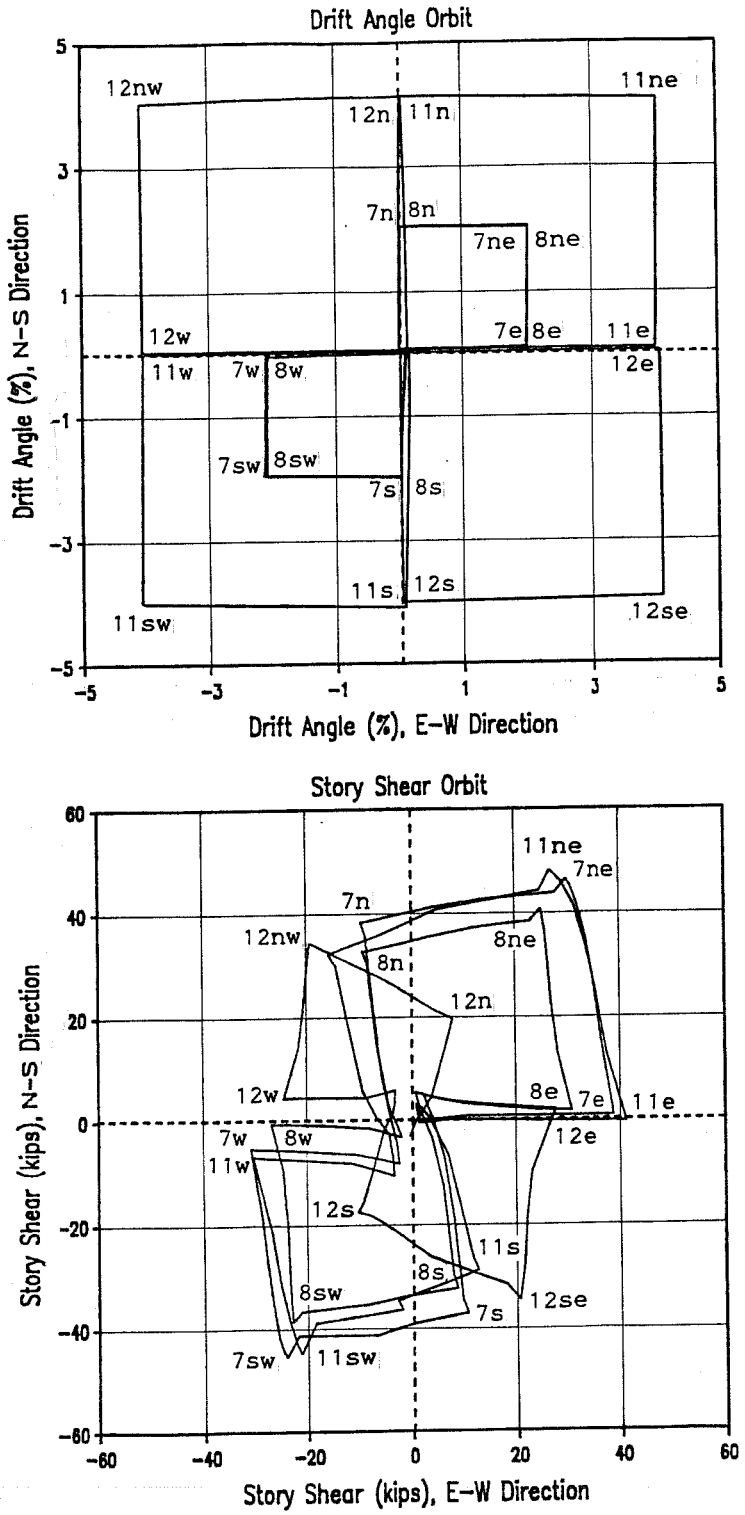

Figure 3.13 Drift Angle and Story Shear Orbits for Specimen J3

the story shear orbits. Loading or even unloading in one direction lowered the story shear in the other direction. In general, the story shear orbit traces fairly consistent response in all quadrants with some loss of capacity in the second cycle of loading to a given drift level. The capacity deteriorated markedly at 4% drift levels.

3.2 Shear Behavior of Beam-Column Joints

3.2.1 Joint shear distortion is plotted against story shear in Figs. 3.14(a) through 3.14(c). First yielding of joint lateral reinforcement is shown with a mark JY.

Specimen J1 sustained higher joint shear than the recommended design strength of $15\sqrt{f'_c}$, as shown in Fig. 3.14(a). The joint reinforcement yielded under loading to 2% drift (cycle 4). The shear distortion increased rapidly in cycle 6 to 4% drift indicating shear failure in the joint. The shear distortion was defined as the average of the inclinometer measurements on the east and west sides of the joint. However, the two measurements showed different features with loading directions. The measurement on the east side showed larger distortion under negative loading (downward loading for the east beam), while that on the west side showed larger distortion under positive loading (downward loading for the west beam). The tensile force at the top of the beam seemed to increase local distortion which produced greater joint shear distortion when the beams were loaded downwards.

For Specimen J2, the story shear-joint shear distortion relations showed an apparent degradation of the joint in shear, as seen in Fig. 3.14(b). The joint shear distortion, particularly in the EW direction, increased with load cycles even under loading in the transverse direction. First yielding of the joint reinforcement occurred under loading to 2% drift (cycle 5 in the EW direction and cycle 7 in the NS direction). The rapid increase in shear distortion in biaxial cycles to 4% drift indicates that the specimen failed in joint shear. The larger shear distortion under negative loading in the EW direction and under positive loading in the NS direction was due to locating the instrumentation at the south-east corner of the joint. It should be noted that the maximum joint shear exceeded the recommended design strength of $20\sqrt{f'_c}$ in both directions.

Specimen J3 reached higher joint shear than the recommended design strength of $15\sqrt{f'_c}$, as shown in Fig. 3.14(c). The joint reinforcement yielded under loading to 4% drift (cycle 10 in the EW direction and cycle 11 in the NS direction). The joint shear distortion in the EW direction was defined as the average of two measurements on the east and west sides of the joint. The two measurements had the same directional features as in Specimen J1. The distortion in the EW direction was smaller than in the NS direction or in the other specimens because the shear force was smaller. The shear distortion increased rapidly during biaxial cycles to 4% drift in both directions.

Figure 3.15 shows drift angle components in the EW direction plotted against story drift. Each component was calculated using the procedure outlined in Fig. 2.17. In the three specimens, the joint component increased steadily with load cycles while the other components decreased or did not change. From this viewpoint, the specimens are considered to have failed in joint shear. Particularly in Specimen J1 the joint component rapidly increased with story drift. The response of the specimen was heavily influenced by shear distress in the joint at large drift levels.

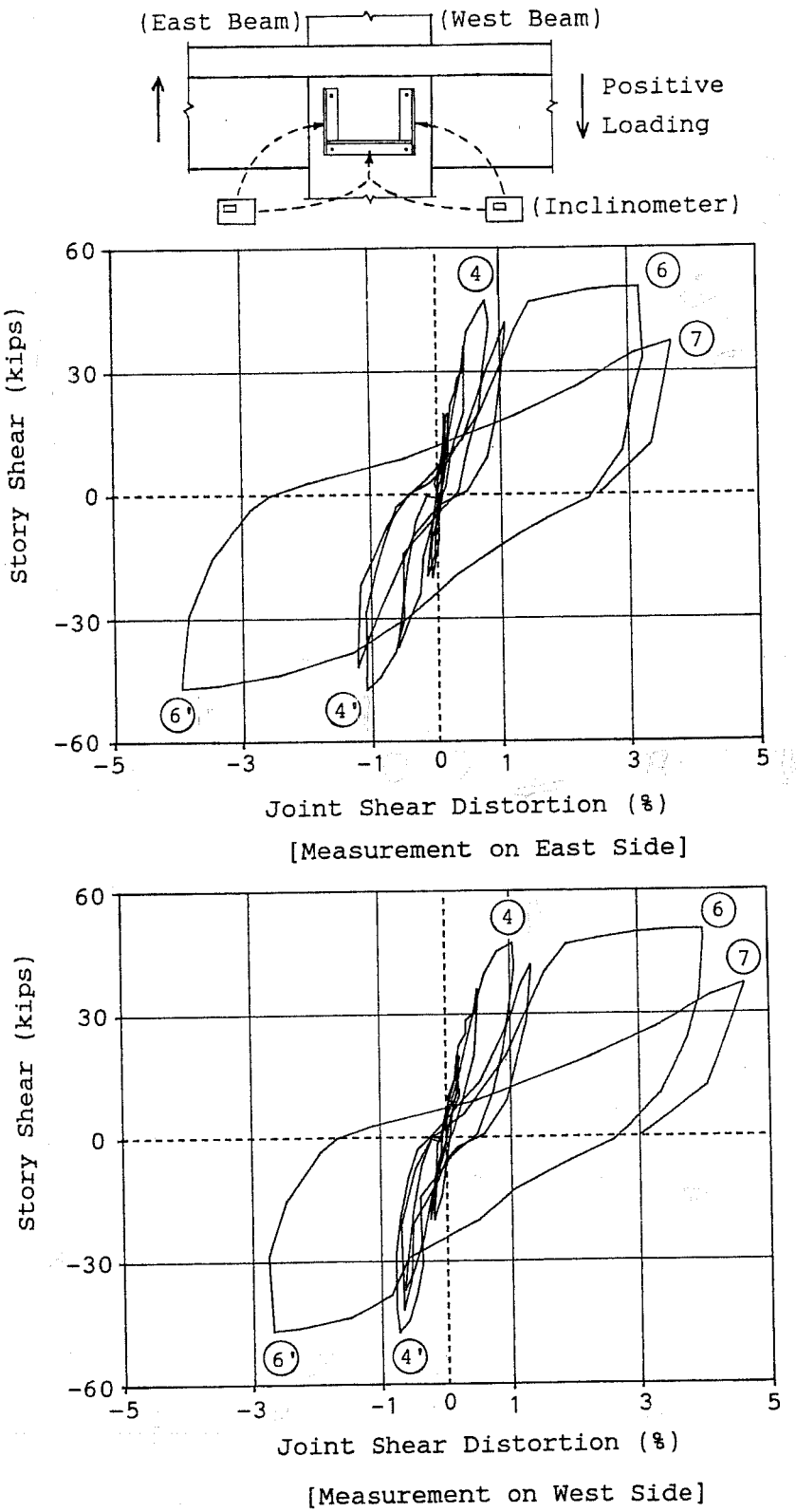

Figure 3.14(a) Story Shear-Joint Shear Distortion (Specimen J1) - continued

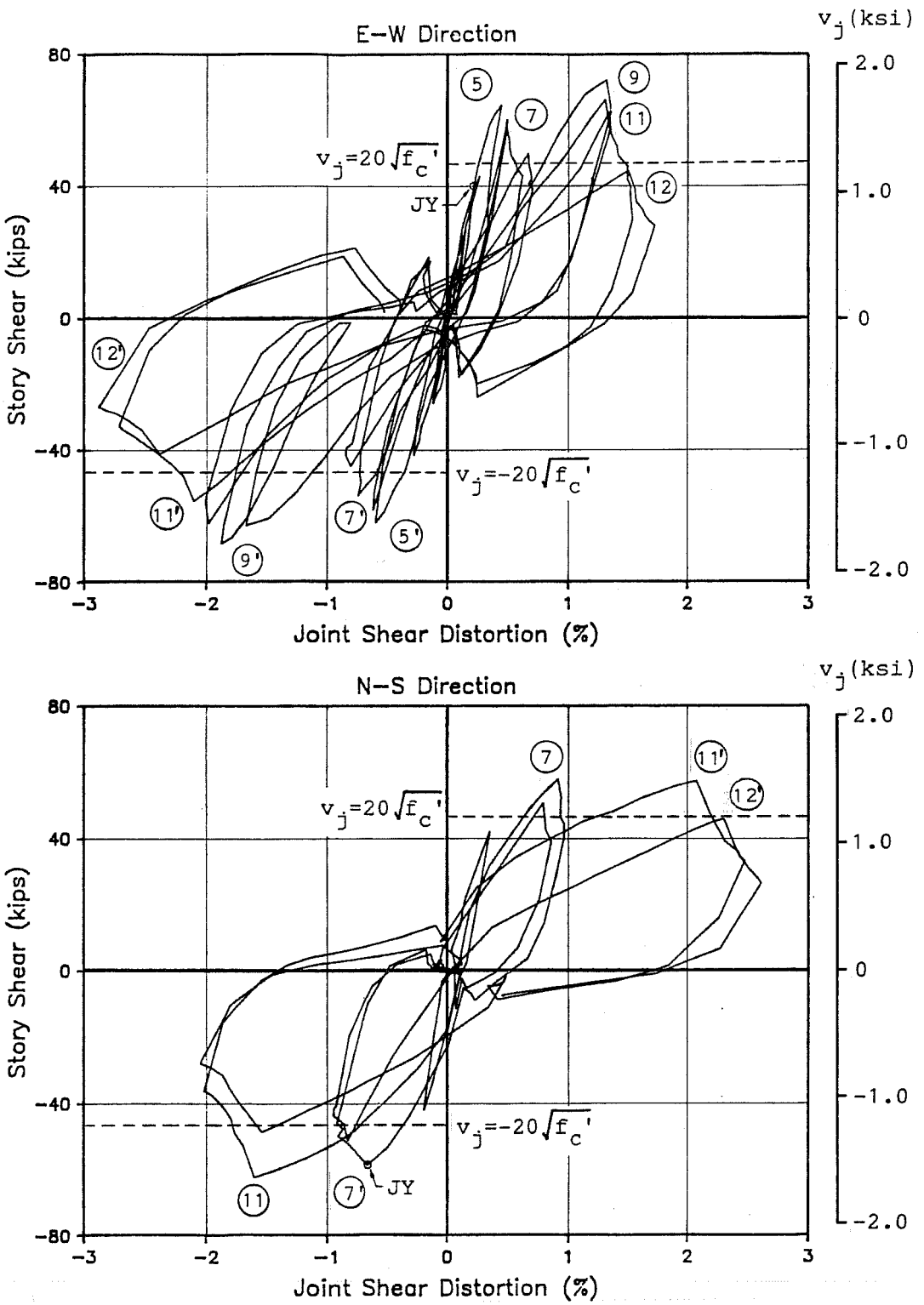

Figure 3.14(b) Story Shear-Joint Shear Distortion (Specimen J2)

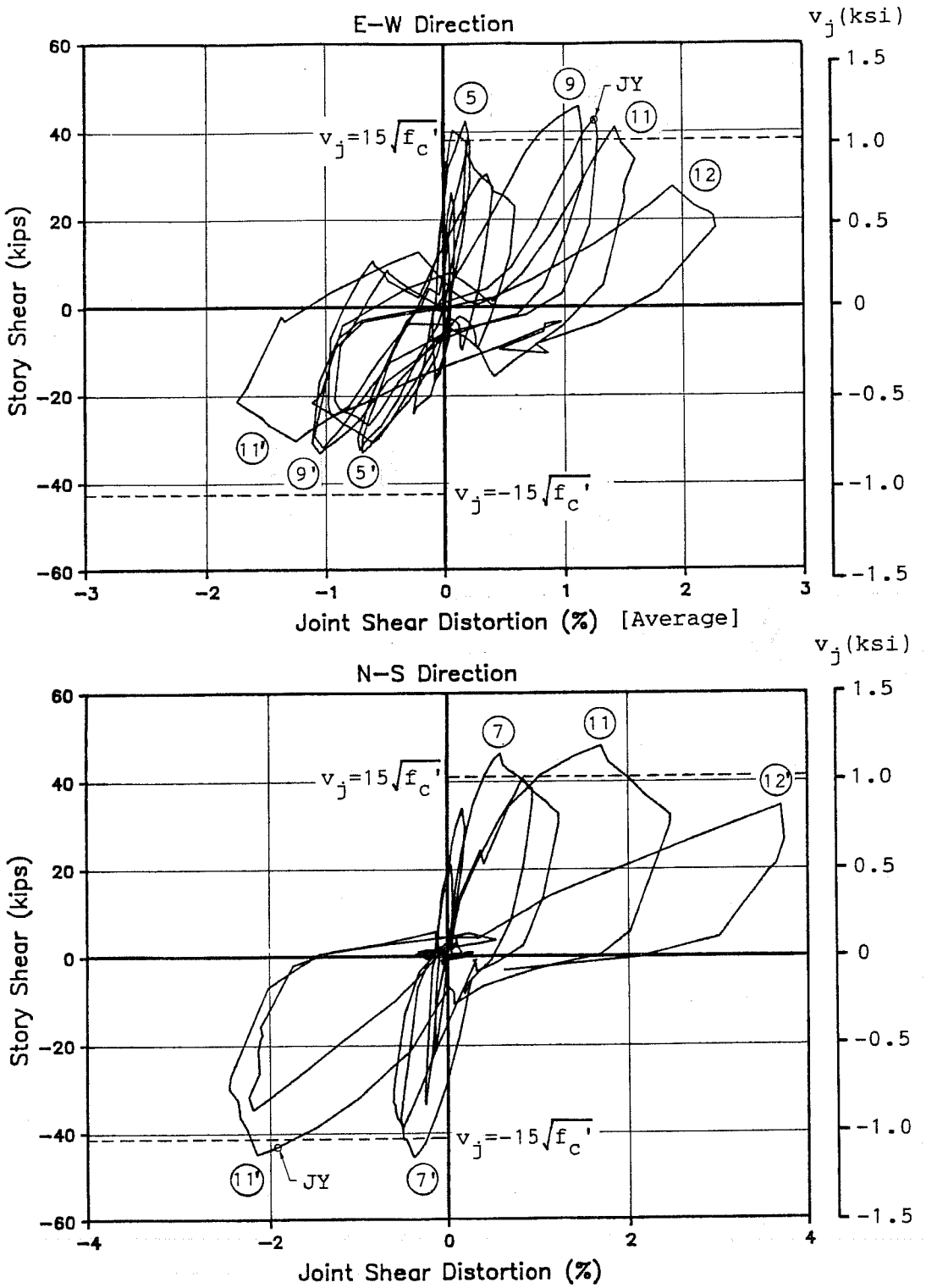

Figure 3.14(c) Story Shear-Joint Shear Distortion (Specimen J3)

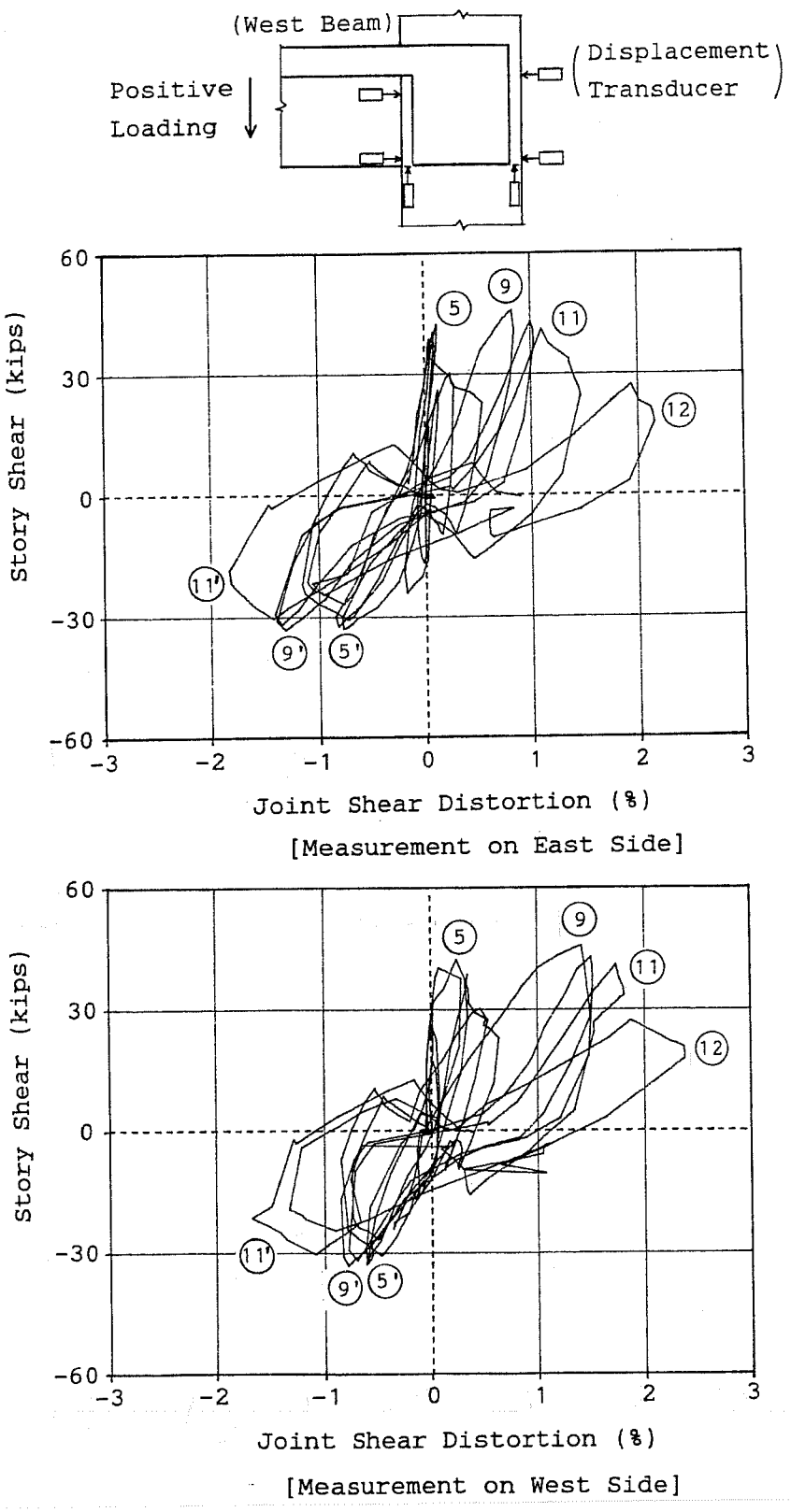

Figure 3.14(c) Story Shear-Joint Shear Distortion (Specimen J3) = continued

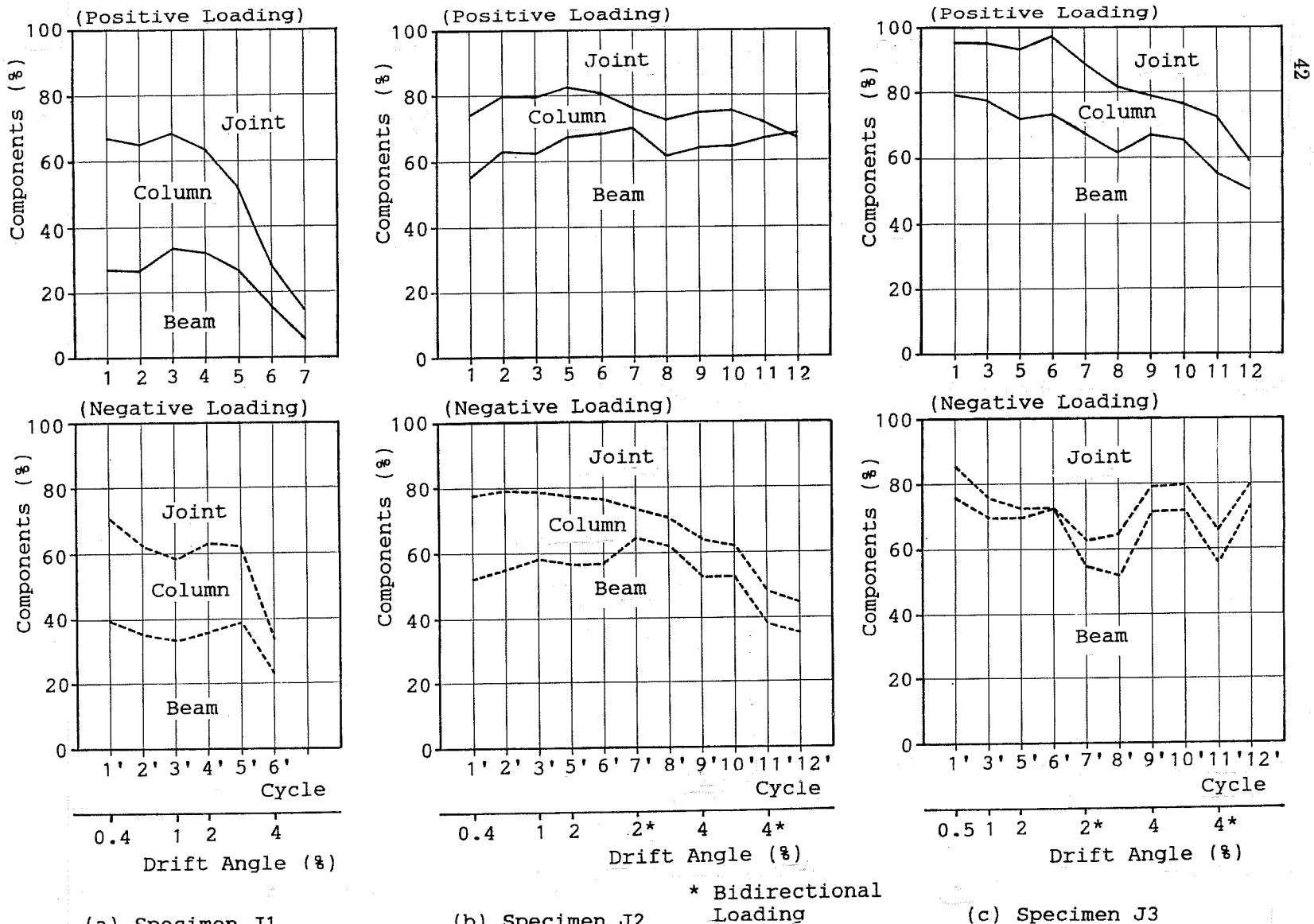

Figure 3.15 Drift Angle Components in East-West Direction

Figure 3.16 shows joint rotations α and β for Specimen J2 in the EW direction. Rotation α, measured along a vertical side of the joint, was much larger than rotation β, measured along a horizontal side. Therefore, the joint shear distortion, defined as the difference between the two rotations, was dominated by rotation α. It should be noted that rotation β was a measure of column deformations.

Figure 3.17 shows displacement measurements for rotation α of Specimen J2 in the EW direction. The top transducer measured displacement only under negative loading, although the bottom transducer measured displacements in both loading directions. Thus, the displacement at the top caused the directional features of the joint shear distortion.

3.2.2 Strains in joint reinforcement are shown in Figs. 3.18(a) through 3.18(c). Five sets of transverse reinforcement were placed within the joint; three (located at Z2, Z3 and Z4) were between the top and bottom beam bars, and the other two (Z1 and Z5) were outside the beam bars. In all the specimens, the strains increased with drift angle, particularly in the reinforcement between the beam bars.

For Specimen J1, strains were measured in all five sets. The reinforcement between the beam bars exhibited much higher strains than outside the beam bars, as seen in Fig. 3.18(a).

For Specimens J2 and J3, the strains in the EW direction increased under biaxial loading in the NS direction. The results indicate that the reinforcement was effective in confining the joint concrete. As seen in Fig. 3.18(c), the strains measured at Y1 on the east side of the joint in J3 were relatively low, although the cover concrete on the east side spalled. It is likely that heavy congestion of beam and column bars on the east side accelerated spalling of the concrete and that the joint reinforcement parallel to this side did not provide restraint to spalling.

3.2.3 Joint shear strength is discussed using story shears measured uniaxially and biaxially. It is important to note that all the specimens developed beam flexural yielding before failing in joint shear. Therefore, the measured maximum strength of the specimens may have been reduced because the capacity of the beams governed.

Table 3.1 is a summary of the maximum story shears measured during uniaxial and biaxial cycles at 4% drift levels. The table also includes the story shears calculated from the joint shear strength following the recommendations or guidelines of Japan[6], New Zealand[5], and the United States[3]. The equations for the joint shear strength are given in Appendix C. The measured biaxial shear was defined as a square root of the sum of squares of the shears measured in orthogonal directions. For the calculated biaxial shear, circular or elliptical interaction curves were assumed. In all three specimens, the measured maximum shear exceeded the calculated strengths under uniaxial or biaxial loading. The NZS approach resulted in the lowest calculated strength because the concrete contribution was lowest. The ACI 352 approach underestimated the maximum shear by 20 to 50%. Among the specimens, J2 sustained the highest shear, probably because the joint was confined with beams in both directions. The maximum shears in J3 were comparable to those in J1. It should be noted that the measured biaxial strength exceeded the measured uniaxial strength in both J2 and J3.

Figure 3.19 shows one quadrant of story shear orbits compared with calculated beam and column moment capacities (see Appendix C for calculations). The different values of joint shear

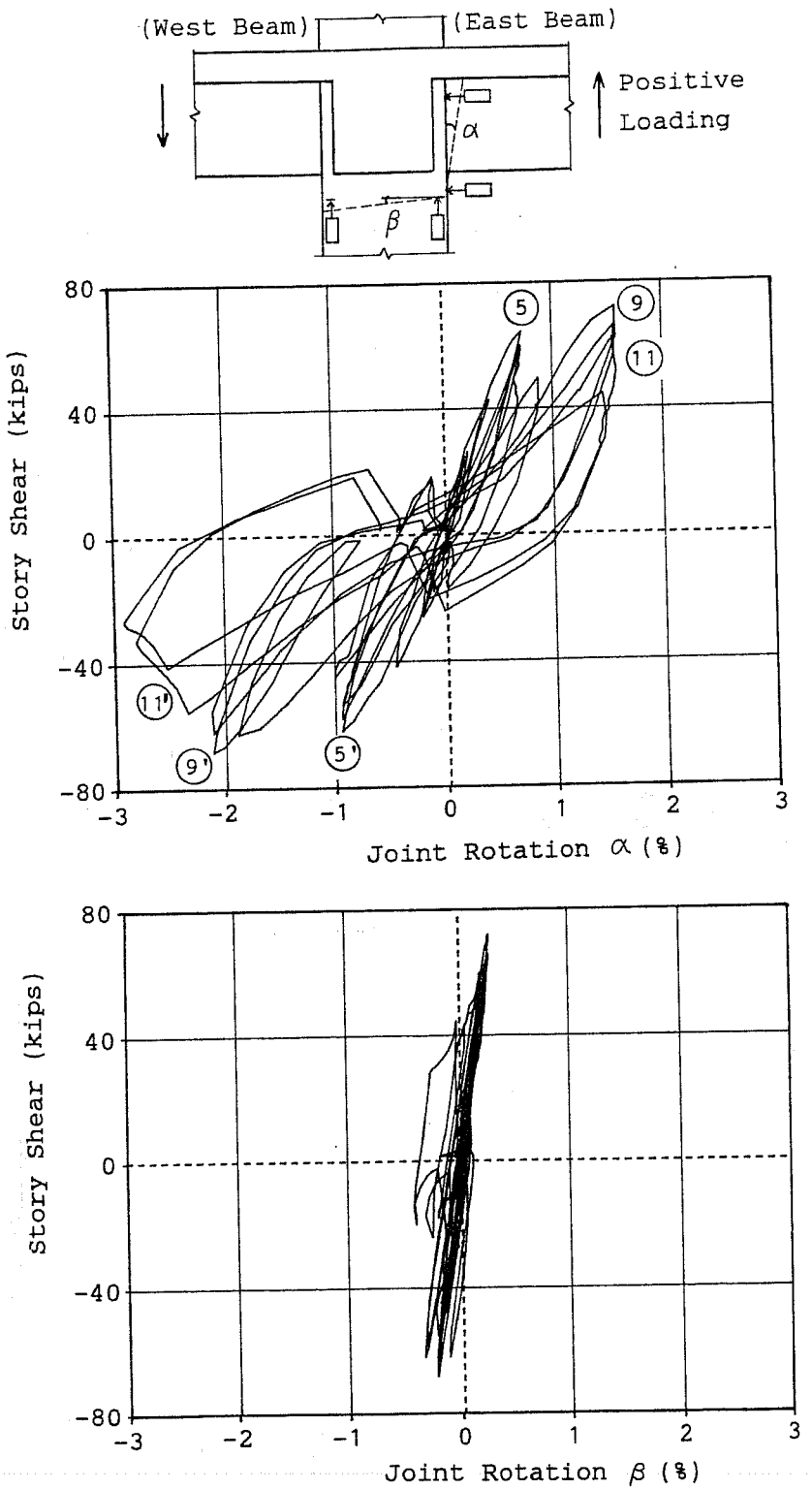

Figure 3.16 Joint Rotations for Specimen J2 in E-W Direction

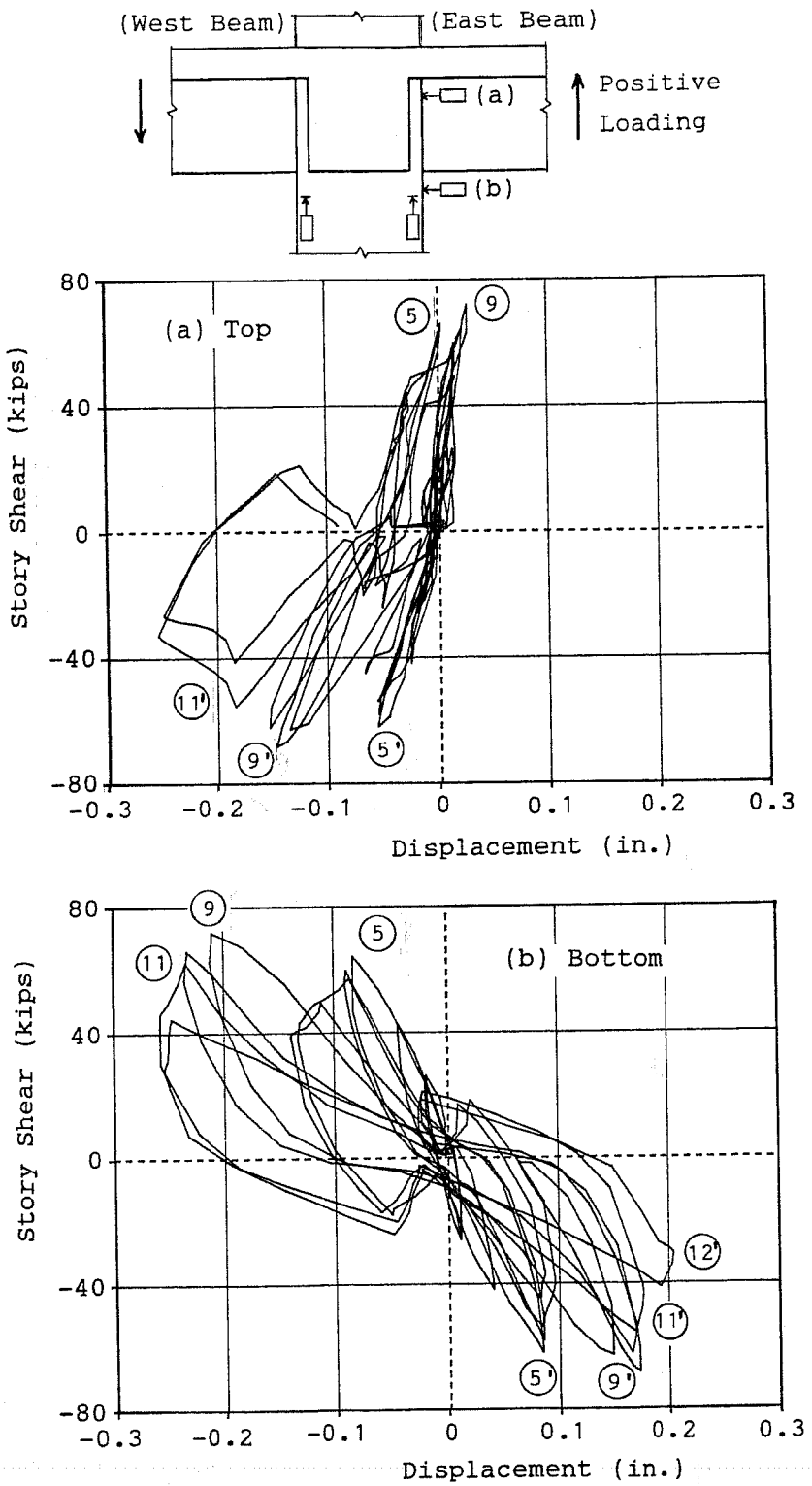

Figure 3.17 Displacement Measurements at Joint for Specimen J2

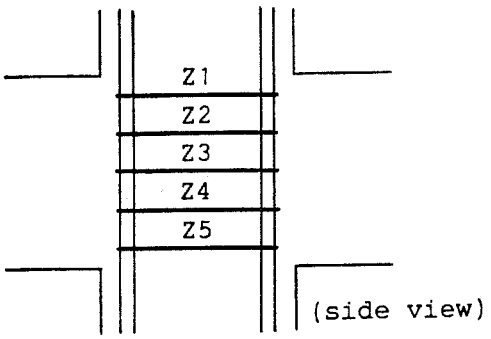

Joint Hoop Position

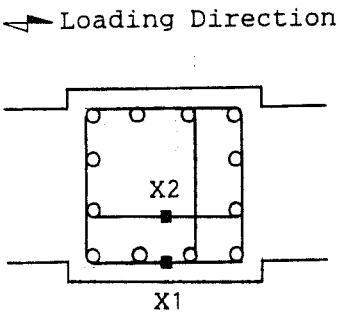

Strain Gauge Location

Loading Peaks

Line	Rx(%)	Ry(%)	LC
—·—	+0.4	0	1
------	+1	0	3
— — —	+2	0	4
———	+4	0	6

where

Rx : drift angle in E-W direction

Ry : drift angle in N-S direction

LC : loading cycle

▷- : yield strain

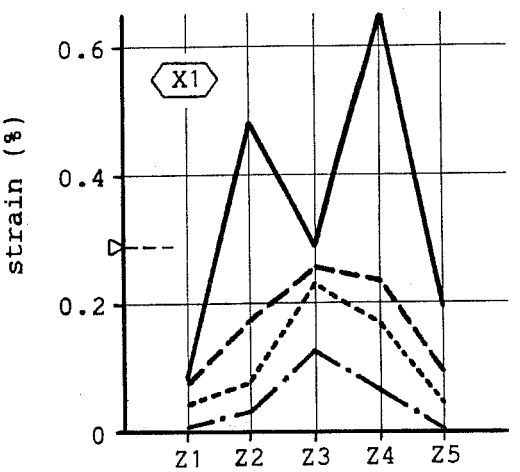

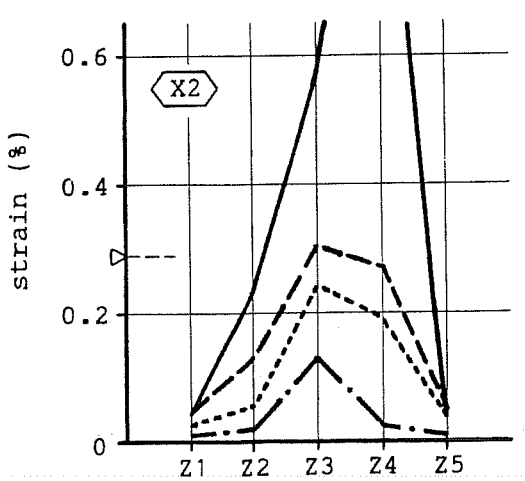

Figure 3.18(a) Joint Hoop Strains at Loading Peaks (Specimen J1)

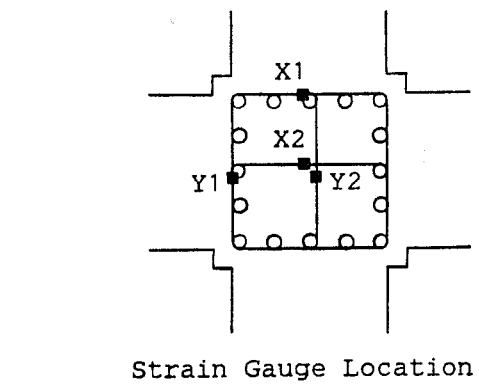

Strain Gauge Location

North

Line	Rx(%)	Ry(%)	LC
—·—	+0.4	0	1
------	+1	0	3
------	0	+1	4
——	+2	0	7
— —	+2	+2	7
———	+4	0	9
———	+4	-4	11

(i) E-W Direction

(ii) N-S Direction

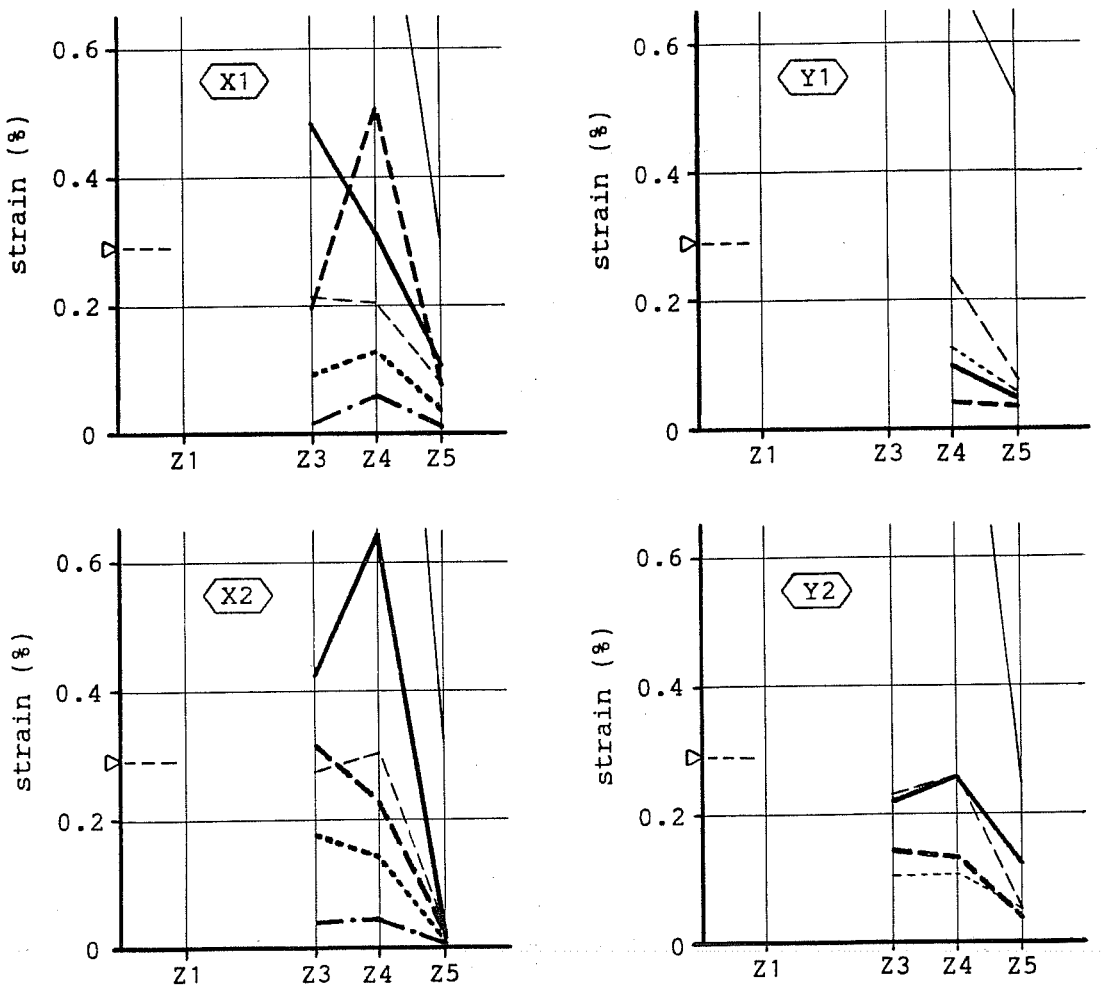

Figure 3.18(b) Joint Hoop Strains at Loading Peaks (Specimen J2)

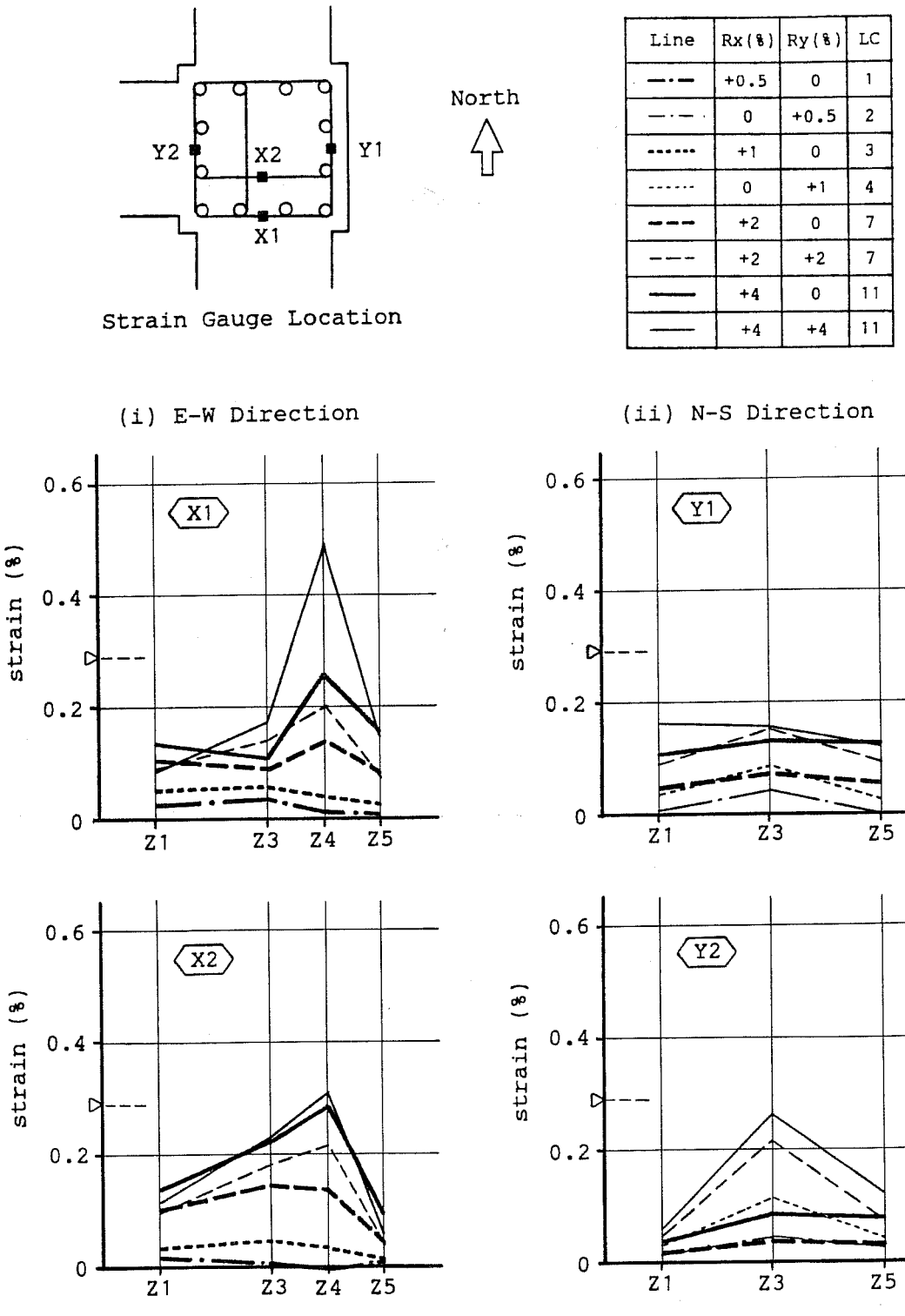

Figure 3.18(c) Joint Hoop Strains at Loading Peaks (Specimen J3)

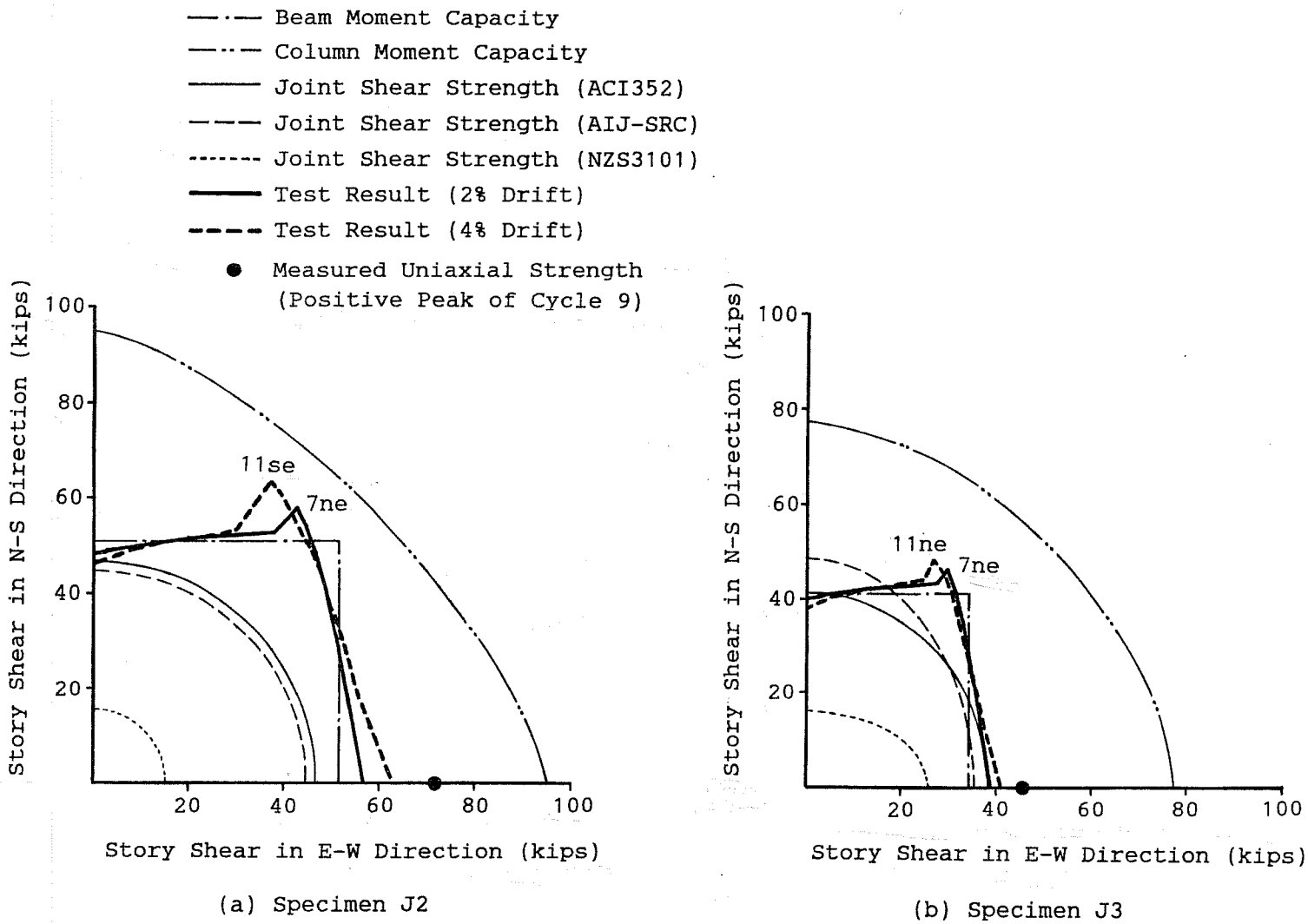

(a) Specimen J2

(b) Specimen J3

Figure 3.19 Story Shear Orbits in Comparison with Calculated Capacities

Table 3.1 Measured Maximum Story Shear in Comparison with Calculated Joint Shear Strength

Story Shear	Specimen J1 (Uniaxial) [EW]	Specimen J2		Specimen J3	
		Uniaxial [EW]	Biaxial	Uniaxial [EW]	Biaxial
Measured Story Shear (kips)	50.3	72.0	73.4 [EW: 37.6] [NS: 63.0]	45.8	54.8 [EW: 26.5] [NS: 48.0]
Calculated Story Shear (kips)					
a) ACI 352	35.6 (1.41)	46.8 (1.54)	46.8 (1.57)	38.2 (1.20) [NS: 41.3]	40.6 (1.35)
b) AIJ-SRC	46.3 (1.09)	44.7 (1.61)	44.7 (1.64)	35.3 (1.30) [NS: 48.5]	44.1 (1.24)
c) NZS-3101	16.0 (3.14)	15.3 (4.70)	15.3 (4.79)	25.7 (1.78) [NS: 16.0]	17.3 (3.17)

() : ratio of measured story shear to calculation

(i) Calculated Uniaxial Story Shear

$$Vn = \frac{b_j h_j j_b v_j}{H(1 - \frac{h_j}{L} - \frac{j_b}{H})}$$

v_j: joint shear strength using codes a to c

L: beam length (L = 192")

H: column height (H= 165")

b_j: joint width

$$[b_j = (b_b + b_c)/2 \quad (a\&b) \quad or \quad b_j = b_c \quad (c)]$$

h_j: joint depth

$$[h_j = h_c \quad (a\&c) \quad or \quad h_j d_c * 7/8 \quad (b)]$$

j_b: $= d_b * 7/8$ (d_b:beam effective depth)

(ii) Calculated Biaxial Story Shear

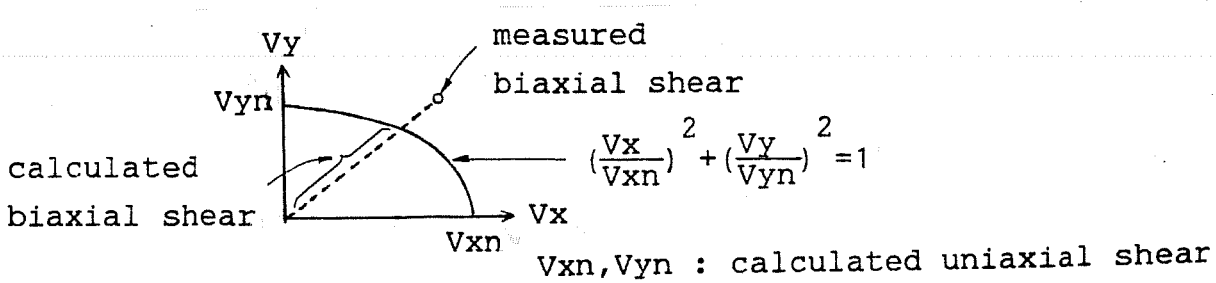

strength based on the AIJ, NZS and ACI approaches, respectively, are also plotted by assuming quadratic curves; circular curves for J2 and elliptical curves for J3. Specimen J2 had the same strength in both principal directions, but J3 had different strength due to different contributions of concrete. The assumed quadratic curves appears to evaluate the biaxial strength fairly but somewhat conservatively. It should be noted that the story shear orbit did not reach the column moment capacity but the column developed yielding of longitudinal bars and crushing of concrete in the two specimens.

3.3 Bond Behavior of Longitudinal Reinforcement

The bond behavior of longitudinal reinforcement is discussed below using deformations and strains measured in the EW direction during uniaxial cycles. Strains were converted to stresses using a stress-strain relation shown in Appendix C. The emphasis is placed on the behavior of beam longitudinal reinforcement.

3.3.1 Member end deformations were examined in terms of beam end rotations (Fig. 3.20), beam and column end curvatures (Figs. 3.21 through 3.25) and displacement measurements at beam and column ends (Figs. 3.26 through 3.30). It should be noted that the deformations included flexural deformations at the member end and bond slip deformations within the joint. Shear deformations at the member end were thought to be small. However, beam end rotations seemed to be affected slightly by joint shear distortion, particularly for Specimens J2 and J3. Displacement transducers for the beam end rotations were mounted on the specimen about two inches above or below the beam face so that the transducers incidentally measured small horizontal deformations which occurred over the two inches at column ends, mainly due to joint shear distortion.

Figure 3.20 shows the beam end rotations plotted against beam tip deflections. The beam tip deflection was calculated from story drift using the deformation pattern shown in Fig. 2.17. In Specimen J1, both the beam end rotation (angle change in region adjacent to column face) and beam tip deflection did not change while the drift angle increased from 1% to 4%. In specimens J2 and J3, the beam deformations increased with drift angle. The beam end rotation contributed an increasing amount of the beam tip deflection. Under negative bending in J3, the beam end rotation contributed nearly all of the beam deflection, indicating anchorage distress in the hooked top beam bars.

Figures 3.21 through 3.25 show the beam or column end curvatures plotted against beam of column (story) shears, respectively. The beam end curvatures for Specimen J1, measured with a digital inclinometer, remained small throughout the test, as shown in Figure 3.21. Those for Specimens J2 and J3 measured in region 1 (immediately adjacent to column face) exhibited large inelastic deformations and showed pronounced pinching in the beam shear-curvature relations, as seen in Figure 3.22. Specimen J2 exhibited larger curvatures under positive bending than under negative bending at 4% drift levels. On the contrary, J3 exhibited much larger curvatures under negative bending than under positive bending in cycles to 4% drift. As shown in Fig. 3.23, the beam end curvatures measured in region 2 (adjacent to region 1) were very small. Inelastic deformations were observed only under positive bending. First yielding of the section appears to occur in cycle 9 to 4% drift for J2 and in cycle 5 to 2% drift for J3. The results indicate that the beam plastic hinge under positive bending penetrated into region 2 during 2 to 4% drift cycles but the section in this

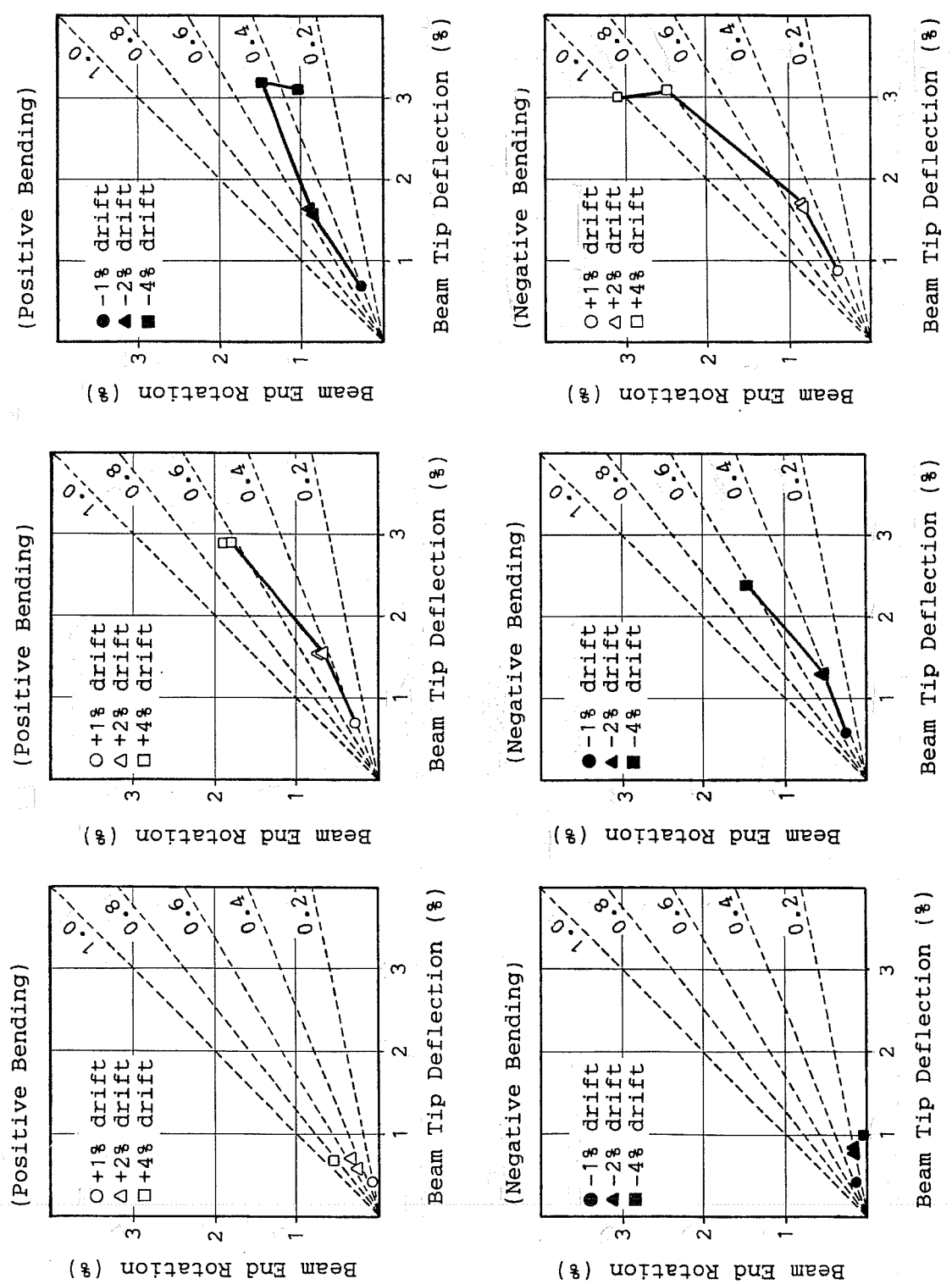

Figure 3.20 Beam End Rotation vs. Beam Tip Deflection Relations in E-W Direction

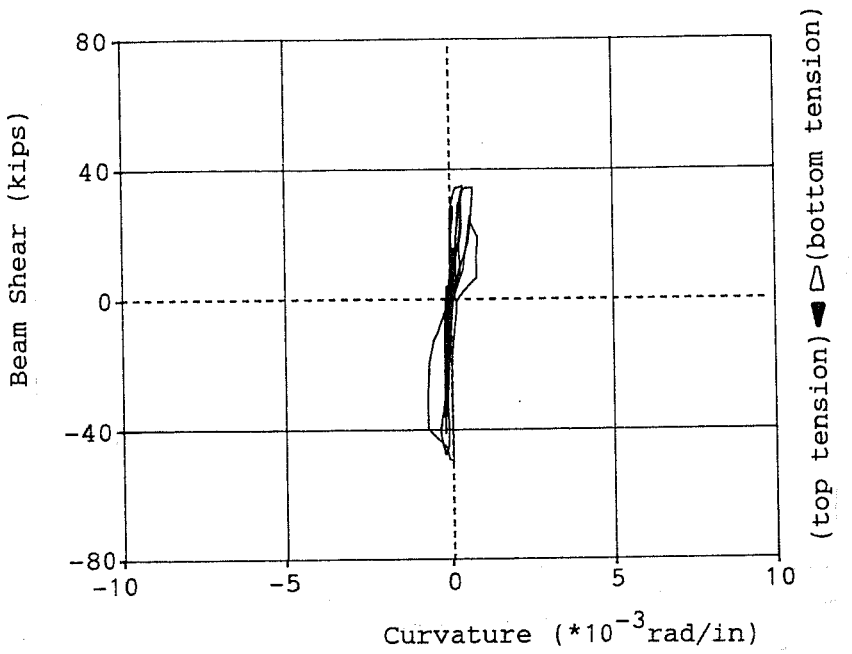

(a) East Beam End

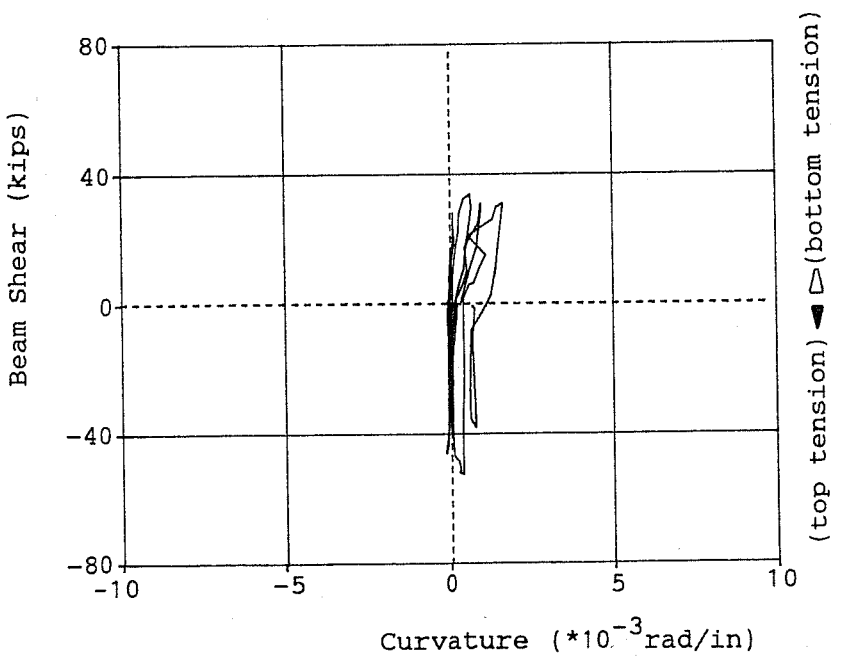

(b) West Beam End

Figure 3.21 Beam Shear-Averaged Curvature at Beam Ends for Specimen J1 (Digital Inclinometer Measurement)

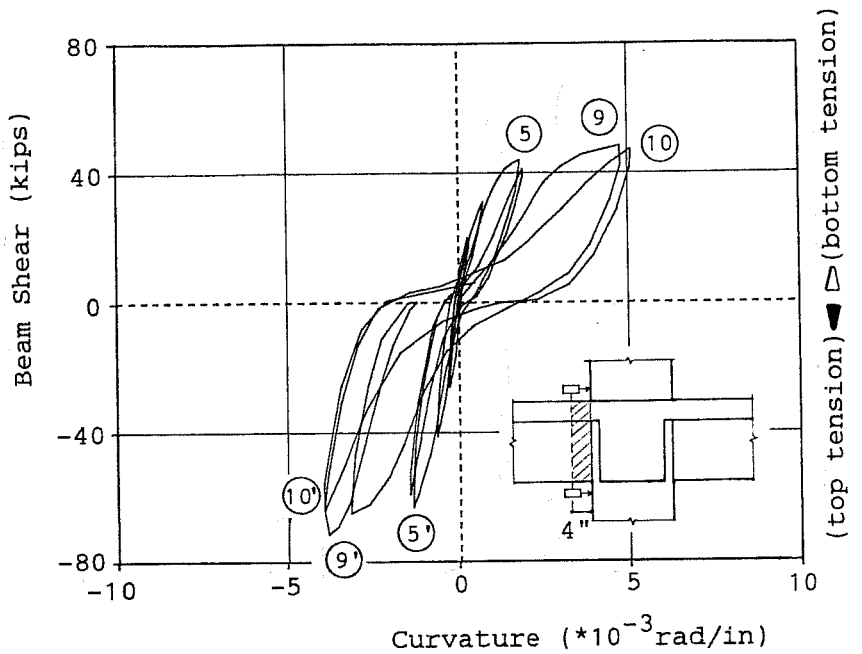

(a) Specimen J2 (East Beam)

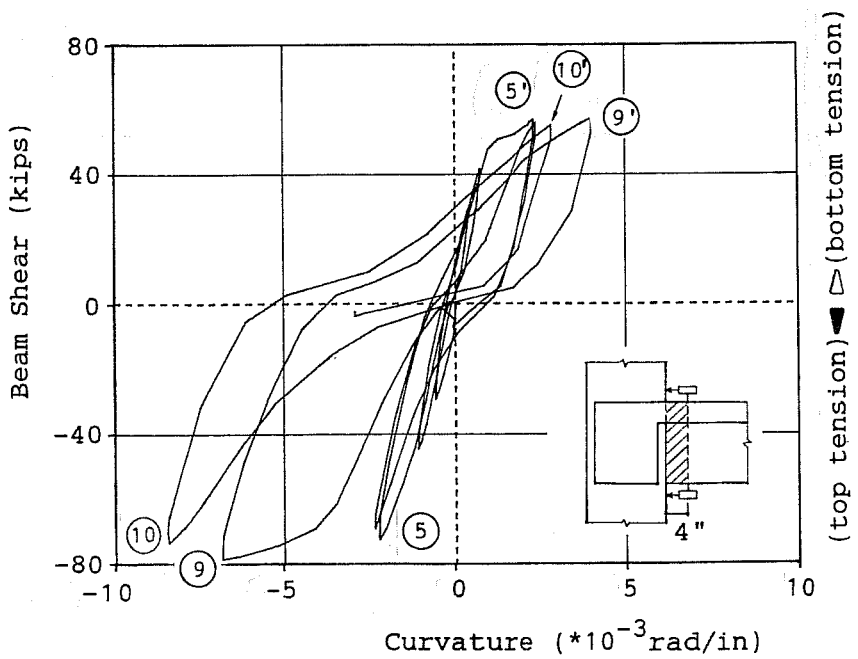

(b) Specimen J3 (West Beam)

Figure 3.22 Beam Shear-Averaged Curvature at Beam End (Region 1) during Unidirectional Loading in E-W Direction

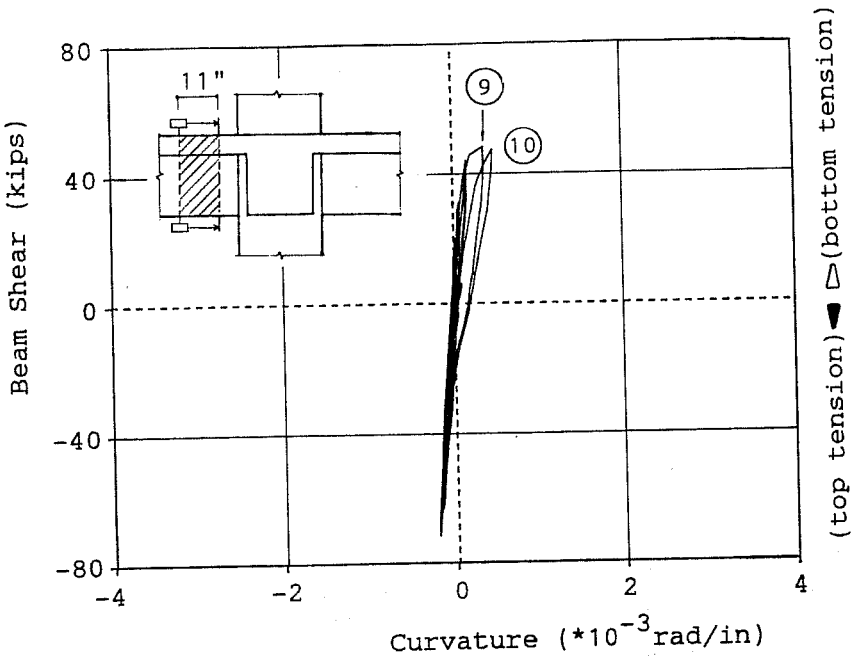

(a) Specimen J2 (East Beam)

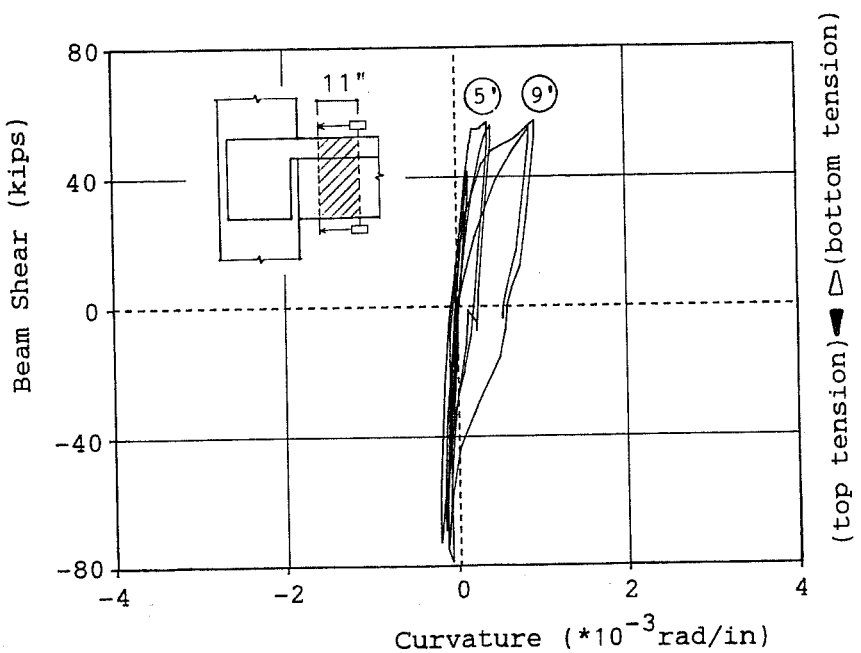

(b) Specimen J3 (West Beam)

Figure 3.23 Beam Shear-Averaged Curvature at Beam End (Region 2) during Unidirectional Loading in E-W Direction

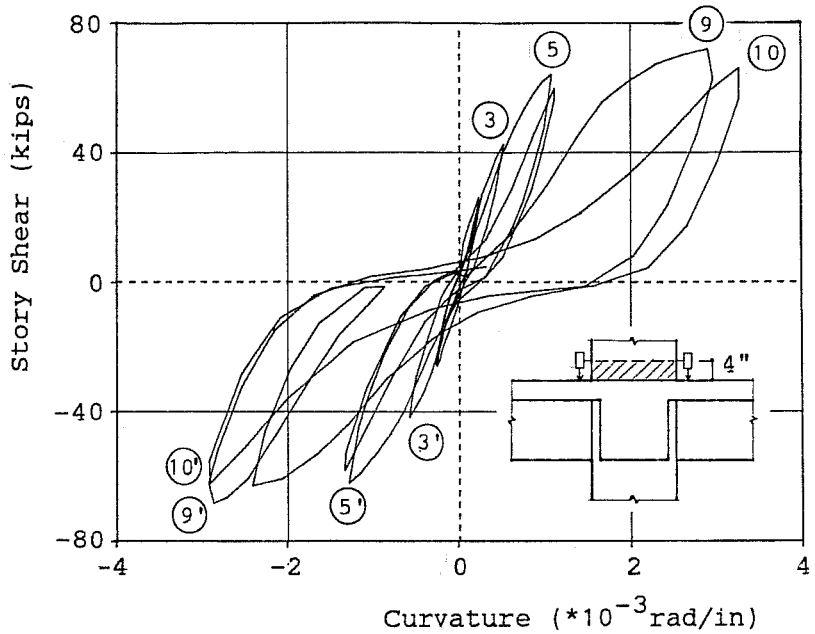

(a) Specimen J2

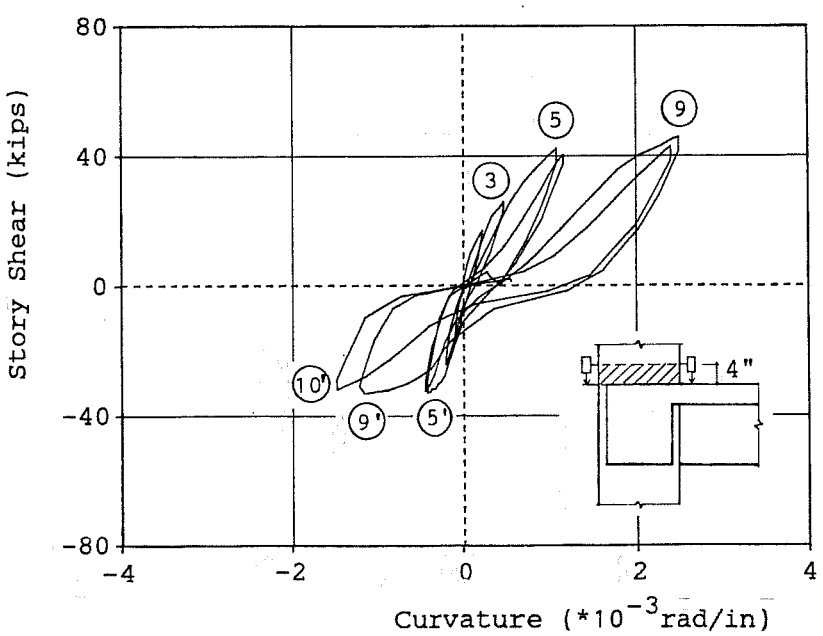

(b) Specimen J3

Figure 3.24 Story Shear-Averaged Curvature at Upper Column Base during Unidirectional Loading in E-W Direction

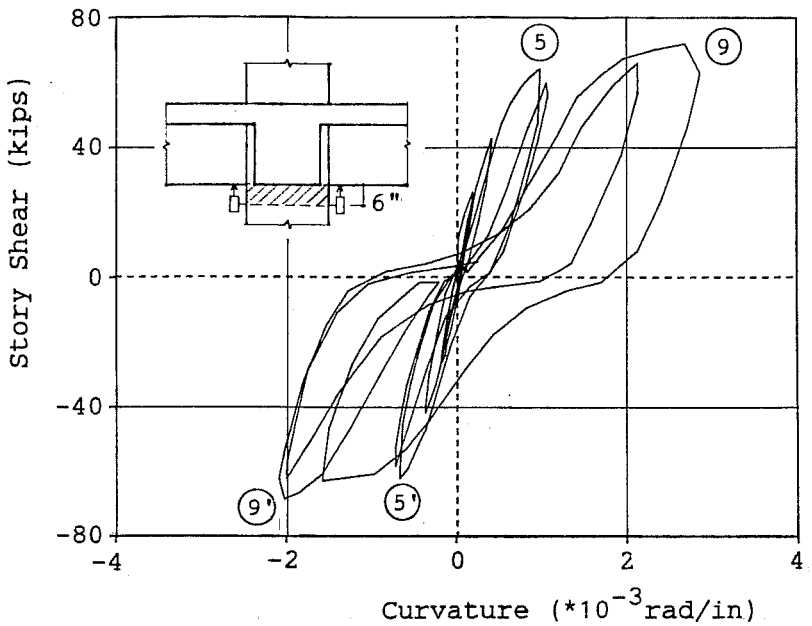

(a) Specimen J2

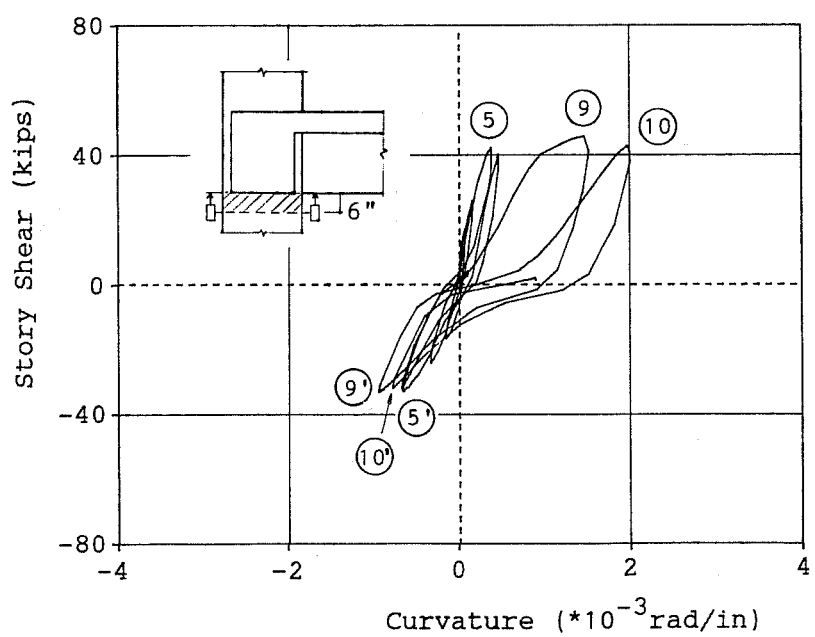

(b) Specimen J3

Figure 3.25 Story Shear-Averaged Curvature at Lower Column Capital during Unidirectional Loading in E-W Direction

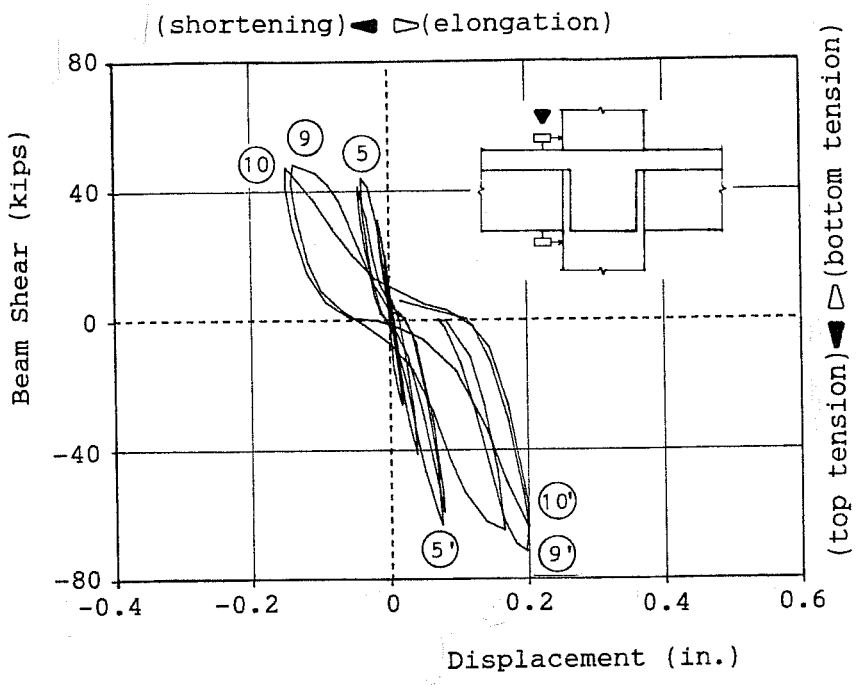

(a) Transducer on Top Face

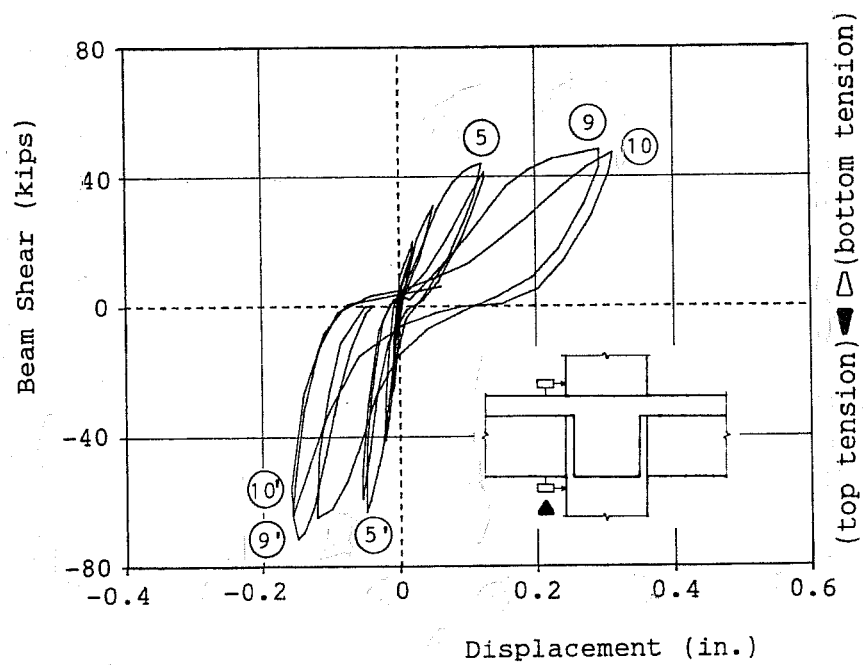

(b) Transducer on Bottom Face

Figure 3.26 Displacement Measurements at East Beam End in Unidirectional Loading (Specimen J2)

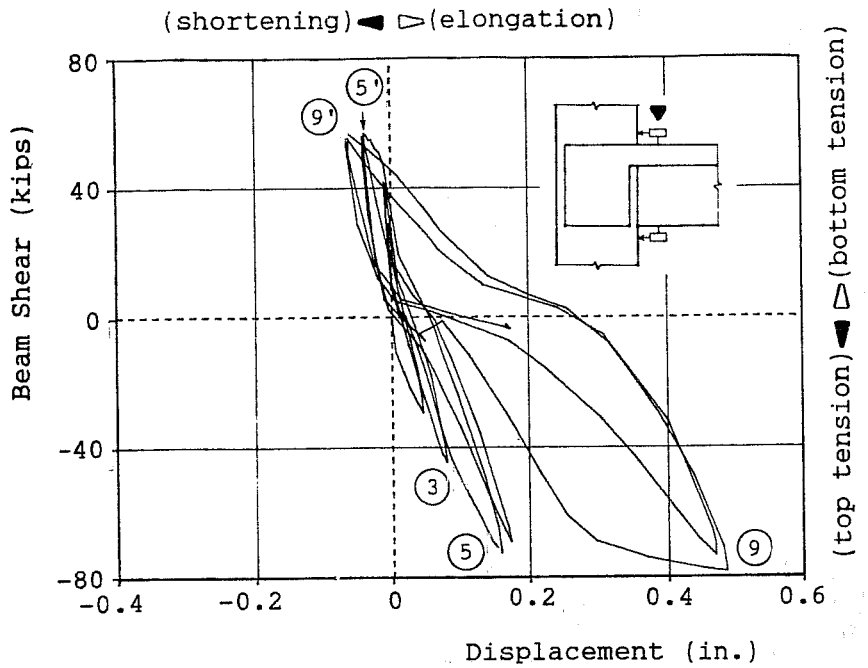

(a) Transducer on Top Face

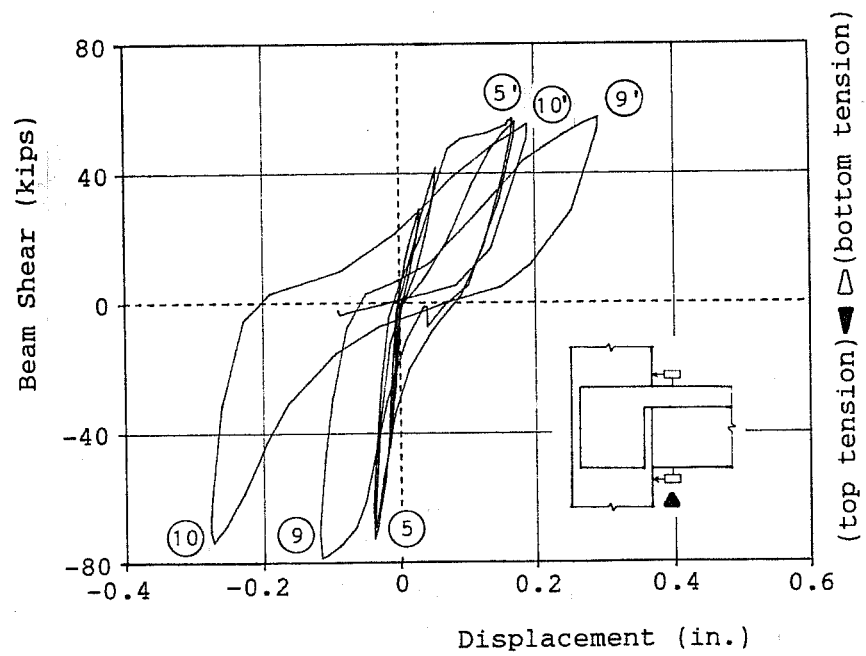

(b) Transducer on Bottom Face

Figure 3.27 Displacement Measurements at West Beam End in Unidirectional Loading (Specimen J3)

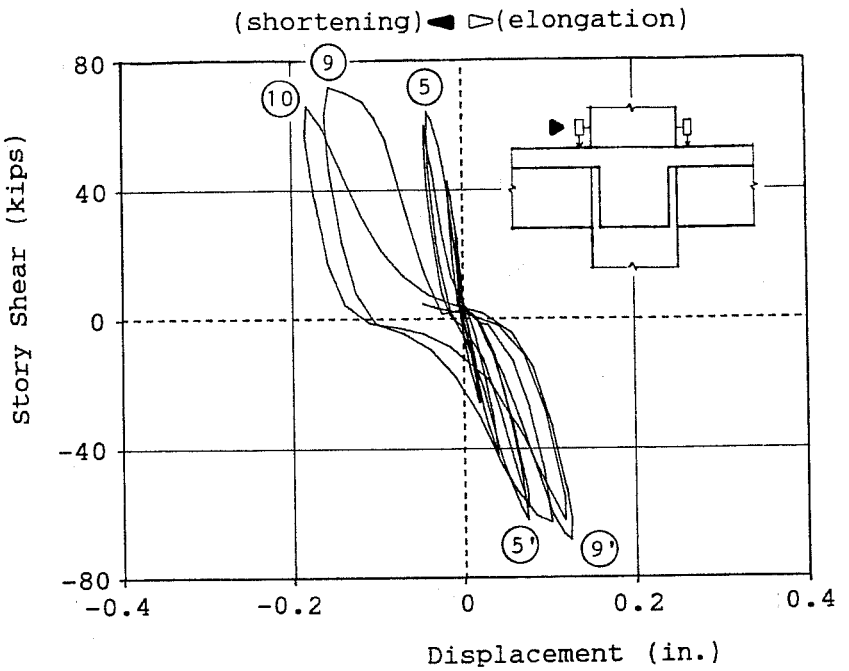

(a) Transducer on East Face

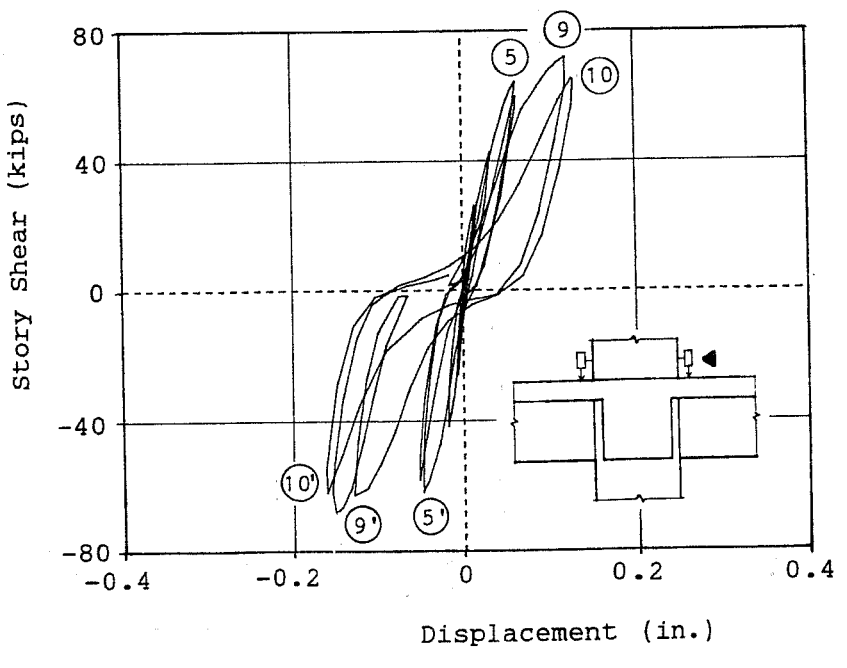

(b) Transducer on West Face

Figure 3.28 Displacement Measurements at Upper Column Base in Unidirectional Loading (Specimen J2)

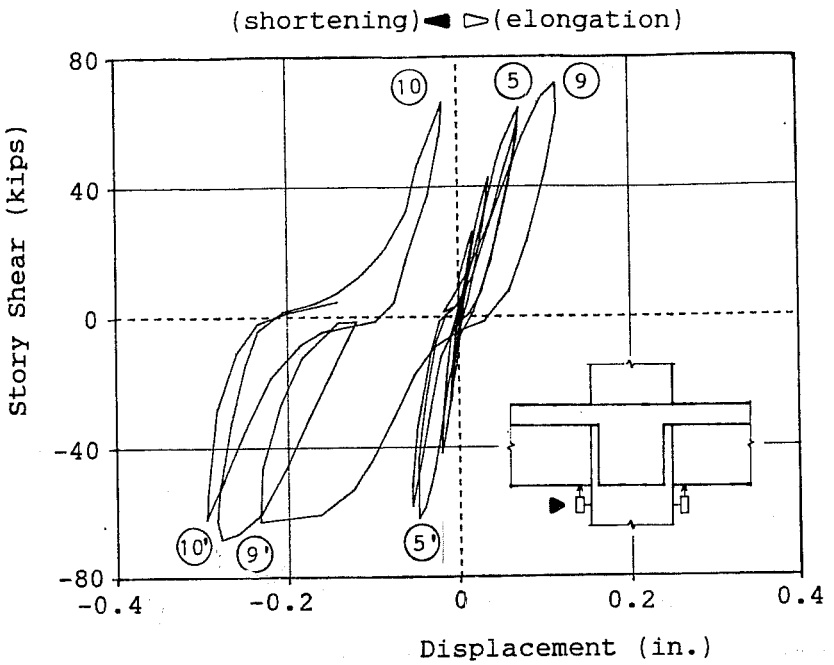

(a) Transducer on East Face

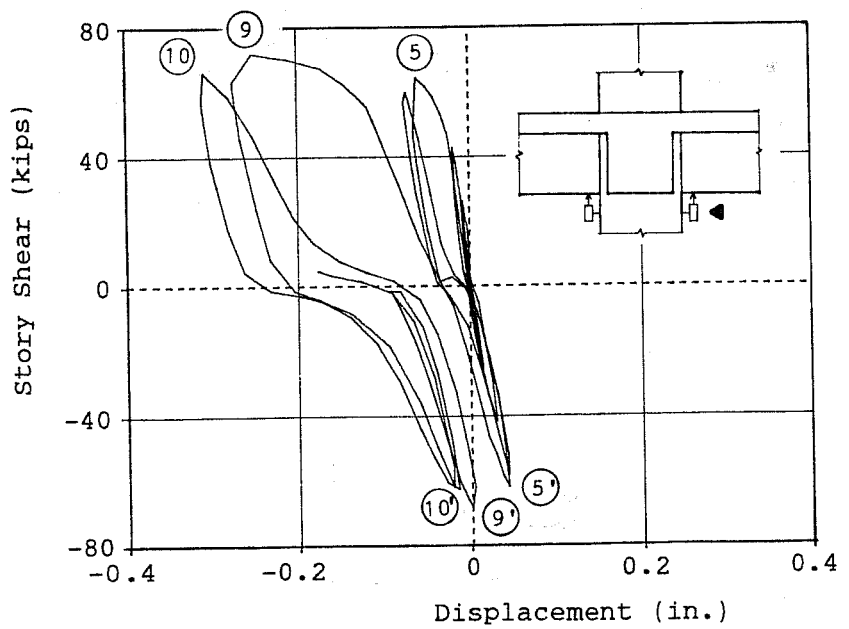

(b) Transducer on West Face

Figure 3.29 Displacement Measurements at Lower Column Capital in Unidirectional Loading (Specimen J2)

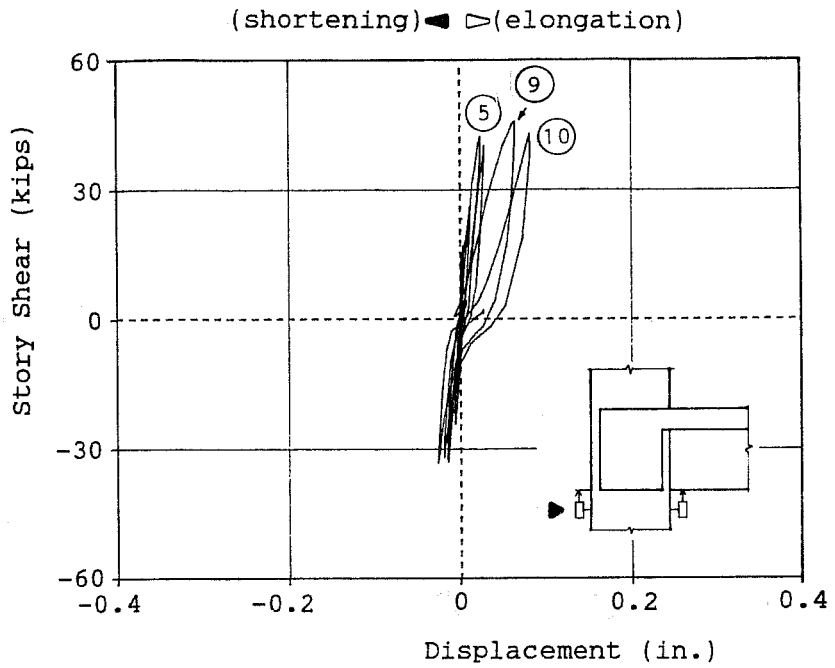

(a) Transducer on East Face

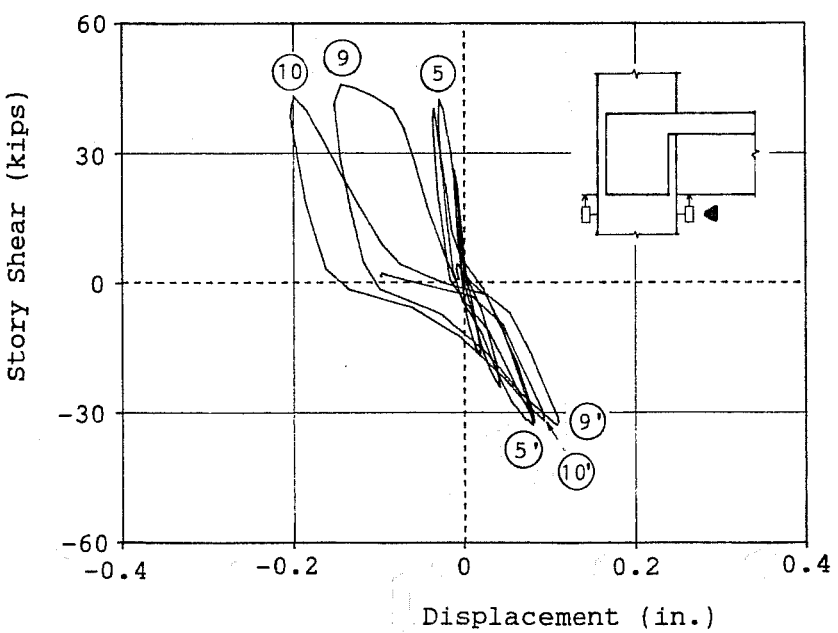

(b) Transducer on West Face

Figure 3.30 Displacement Measurements at Lower Column Capital in Unidirectional Loading (Specimen J3)

region remained elastic under negative bending. As shown in Figs. 3.24 and 3.25, the column and curvatures for J2 and J3 also showed considerable pinching in the story shear-curvature relations. The curvature in J2 were larger than those in J3 because J2 was subjected to higher story shears. Besides, the column stiffness relative to the beam stiffness was lower in J2 than in J3 because J2 was an interior joint with two beams and J3 was an exterior joint with one beam. Therefore, the beam in J3 had to undergo larger deflections than the beams in J2 at the same story drift. That is why the beam end curvatures in J3 were generally larger than those in J2 as shown previously in Figs. 3.22 and 3.23.

Figures 3.26 through 3.30 show the displacement measurements used to calculate curvatures at beam and column ends. It should be noted that the measurements slightly overestimated deformations at extreme fibers because transducers were mounted about two inches above or below the concrete surface. For specimen J2, as shown in Fig. 3.26, large elongation at the bottom of the beam corresponds with the large values of beam end curvature under positive bending. For Specimen J3, as shown in Fig. 3.27, the transducer at the top of the beam measured large elongation under negative bending in 4% drift cycles, probably due to pull-out deformation of the hooked top beam bars. The transducer at the bottom measured large shortening under negative bending as well as elongation under positive bending in cycles to 4% drift. The shortening reflects crushing of the bottom concrete. As shown in Figs. 3.28 through 3.30, the transducers for column and curvatures measured large shortening particularly at the top of the lower column in cycles to 4% drift. The shortening as caused by crushing and spalling of the column concrete. Thus, pinching in the story shear-column end curvature relations in 4% drift cycles is likely due to the crushing and spalling of concrete.

3.3.2 Strains in beam and column bars are plotted against story shear in Figs. 3.31 through 3.37. As shown in Figs. 3.31(a), 3.32(b) and 3.34(a), the top beam bars in J1 and J3 and the lower layer of beam bars in J2 exhibited tensile strains under upward loading because these bars had a thick top cover (see Appendix A) and participation of slab concrete possibly raised the neutral axis of the beam section above the bars. For J1, the same behavior was observed for slab bottom bars located at nearly the same level as the beam top bars (see Fig. 3.45 in Section 3.4). As described in Section 3.3, large joint distortion occurred in J1 during loading to 4% drift because of joint shear failure. The large distortion was likely to kink (produce high local distortions) the beam bars and increase the tensile strains. In the top beam bars in J2 shown in Fig. 3.32(a), tensile strains under downward loading turned into compression under upward loading during cycles up to 2% drift. In cycles to 4% drift, large tensile strains under downward loading decreased with unloading but resulted in residual tensile strains under upward loading. The results indicate good bond along the top bars.

As shown in Figs. 3.31(b) and 3.33, the bottom bars in J1 and J2 exhibited similar behavior. Tensile strains under upward loading turned into compression under downward loading in only a few initial cycles. Although the tensile strains under upward loading decreased with unloading in larger drift cycles. The strains increased again after the loading direction was reversed and exhibited small loops under downward loading in the story shear-strain relations. It seems that the increases in the tensile strains under downward loading were caused mainly by redistribution of compressive stresses from the bottom bars into the bottom concrete and were enhanced by bond deterioration which probably occurred at the maximum drift levels. In the bottom bars in J3 shown

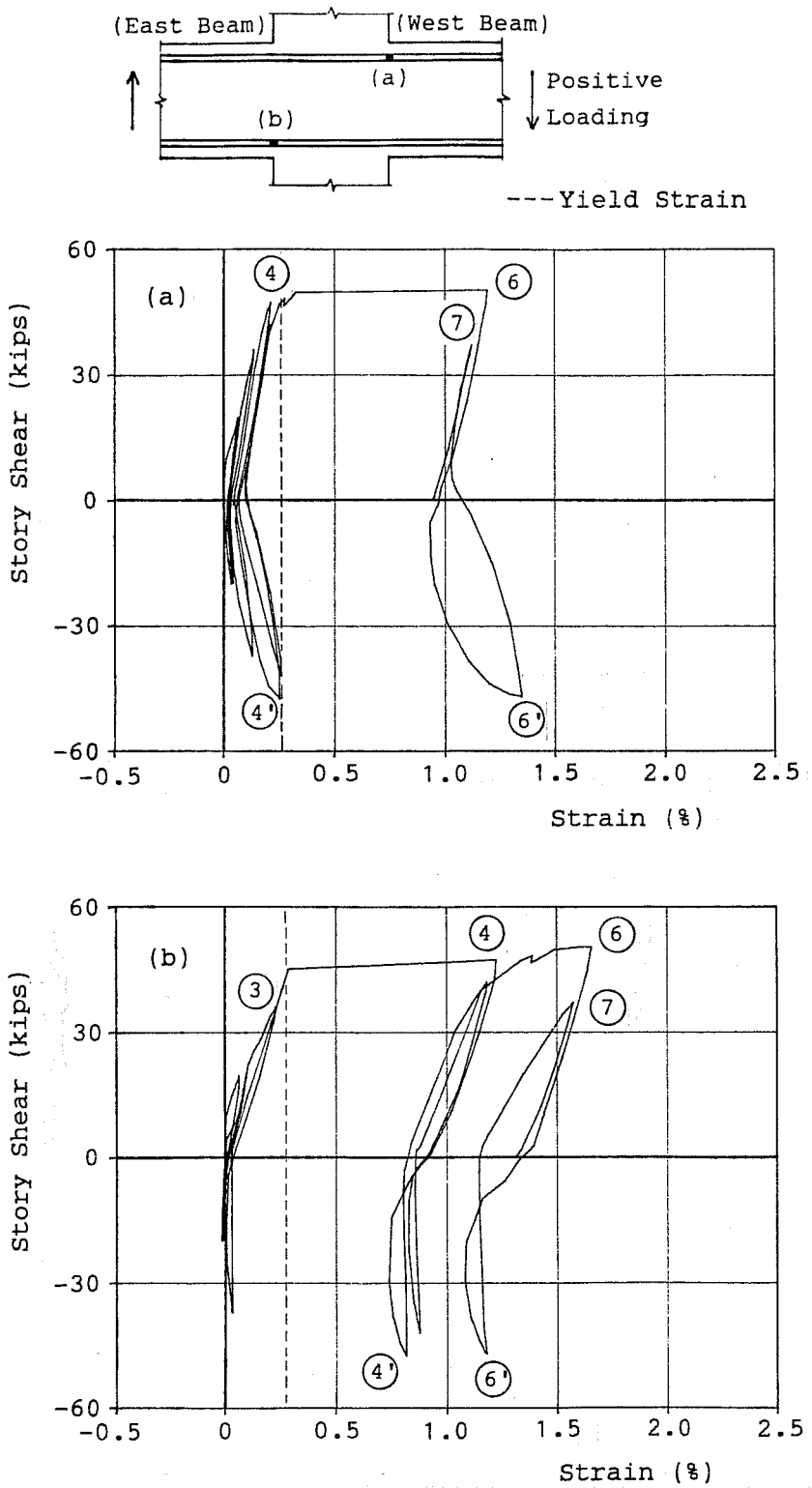

Figure 3.31 Strain Measurements on Beam Bars (Specimen J1)

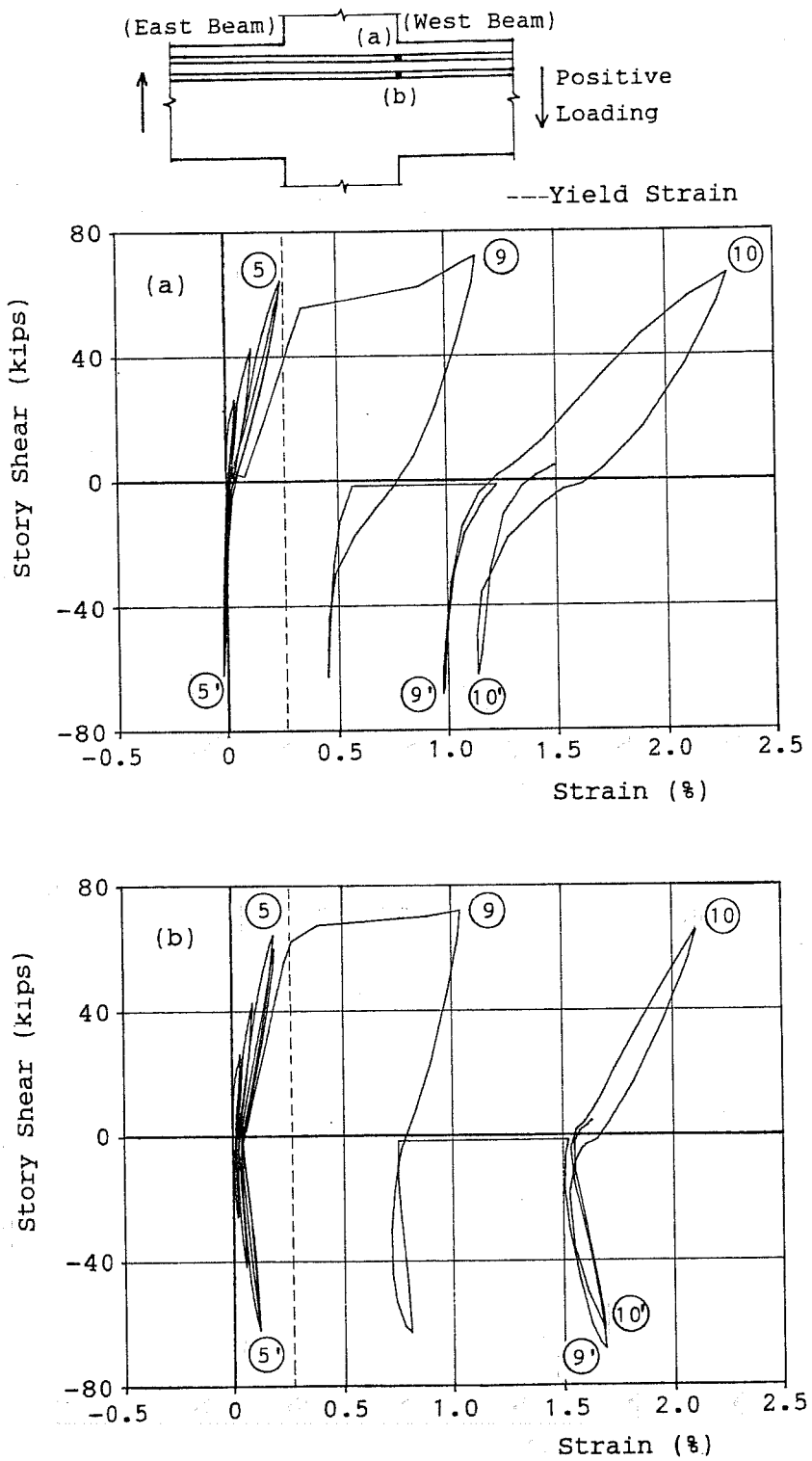

Figure 3.32 Strain Measurements on Beam Top Bars at Joint End in Unidirectional Loading (Specimen J2)

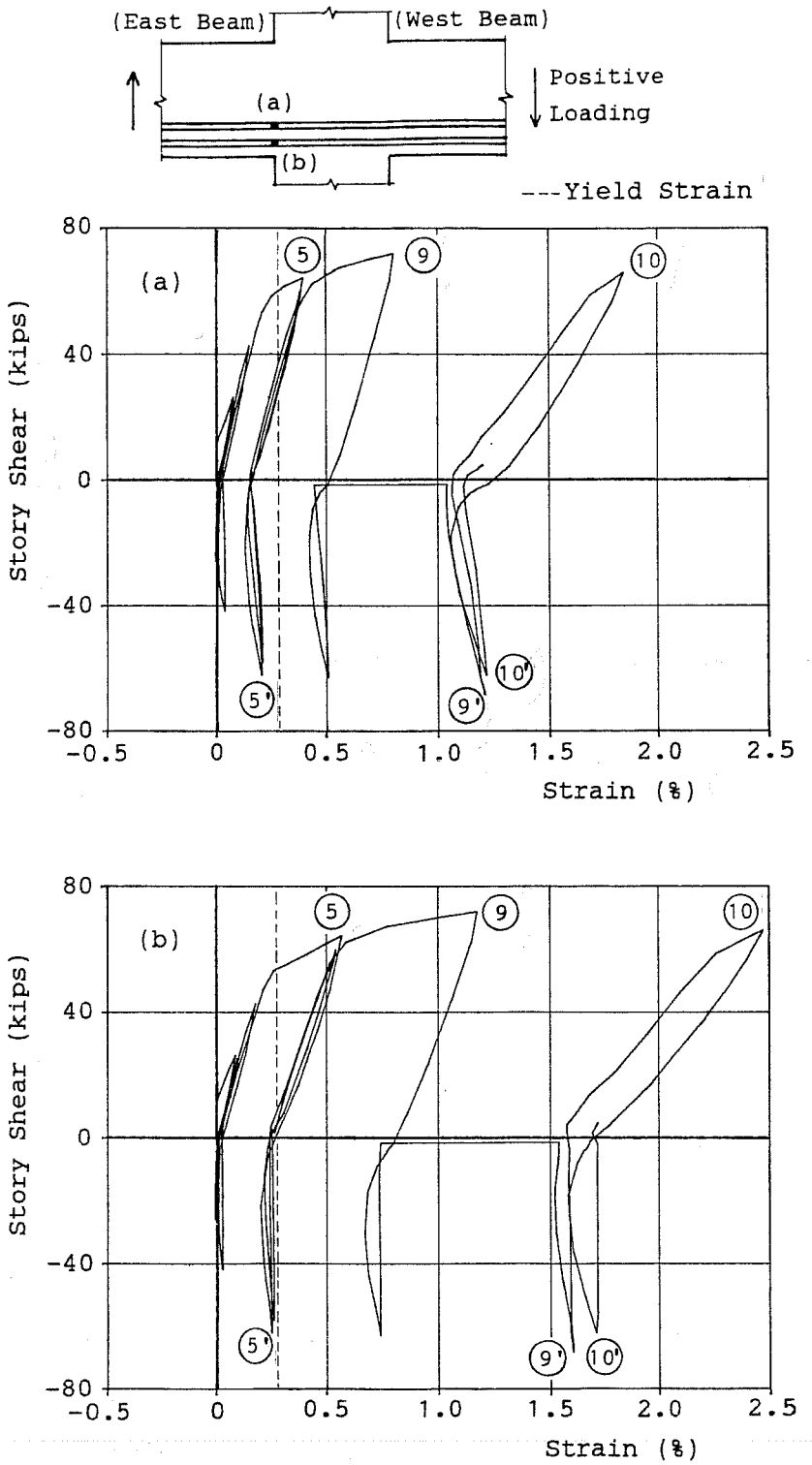

Figure 3.33 Strain Measurements on Beam Bottom Bars at Joint End in Unidirectional Loading (Specimen J2)

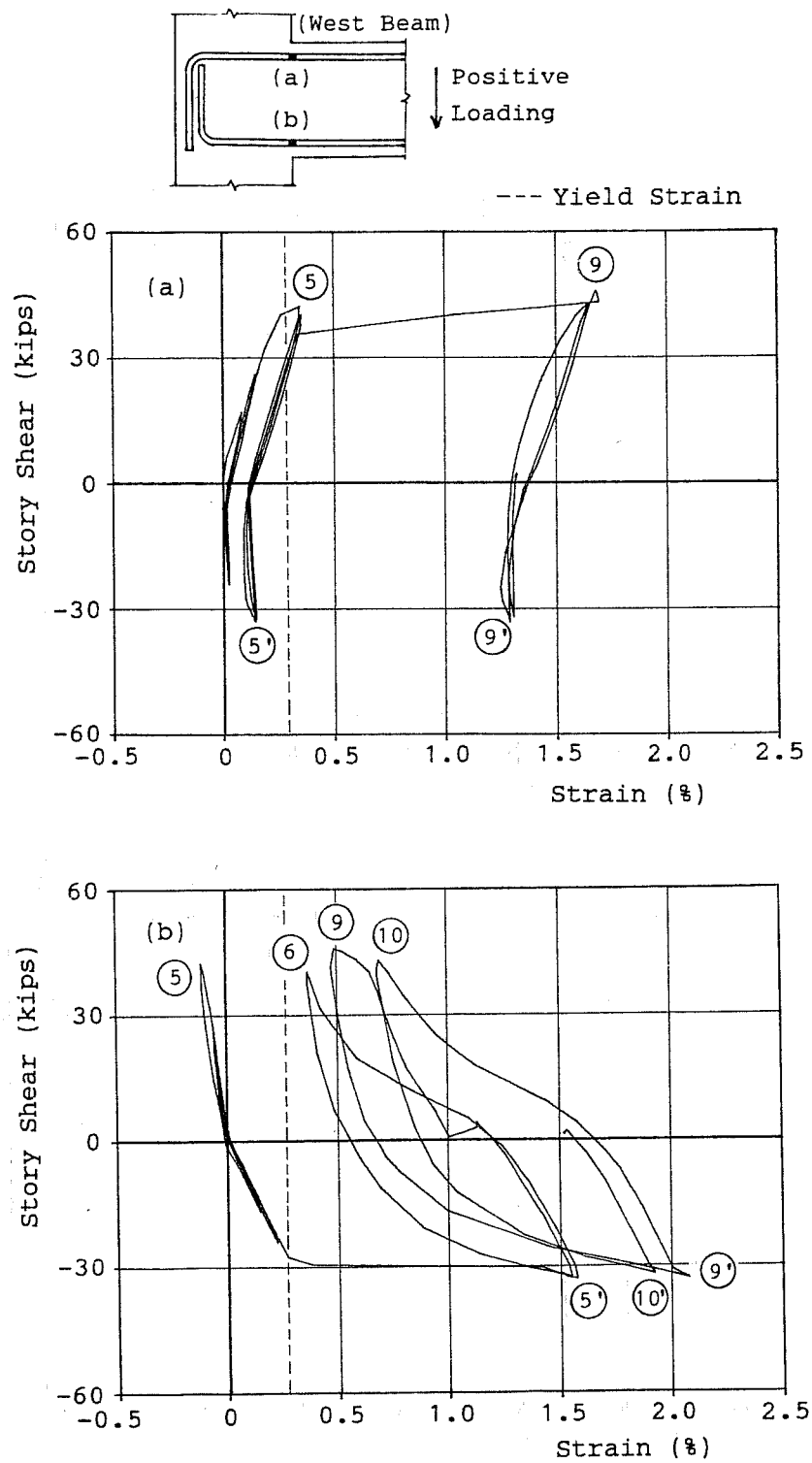

Figure 3.34 Strain Measurements on Beam Bars at Joint End in Unidirectional Loading (Specimen J3)

in Fig. 3.34(b), tensile strains under upward loading decreased with downward loading. Compared with J1 and J2, J3 had a thinner cover to the bottom beam bars and developed crushing of the bottom concrete at an earlier stage so that the bottom cover concrete was less effective in redistributing compressive stresses. In addition, the bottom bars were provided with good bond by hooked bar anchorages.

As seen in Figs. 3.35 through 3.37(a), column bars in the three specimens developed tensile strains in both loading directions and exhibited saddle-shaped hysteresis in the story shear-strain relations. The saddle shaped hysteresis is likely due to joint shear because strains measured 10 in. below the beam bottom in J3 exhibited normal tension-to-compression hysteresis as shown in Fig. 3.37(b).

The diagonal compressive strut must have formed in the joint to resist shear forces. Forces induced in the strut were balanced by horizontal and vertical joint shears. The vertical component of the strut force was geometrically related to the horizontal component which was in equilibrium with the horizontal joint shear, depending on dimensions of the joint. On the other hand, vertical joint shear was also geometrically related to horizontal joint shear in terms of bending moments about the joint, depending on overall specimen dimensions of the specimen. Therefore, force equilibrium conditions in the joint were influenced by the geometrical relationships between the joint dimensions and overall dimensions. When the vertical component of the strut force is greater than the vertical joint shear determined from a bending moment diagram, an additional force is needed. If the column is subjected to axial load, the load acts as the additional force to reduce the difference in the vertical forces. If not, the difference produces tension in the compressive reinforcement. As a result, the column bars exhibited tensile strains under loading which was expected to produce compressive strains.

3.3.3 Stress distributions along beam bars are shown in Figs. 3.38 through 3.40. The top bars in J1 and the lower layer of bars in J2 exhibited nearly uniform tensile stresses across the joint, indicating low bond stresses. The bars were in tension at both ends of the joint as discussed previously. However, tensile stresses decreased rapidly along the top bars in J2. Yielding of the outer layer of top bars at one end of the joint penetrated into the joint region toward the other end and increased bond stresses over a reduced length of bar as drift angle increased.

At 0.4% drift level, the bottom bars in J1 and J2 showed distributions in which tensile stresses at one end of the joint decreased along the bars and turned into compression at the other end. Although the bottom bars developed tensile stresses within the entire joint depth at 1 to 2% drift levels, large tensile forces at the top of the beam imposed compressive stresses on the bottom bars at 4% drift levels.

In J3, tensile stresses were distributed along lead embedments of the hooked top and bottom bars. The tensile stresses increased with drift angle and reached yield at the start of the bend in cycles to 2 to 4% drift. Anchorage of the bars was mainly provided by the hooks at large drift levels.

3.3.4 Average bond stress were calculated from measured bar stresses and maximum values are shown in Table 3.2. The table also includes calculated bond index values[7] and design bond stress values[4]. The bond index is an average bond stress over the joint depth based on the assumption that a bars has developed tensile yielding at one end of the joint and compressive yielding

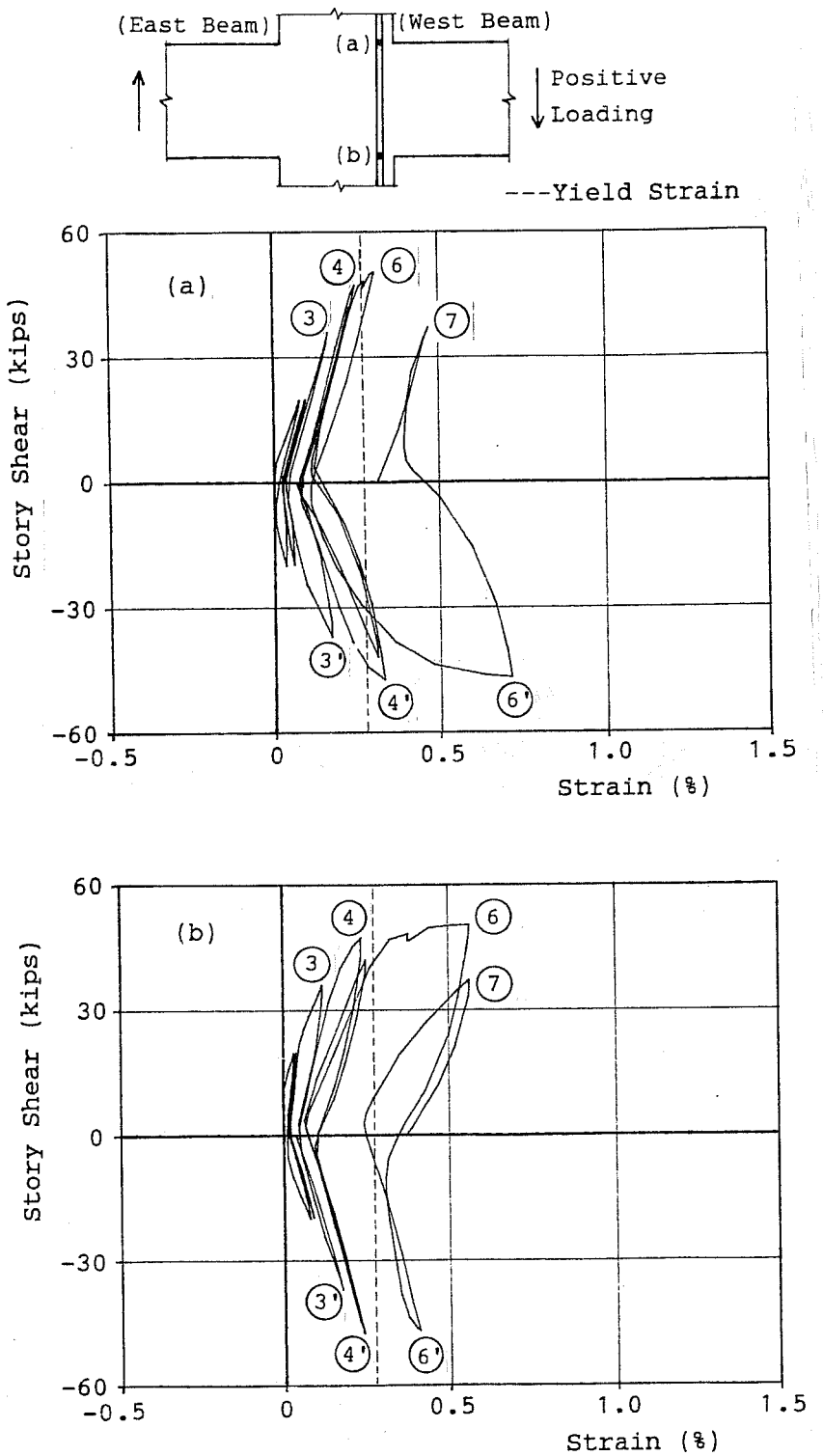

Figure 3.35 Strain Measurements on Column Bar (Specimen J1)

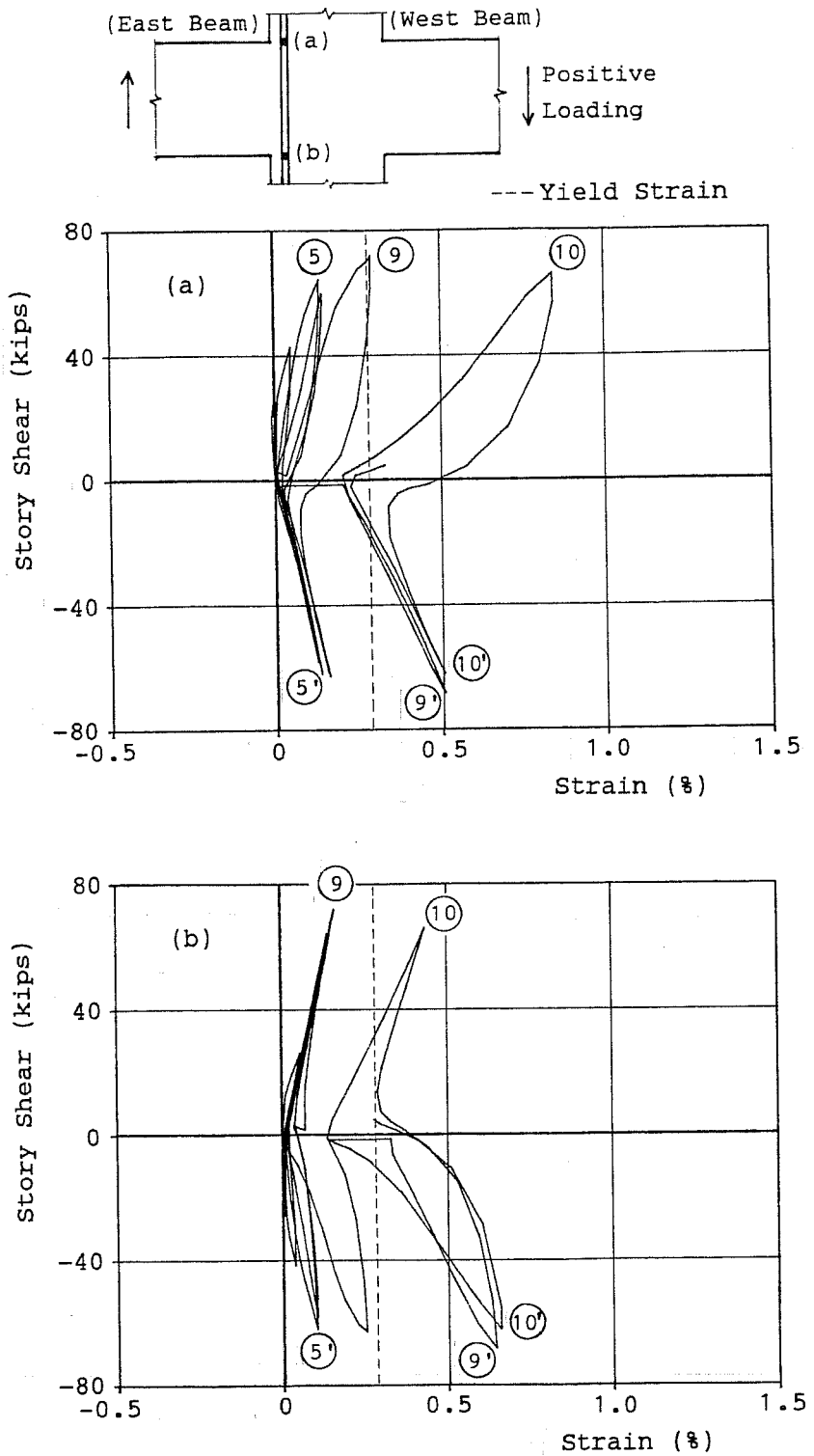

Figure 3.36 Strain Measurements on Column Bar at Joint End in Unidirectional Loading (Specimen J2)

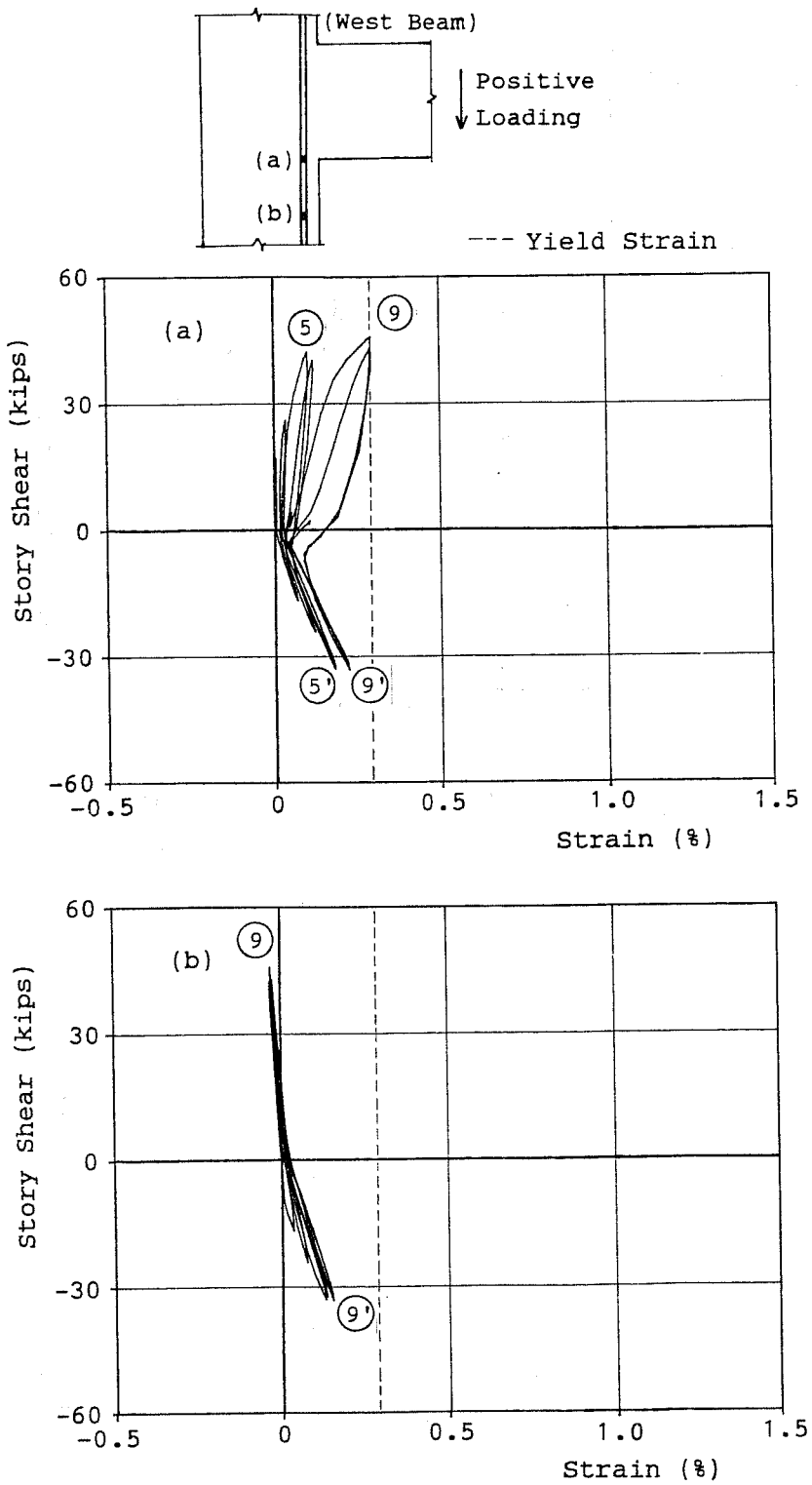

Figure 3.37 Strain Measurements on Column Bar at Joint End in Unidirectional Loading (Specimen J3)

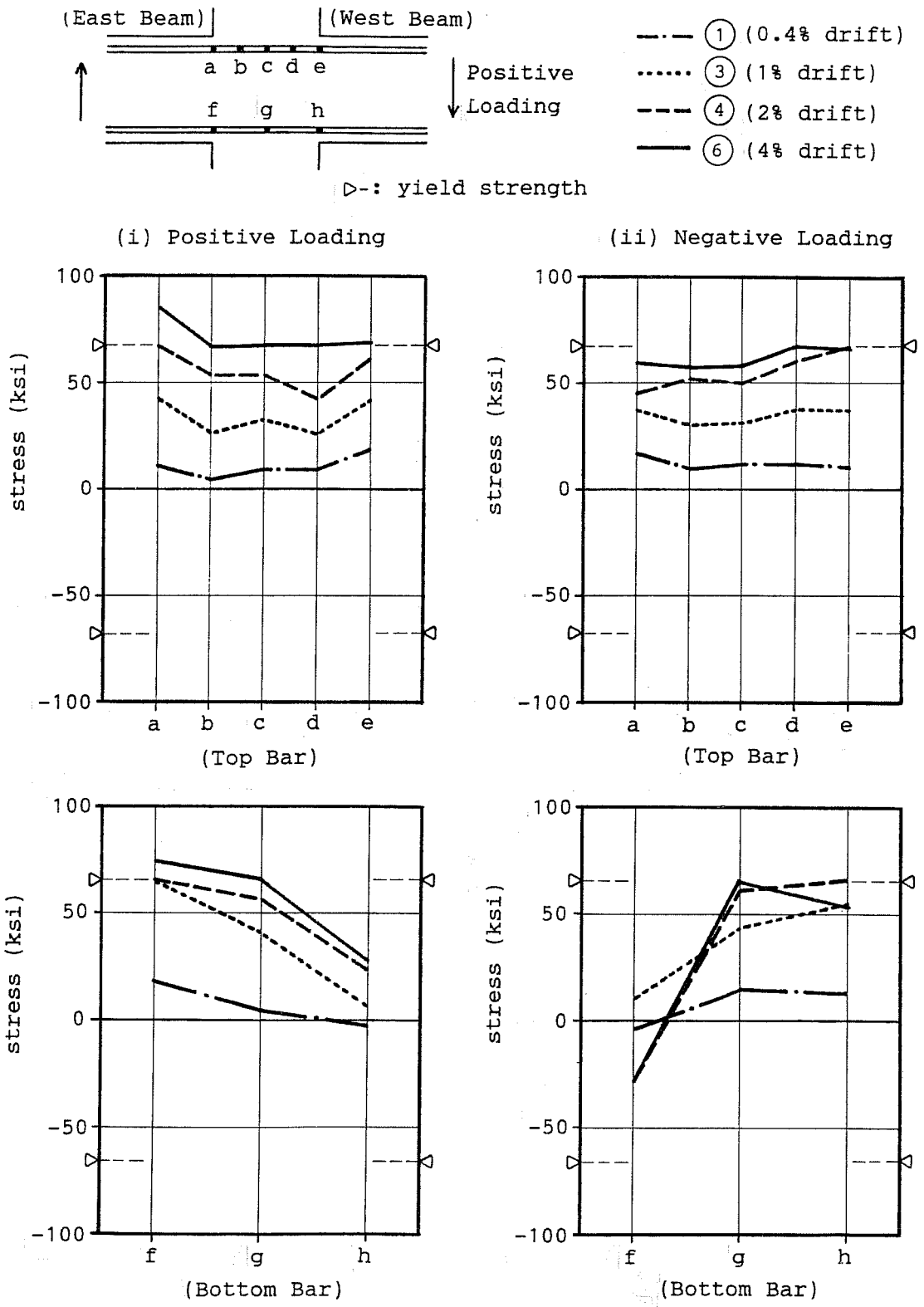

Figure 3.38 Stress Distribution Along Beam Bars (Specimen J1)

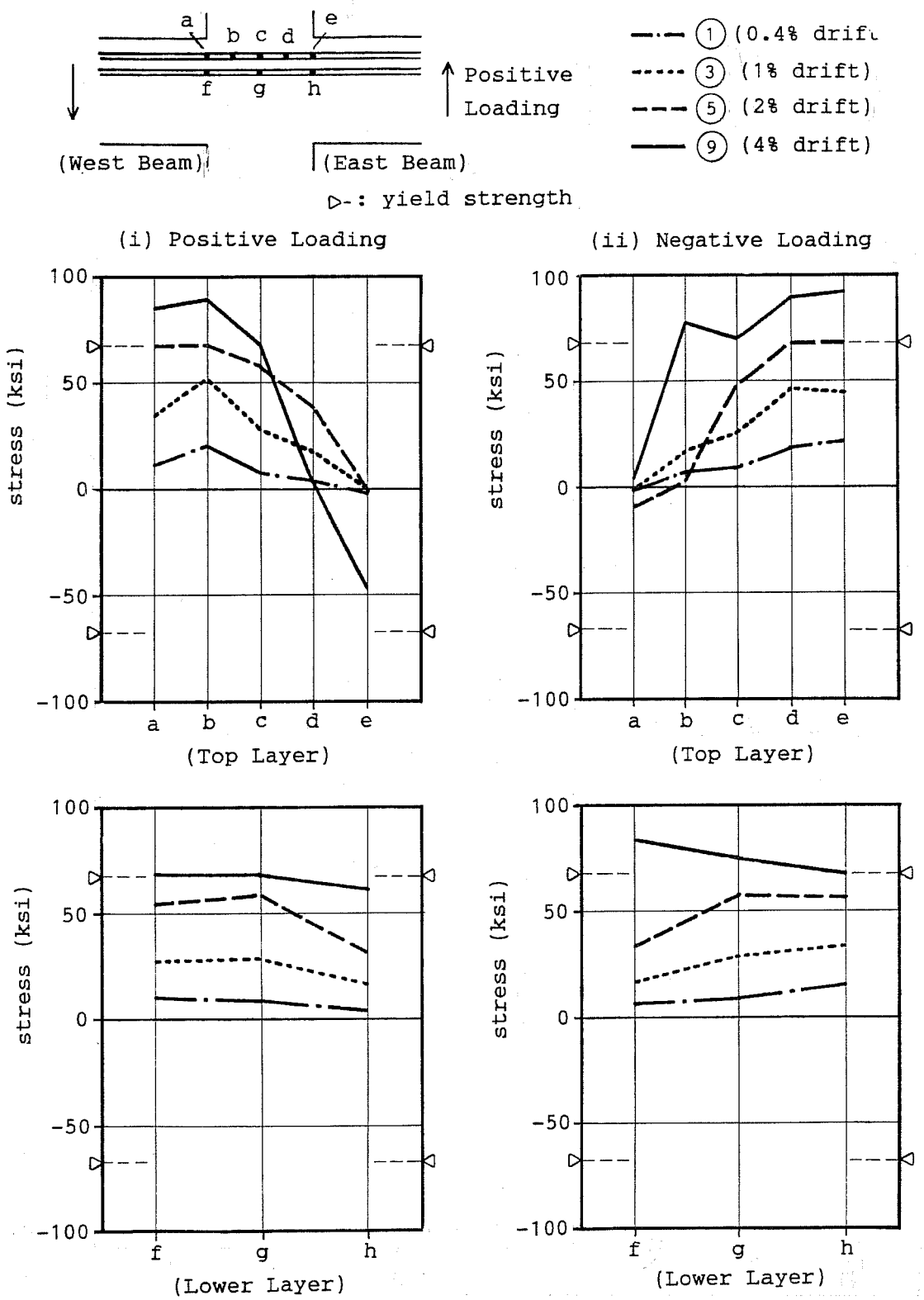

Figure 3.39(a) Stress Distribution Along Beam Top Bars (Specimen J2)

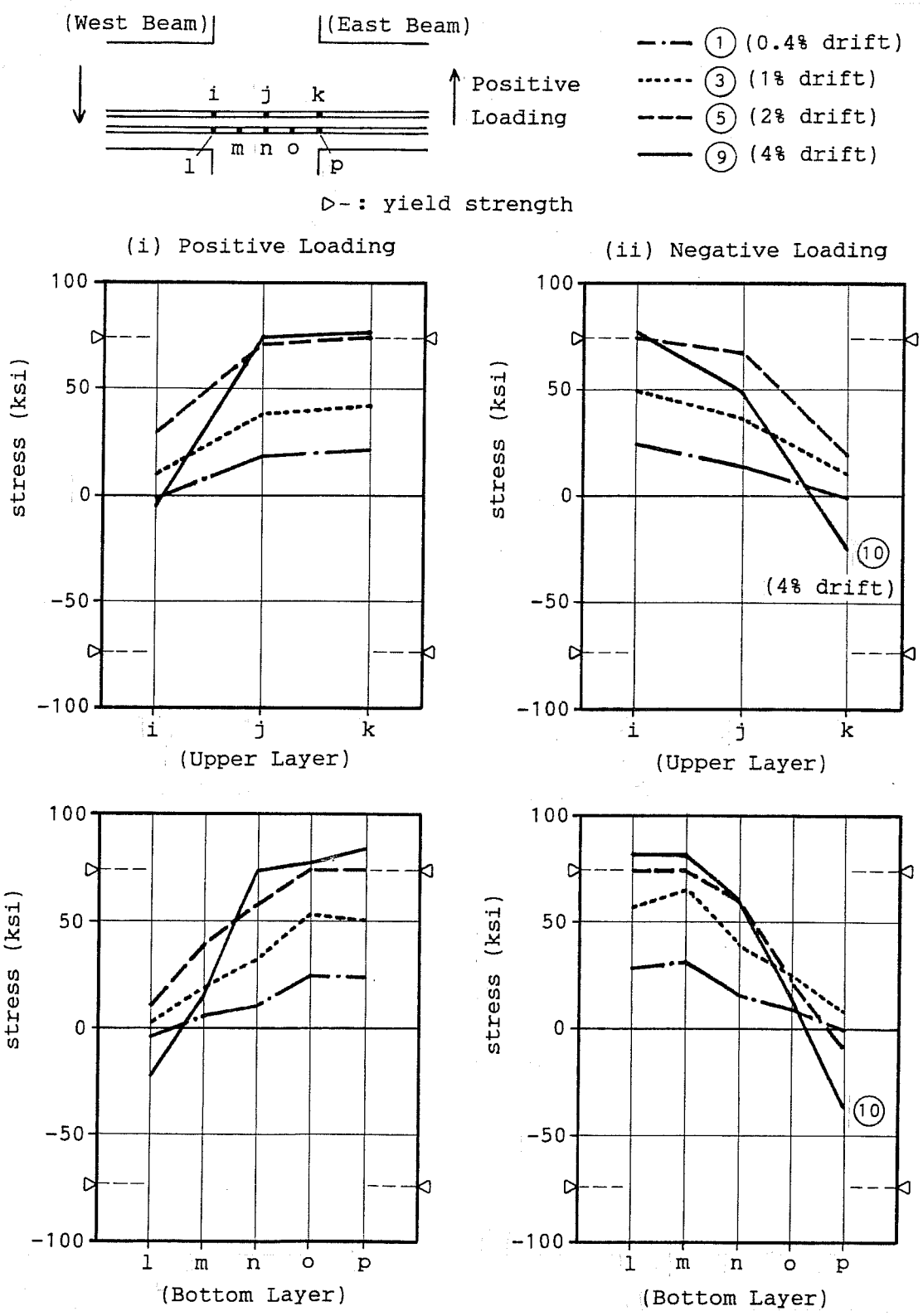

Figure 3.39(b) Stress Distribution Along Beam Bottom Bars (Specimen J2)

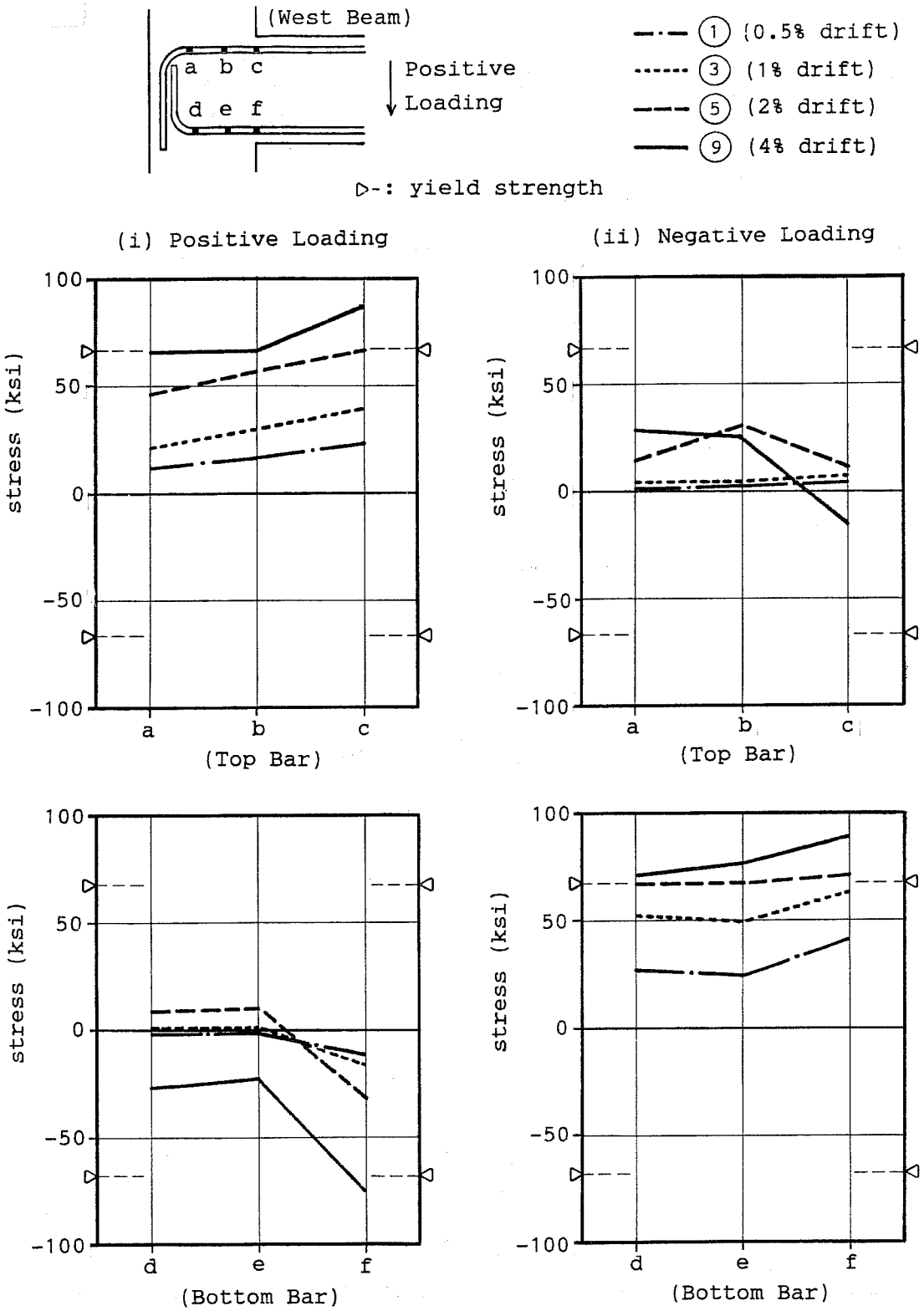

Figure 3.40 Stress Distribution Along Beam Bars (Specimen J3)

Table 3.2 Maximum Bond Stress in Comparison with Calculations for Straight Bar Development

Position		Bar Size	(1) Ratio h/d_B	Measurements		Calculated Bond Stress	
				(2) Bond Stress u_m (psi)	(3) LC (R[%])	(4) Bond Index u_i (psi)	(5) Design Bond u_d (psi)
Beam Top Bar	J1	#8	20	940	7 (+4.0)	1680	470
	J2	#8	20	2210	10 (+4.0)	1680	480
Beam Bottom Bar	J1	#7	23	1120	4 (-1.4)	1440	540
	J2	#6	27	1580	10 (+2.2)	1390	650
Column Bar Top	J1	#8	20	690	2 (+0.4)	1680	470
	J2	#9	18	2030	12 (-2.0EW) 12 (+4.2NS)	1880	430
	J3	#9	18	1590	12 (+4.1EW) 12 (-0.2NS)	1880	480

where:

(1) h = column depth or beam depth, d_B = bar diameter

(2) $u_m = (f_2 - f_1)\, d_B/4h$, $f_{1,2}$ = bar stress

(3) LC = loading cycle, R = drift angle at max. bond

(4) $u_i = f_y d_B/2h$, f_y = bar yield strength

(5) $u_d = \sqrt{f'_c}/0.04\pi d_B)$, f'_c = concrete strength

(bond stress based on 12.2.2 of ACI 318-83)

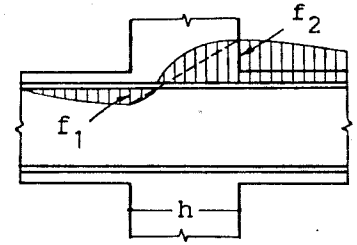

at the other end simultaneously. The design bond stress is an average bond stress over the basic development length of a bar specified by Section 12.2.2. of ACI 318. As shown in the table, J1 developed low bond stresses ranging from 40% to 80% of the bond index values. The response of J1 was dominated by joint shear distortion and the beam and column underwent small deflections which produced relatively low stresses in the reinforcement. In J1, the bond stress along beam bottom bars was higher than those along beam top bars and along column bars which were in tension at both ends of the joint. Specimen J2 exhibited higher bond stresses than the calculated bond index values. The maximum bond stresses occurred at 4% drift levels uniaxial loading for beam bars and biaxial loading for column bars. The bottom bars had a larger value of the column depth to bar diameter ratio but developed lower bond stresses than the top beam bars. Specimen J3 reached maximum bond stress along column bars in the last biaxial cycle to 4% drift. It should be noted that the design bond stress values were considerably lower than measured bond stresses in all cases.

Figure 3.41 shows average bond stresses along beam bars in J2 during uniaxial cycles to 4% drift. The bond stress along the top bar reached maximum values at loading peaks. The highest bond stress occurred at the positive peak of cycle 10 (LP231). The bond stress along the bottom bar was generally lower than that along the top bar and reached maximum values prior to loading peaks. The bond stress reached the highest value at LP228 and then decreased with loading to LP231.

Figure 3.42 shows beam bar stresses which caused maximum bond stresses in J2 during uniaxial cycles to 4% drift. Load points are given in the loading history which includes an extra path from LP205 to LP217 due to fracture of the pin connection in the east ram. The bar stresses in the top bar, particularly the compressive stress, increased with loading from LP192 to LP231, indicating good bond behavior. At LP228, the bottom bar developed the largest compressive stress which produced the highest bond stress. At this stage, most of the tensile force at the top was balanced by the compressive force in the bottom bars and the bottom concrete carried only a small amount of the compressive force, as seen from the section analysis of the west beam end. However, loading from LP228 to LP231 decreased the compressive stress in the bottom bar and thus lowered the bond stress. At LP231, the bottom concrete carried a large amount of the compressive force, probably because cracks in the bottom concrete closed at the beam end.

Figure 3.43 shows stress-strain relations for beam bars in J2 during uniaxial cycles to 4% drift. Strain gage locations are given in Fig. 3.42. At locations BT29 and BT35 in the top bar, both tensile and compressive stresses reached maximum values at loading peaks marked with an asterisk. At locations of BB45 and BB51 in the bottom bar, compressive stresses reached maximum values prior to peaks and then decreased with loading to the peaks, although tensile stresses reached maximum values at loading peaks. This behavior corresponds with the small loops under downward loading in story shear-strain relations (see Fig. 3.33).

Summarizing bond behavior in J2, the top beam bars showed no sign of bond deterioration but the bottom beam bars exhibited a loss of bond stress. The loss resulted from a decrease in compressive stresses and was probably caused by redistribution of compressive stresses from the bottom bars into the bottom concrete due to closing of cracks, even though some bond deterioration increased the loss. Stress redistribution is a more likely reason for the loss of compressive stress than bond deterioration because:

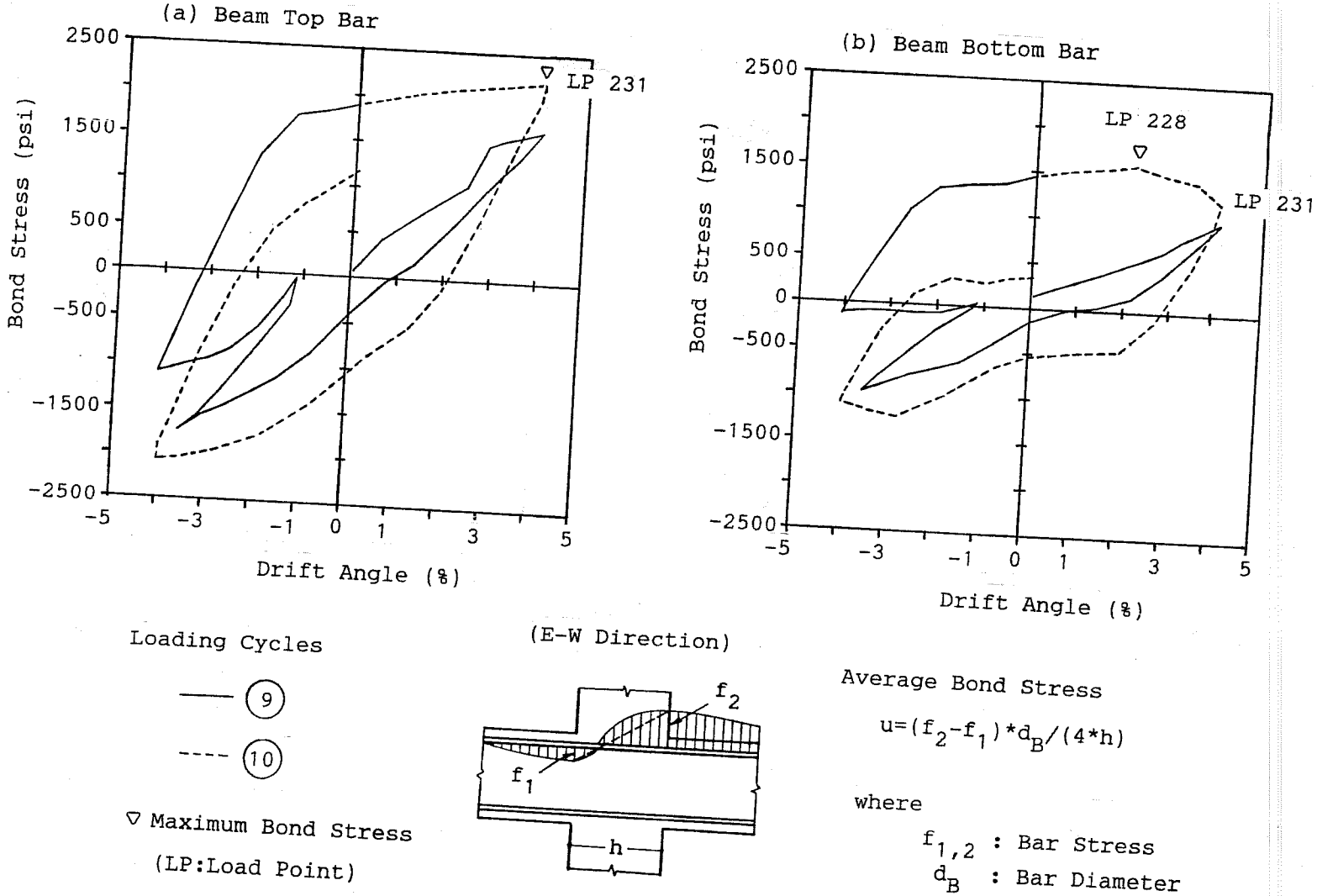

Figure 3.41 Average Bond Stress Along Beam Bars Within Joint in 4% Drift Unidirectional Loading (Specimen J2)

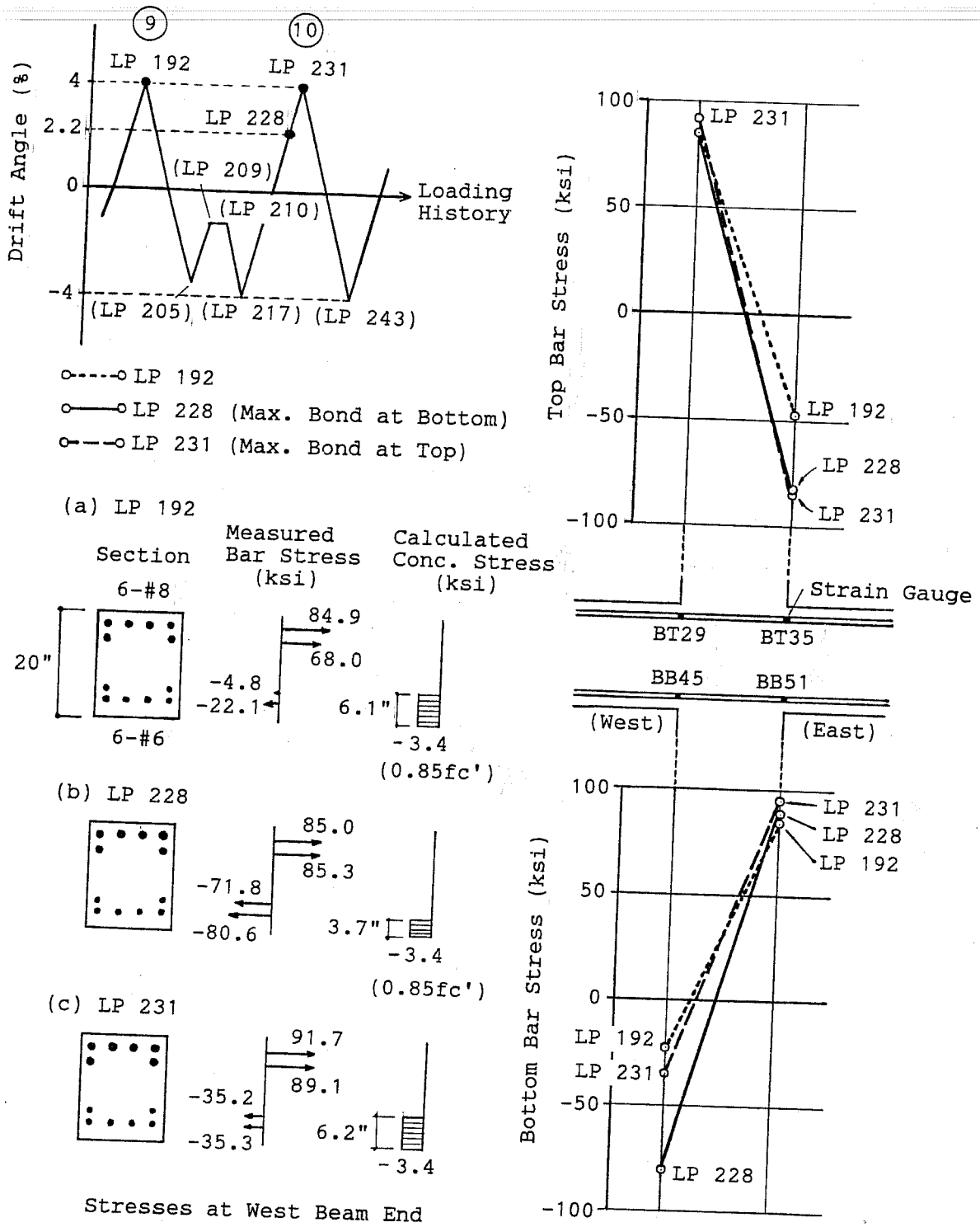

Figure 3.42 Beam Bar Stresses at Maximum Bond Within Joint in 4% Drift Unidirectional Loading (Specimen J2)

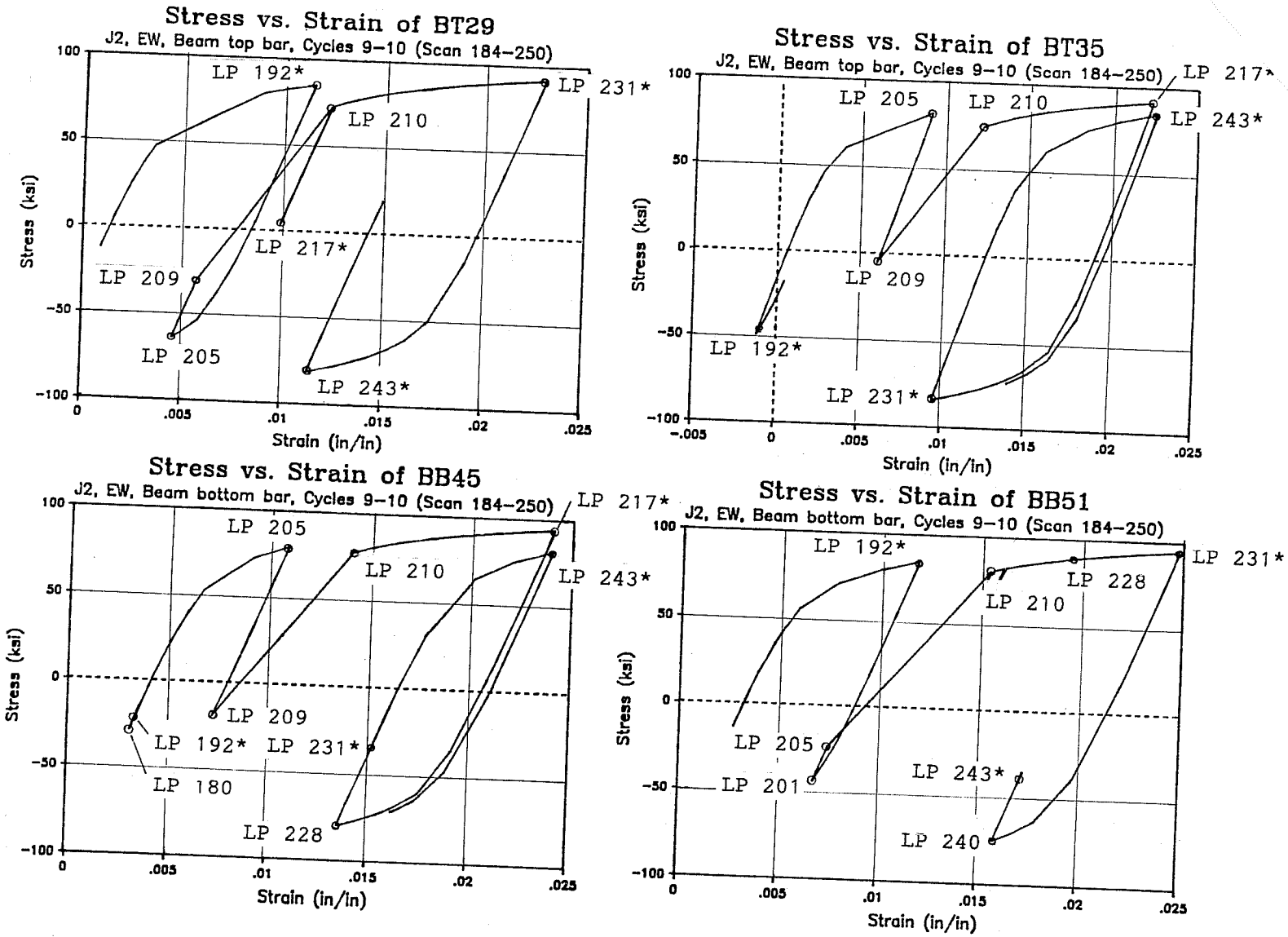

Figure 3.43 Stress-Strain Relations for Beam Bars at Joint End in 4% Drift Unidirectional Loading (Specimen J2)

(1) As shown in Fig. 3.33, the small loops in strain hysteresis observed for the bottom bars under downward loading occurred at an early stage of the test.

(2) The top bars (15 in. of concrete placed below the bar) with a larger diameter developed higher bond stresses than the bottom bars and showed no loss in the bond stress.

(3) The bottom concrete had to carry compressive forces to balance large tensile forces at the top because the beam section had 80% more reinforcement at the top than at the bottom and slab reinforcement participated with top beam reinforcement in generating tensile forces.

With regard to the bond behavior of hooked beam bars in J3, Table 3.3 shows maximum bar stresses measured at the column face in comparison with calculated strengths of hooked bar anchorages. The maximum bar stresses occurred in the uniaxial cycle to 4% drift and exceeded the calculated values using two different equations. However, anchorage distress occurred in the top beam bars with further loading as pointed out previously.

3.4 Effect of Floor Slab

3.4.1 Effect on initial stiffness was examined by comparing measured initial stiffness with calculated uncracked stiffness, as shown in Fig. 3.44. The initial stiffness of the specimen was defined as story shear divided by drift angle measured at the first load stage in cycle 1. The calculated uncracked stiffness was a function of the slab width considered to act with the beam. Among the specimens, J2 exhibited the highest initial stiffness because transverse beams in the NS direction restrained the floor slab. The measured initial stiffness for J2 corresponded with the calculated stiffness in which 80% of the entire slab width participated in beam stiffness. For J1, the measured initial stiffness was nearly equal to the calculated stiffness without a slab. The exterior specimen J3 exhibited the lowest stiffness because only one beam resisted the lateral force or displacement. The measured initial stiffness for J3 was lower than the calculated stiffness because the specimen was subjected to downward loading initially which produced flexural cracking in the slab at the first load stage.

3.4.2 Strains in slab reinforcement are plotted against story shear in Figs. 3.45 and 3.46 for Specimens J1 and J2, respectively. Top slab bars developed large tensile strains under downward loading and enhanced negative bending moment in the beam. Large plastic strains occurred in the top bars under downward loading to 4% drift. Bottom slab bars exhibited tensile strains under both downward and upward loadings. The neutral axis of the section was located above the bottom bars under upward loading.

Slab bar strains measured at loading peaks are shown in Figs. 3.47 through 3.49. In general, the strains increased with drift angle. Under uniaxial loading, strains in the slab bars parallel to the loading direction decreased with distance from the loaded beam, as seen in Fig. 3.47 for J1. On the contrary, strains in the slab bars perpendicular to the loading direction increased with distance from the transverse beam, as shown in Figs. 3.48 and 3.49. The strains along the face of the loaded beam reflect the local distortions produced by the concentrated load at the tip of the beam. In addition, tensile forces at the face of the transverse beam likely imposed in-plane bending moments about the column vertical axis on the slab and thus produced tensile stresses at the face

Table 3.3 Maximum Bar Stress at West Beam End in Comparison with Calculations for Hooked Bar Anchorage (Specimen J3)

Position	Measurements		Calculated Strength	
	(1) Bar Stress f_m(ksi)	(2) LC (R[%])	(3) Bar Stress f_{y1} (ksi)	(4) Bar Stress f_{y2} (ksi)
Top Bar	91.0	9 (+3.4)	75.2	69.3
Bottom Bar	89.4	9 (-4.0)	69.4	74.3

where:

(1) f_m = measured maximum beam bar stress at joint end

(2) LC = loading cycle, R = drift angle at max. stress

(3) $f_{y1} = 75\sqrt{f'_c}\ell_{dh}/d_B$ (ACI 352)

f'_c = concrete strength, d_B = bar diameter, ℓ_{dh}: see below

(4) $f_{y2} = \psi\sqrt{f'_c}[\frac{700(1-0.3d_B)+\ell_s}{0.04A_b}]$ (Marques-Jirsa Eq.)

A_b = bar area, $\psi = 1.4$, ℓ : See Below

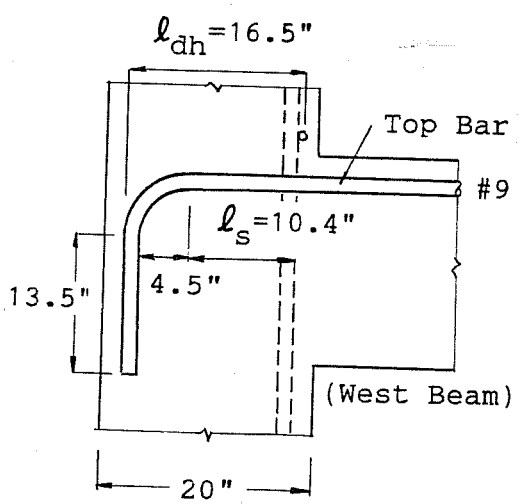

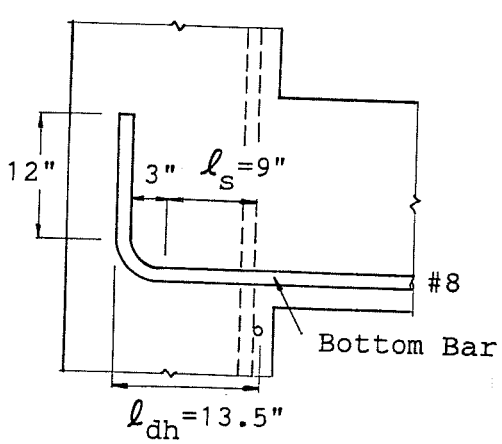

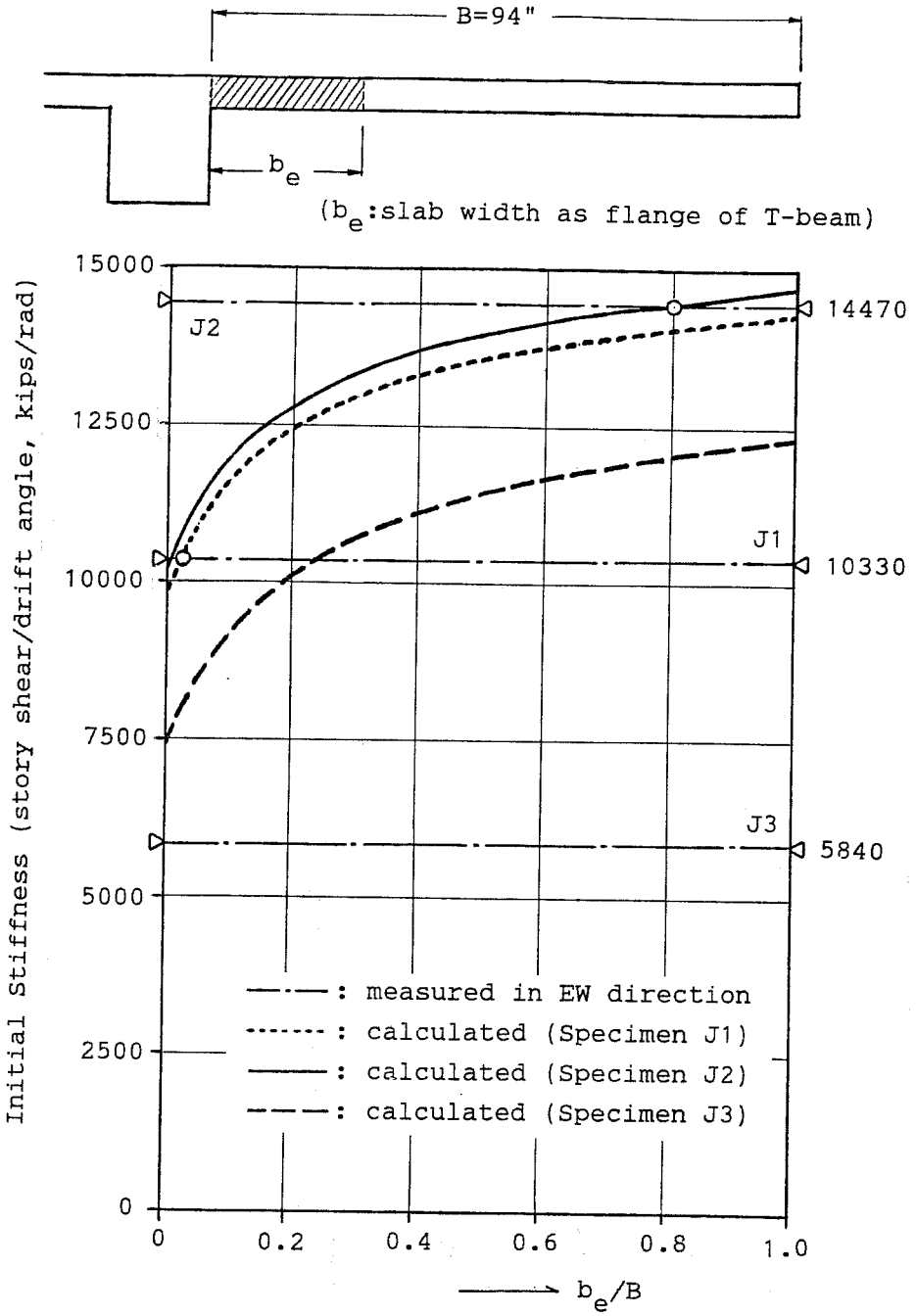

Figure 3.44 Measured Initial Stiffness and Calculated Uncracked Stiffness with Various Slab Widths (E-W Direction)

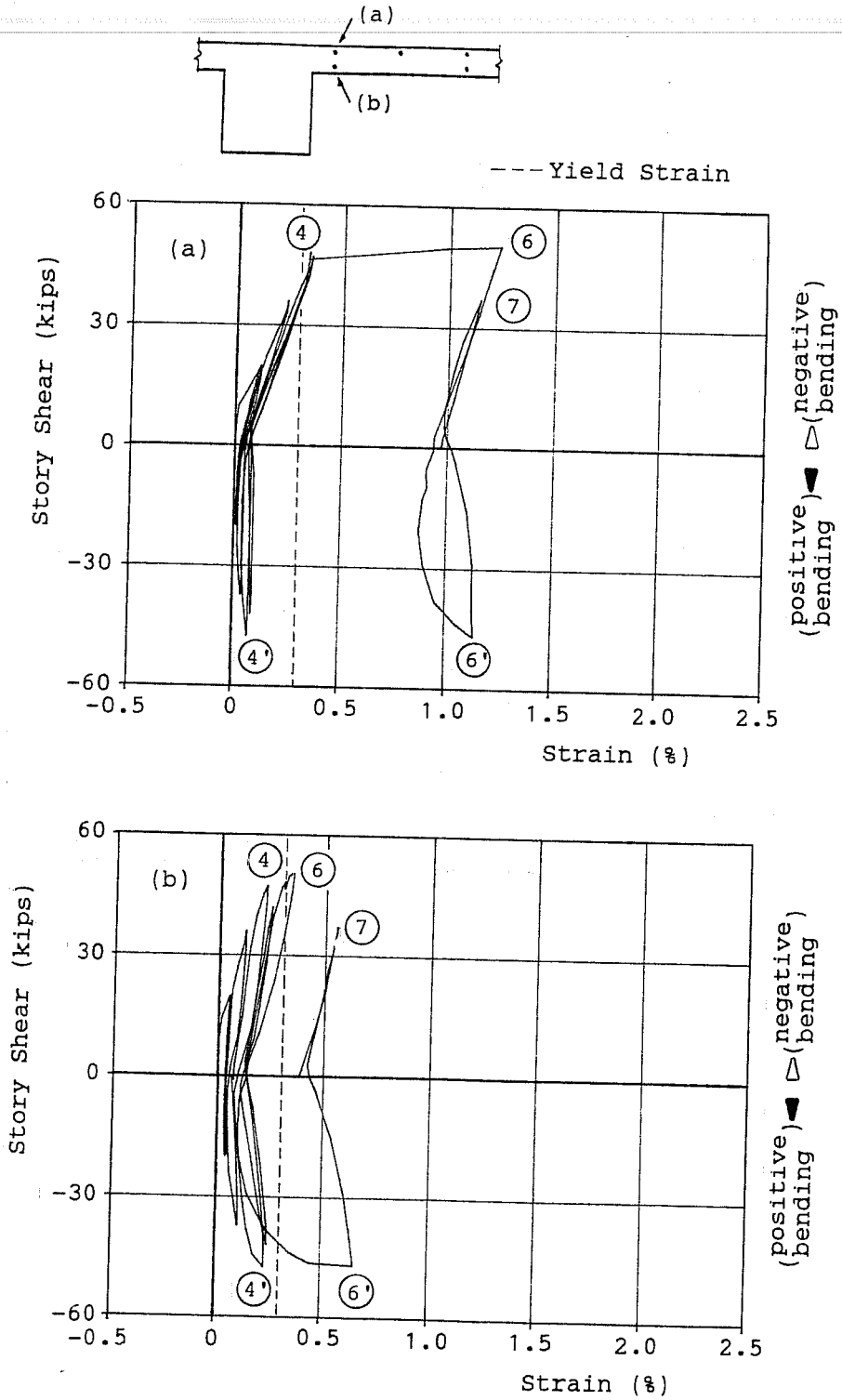

Figure 3.45 Strain Measurements on Slab Bars for Specimen J1

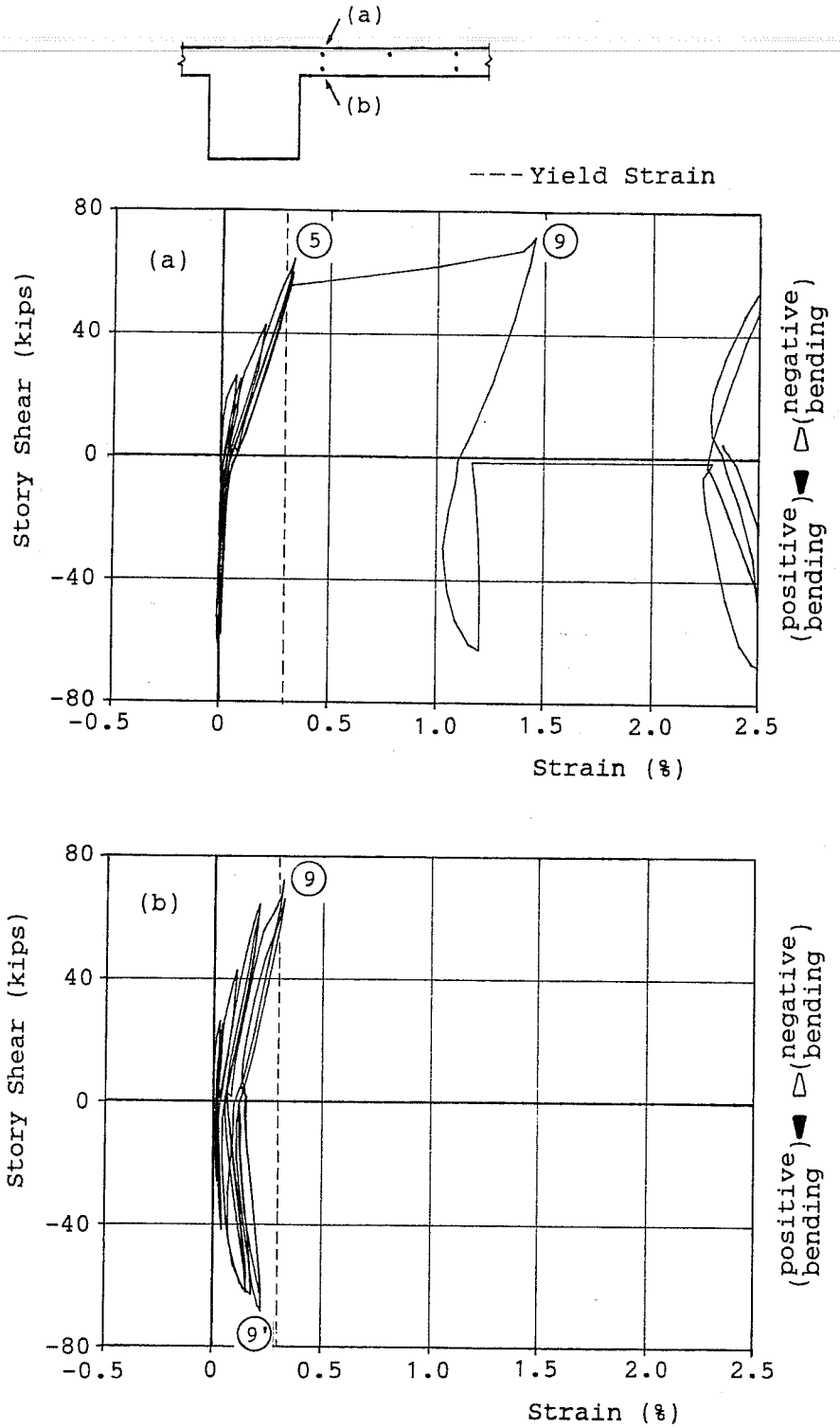

Figure 3.46 Strain Measurements on Slab Bars for Specimen J2 During Unidirectional Loading in E-W Direction

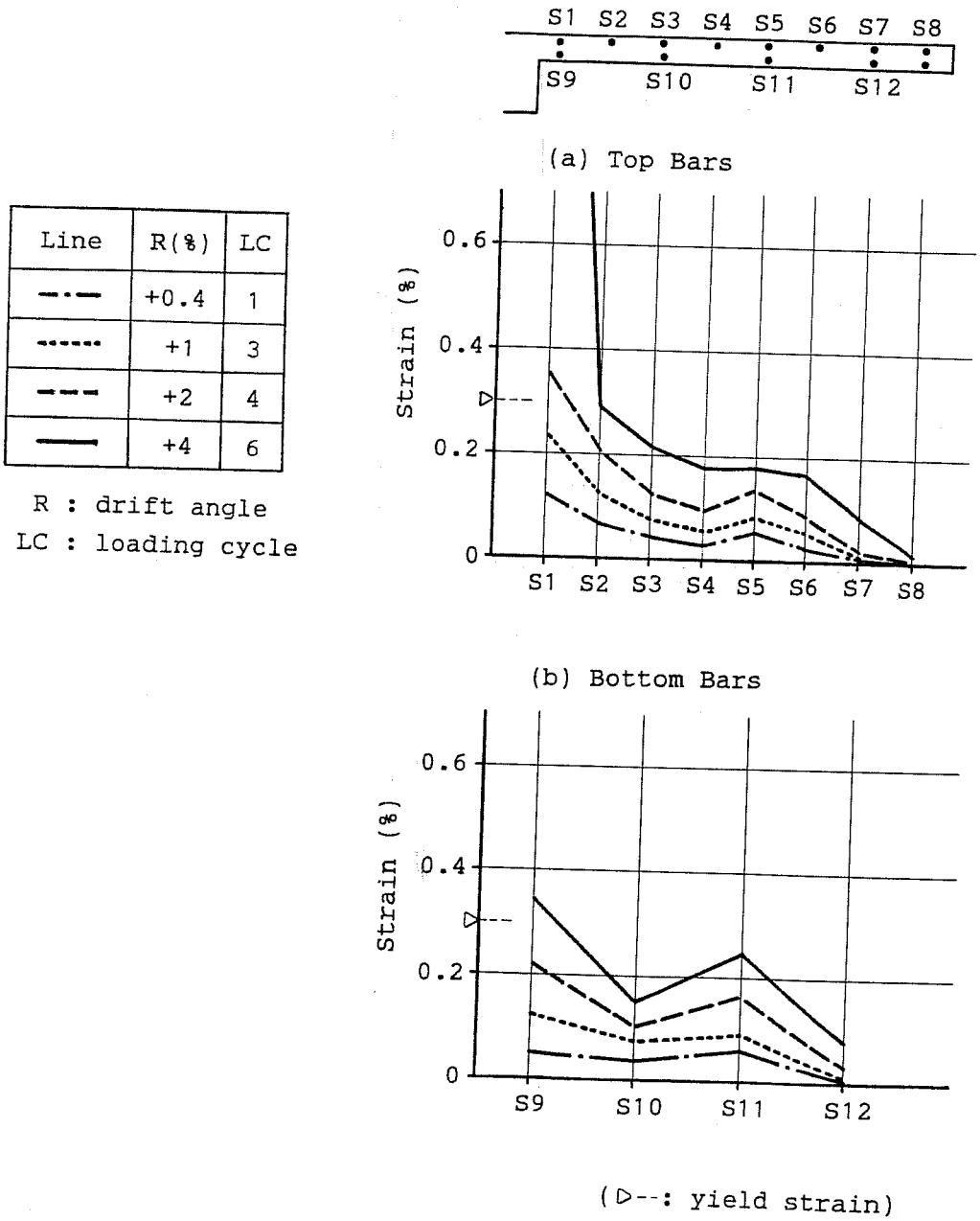

Line	R(%)	LC
—·—	+0.4	1
·····	+1	3
— —	+2	4
———	+4	6

R : drift angle
LC : loading cycle

Figure 3.47 Slab Bar Strains in Negative Bending (Specimen J1)

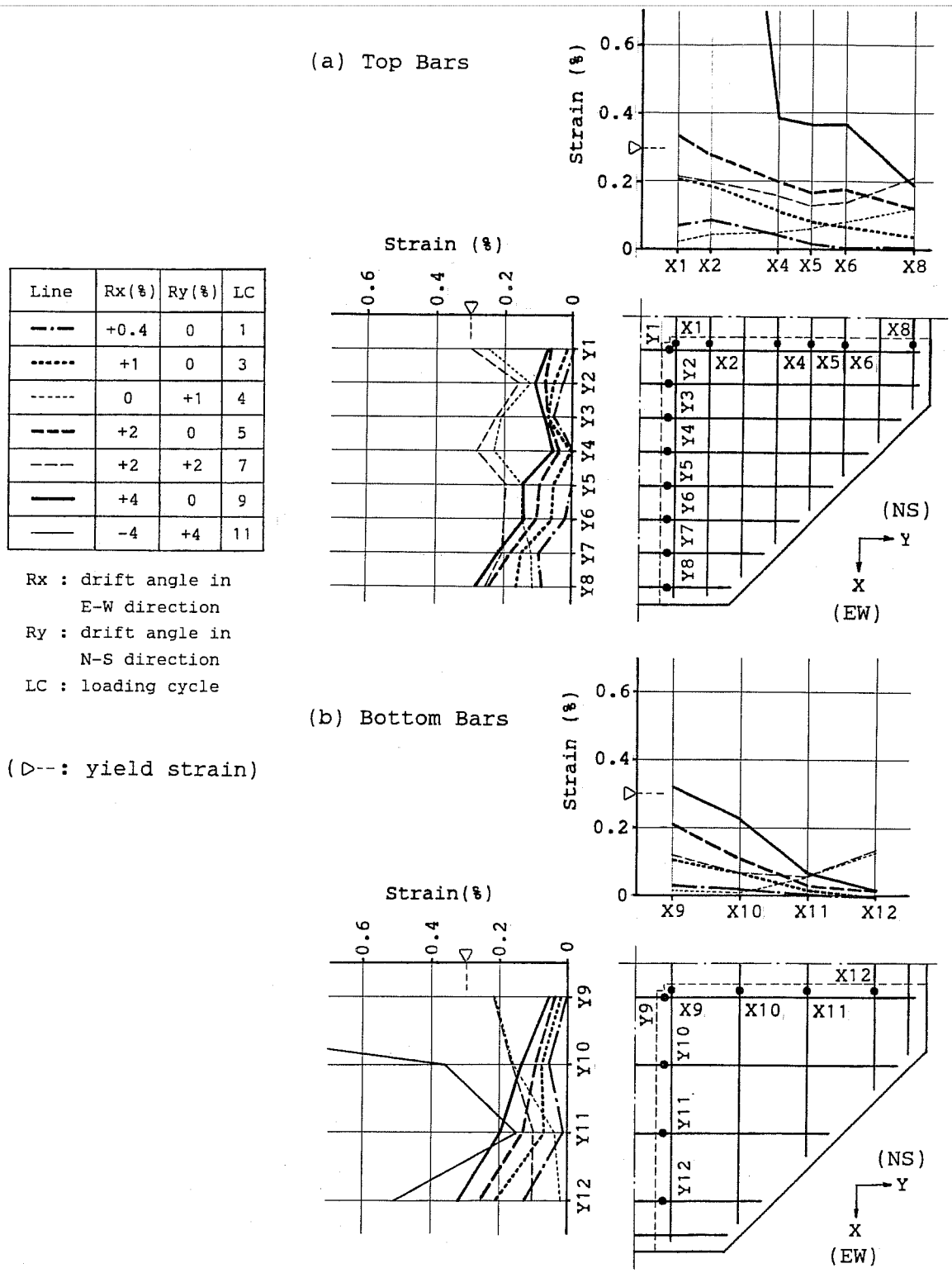

Line	Rx(%)	Ry(%)	LC
—·—	+0.4	0	1
·····	+1	0	3
------	0	+1	4
— — —	+2	0	5
— — —	+2	+2	7
———	+4	0	9
———	-4	+4	11

Rx : drift angle in E-W direction
Ry : drift angle in N-S direction
LC : loading cycle

(▷--: yield strain)

Figure 3.48 Slab Bar Strains in Negative Bending (Specimen J2)

Line	Rx(%)	Ry(%)	LC
—·—·—	+0.5	0	1
—·—	0	-0.5	2
-----	+1	0	3
------	0	-1	4
— — —	+2	0	5
— — —	0	-2	7
———	+4	0	9
———	0	-4	11

Rx : drift angle in E-W direction
Ry : drift angle in N-S direction
LC : loading cycle

(▷-- : yield strain)

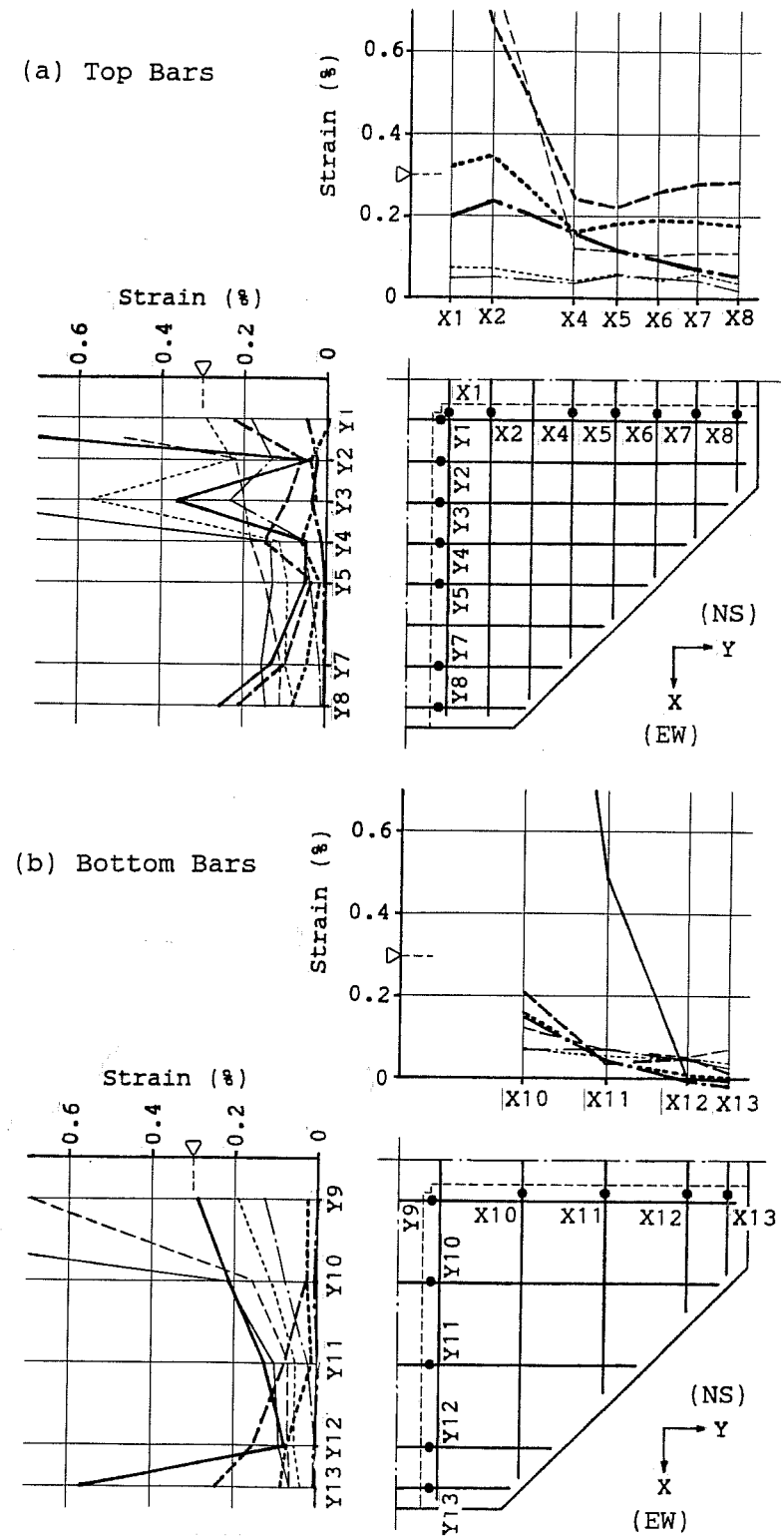

Figure 3.49 Slab Bar Strains in Negative Bending (Specimen J3)

of the loaded beam. Under biaxial loading, slab bar strains were distributed almost uniformly along the beam. In-plane tensile forces in the slab produced diagonal compressive struts in the slab as evidenced by diagonal cracks in the slab radiating outward from the columns. The contribution of the slab in negative bending at the column is due largely to the formation of a "truss" system in the plane of the slab. The struts were located between the diagonal cracks. For equilibrium of the truss, tension in the orthogonal direction is needed and can be provided by slab or beam reinforcement.

3.4.3 Effective slab width for beam moment capacity was examined using measured slab bar stresses as shown in Fig. 3.50. the effective slab width was taken as the ratio of tensile force in the slab reinforcement to the force if all bars yielded. While this may not be a totally accurate measure of the moment resulting from slab steel acting with the beam in negative bending, it does indicate the increasing participation of slab reinforcement at large drift levels. It also indicates the influence of transverse beams. The most effective slab was in J3 where the spandrel resisted bending from a slab on only one side of the beam. Specimen J1, with no transverse beam, showed small slab participation at all drift levels. Two plots are shown for the case where only top slab bars are considered and where all slab bars are considered. In many cases, only top bars are considered to participate in beam moment capacity because bottom bars are designed for positive bending in the center of a slab under gravity loads and are not provided with sufficient anchorage to resist bending moment at the end of the slab under seismic loads. In the specimens, bottom slab bars were continuous over the beam and exhibited tensile stresses at the face of the beam. However, the bottom bars near the free edge in J3 developed compressive stresses under downward loading at large drift levels because of local bending about the slab axis (see Fig. 3.49). Therefore, the effective slab width calculated from all bar stresses for J3 did not increase with loading from 2% to 4% drift.

Table 3.4 shows maximum beam moments measured at the column face in comparison with calculated moment capacities. Two calculations were made for the case where only the beam section was considered (RMcalc) and where 60% of the entire slab width was considered to participate in the beam moment capacity (TMcalc). The value of 60% was determined by referring to the effective slab width at 4% drift levels shown in Fig. 3.50(b). The calculated capacities without a slab considerably underestimated the measured maximum moments. The differences between the measured and calculated values are due to strain hardening in beam bars, particularly under upward loading, and due to participation of slab bars under downward loading. The calculated capacities with 60% slab width resulted in good agreement with the measured maximum moments.

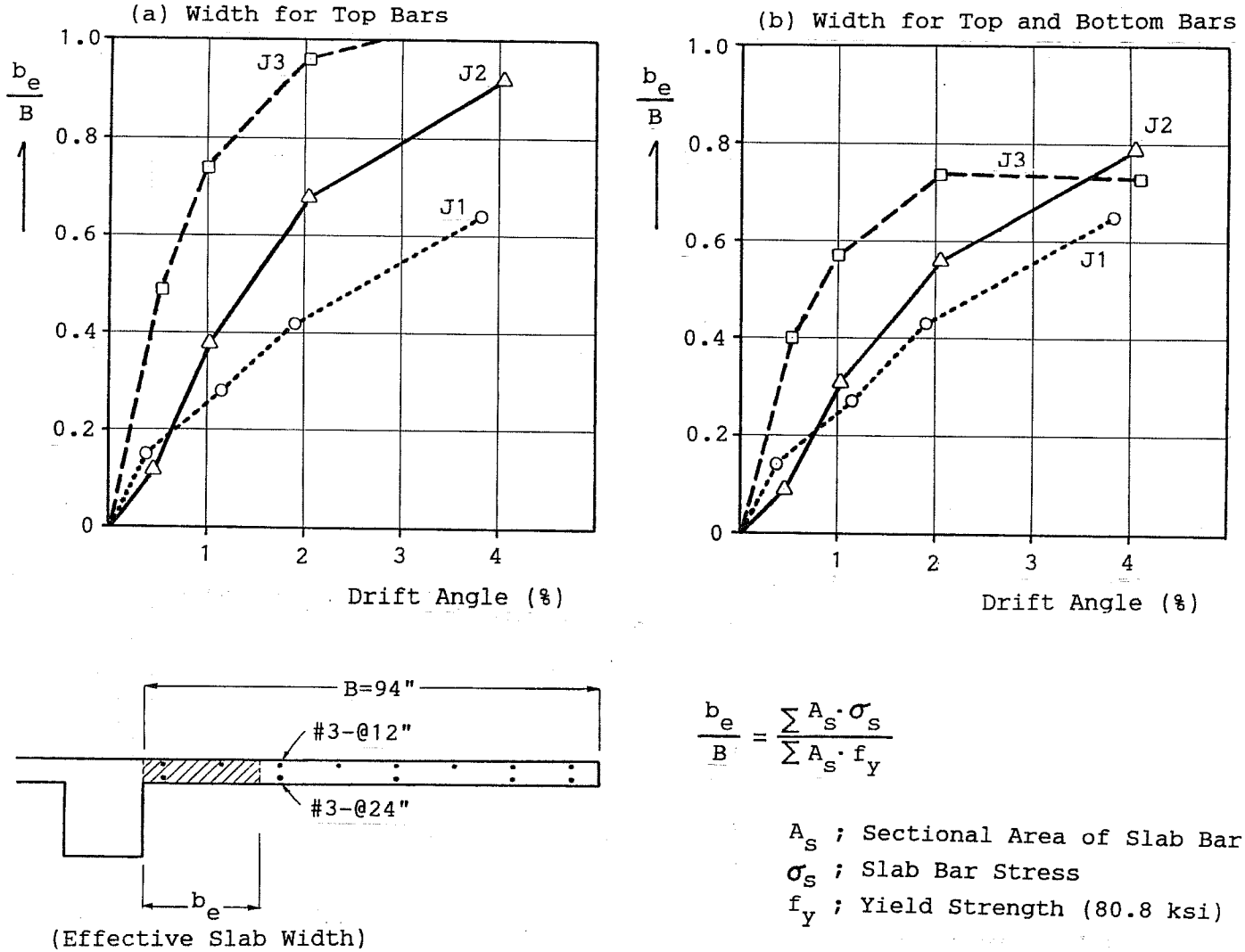

Figure 3.50 Effective Slab Width for Beam Negative Bending in E-W Direction

Table 3.4 Measured Maximum Beam Moment vs. Calculated Moment Capacity

		Positive Bending					Negative Bending				
Beam	Moment	M_{test} (k-in)	R^M_{calc} (k-in)	$\frac{M_{test}}{R^M_{calc}}$	T^M_{calc} (k-in)	$\frac{M_{test}}{T^M_{calc}}$	M_{test} (k-in)	R^M_{calc} (k-in)	$\frac{M_{test}}{R^M_{calc}}$	T^M_{calc} (k-in)	$\frac{M_{test}}{T^M_{calc}}$
J1	East	3010	2460	1.22	2680	1.12	4290	3060	1.40	4760	0.90
	West	2910		1.19		1.09	4520		1.48		0.95
J2	East	4160	2740	1.52	3070	1.35	6160	4300	1.43	5730	1.08
	West	3960		1.45		1.29	6480		1.51		1.13
	North	3790	2940	1.29	3270	1.16	5530	3990	1.39	5460	1.01
	South	3780		1.29		1.15	4940		1.24		0.90
J3	West	4930	3360	1.47	3670	1.34	6770	4400	1.54	6040	1.12
	North	3090	2490	1.24	2660	1.16	4000	3230	1.24	4220	0.95
	South	2810		1.13		1.06	4010		1.24		0.95

where:

M_{test} = measured maximum beam moment at joint end

R^Mcalc = calculated moment capacity as rectangular beam

T^Mcalc = calculated moment capacity as T-beam

(b_e = 0.6B, b_e = effective slab width, B = entire slab width)

4. ANALYSIS OF JOINT SHEAR STRENGTH

4.1 Introduction to Analysis

Shear strength for reinforced concrete beam-column joints was analyzed using tests reported in Japan and in the United States. In the analysis, joints were classified into three types shown in Figs. 4.1 through 4.3. An interior-type joint has two beams in the loading direction and an exterior-type joint has one beam. A corner-type joint is a connection at a roof level. Each type is expected to resist joint shear differently. for example, an interior-type joint is considered to form a diagonal compressive strut between compressive concrete zones in member and sections, while an exterior-type joint is considered to form the strut from the compressive zone in the beam end section to the bend portion of hooked beam bars. Each type has three variations with the number of transverse beams. The transverse beams influence the shear resisting mechanism in the joint by confining joint concrete.

The analysis included 84 interior-type joints, 63 tested in Japan and 21 in the United States, and 27 exterior-type joints, 15 tested in Japan and 12 in the United States. Uniaxial cyclic loads simulating earthquake effects were applied to these specimens. Most of the specimens did not have a floor slab. Test data for the interior-type joints were from Refs. 8 through 27 and those for the exterior-type joints were from Refs. 19 and 26 through 31. The three specimens described in Chapters 2 and 3 were also included in the analysis as interior- type joints (J1 and J2) and an exterior-type joint (J3). However, the analysis did not cover any corner-type joints because few test data were available. Most of the analyzed specimens failed in joint shear before or after developing beam flexural yielding. The specimens which failed in beam flexure were generally omitted from the analysis except those which reached high joint shear due to enhancement by transverse beams. The joint shear strength was evaluated in terms of the maximum shear stress measured in the horizontal joint section as shown in Fig. 4.4. When beam effective depth was not given in the reference, 90% of the full beam depth was assumed in the calculation. The results of the analysis are discussed in Section 4.2 for interior-type joints and in Section 4.3 for exterior-type joints.

According to the recommendations of ACI 352[3], the interior-type joint with two transverse beams shown in Fig. 4.1(c) is an interior joint with a design shear strength of $20\sqrt{f'_c}$ (f'_c = concrete strength) and those shown in Figs. 4.1(a)., 4.1(b) and 4.2(c) are exterior joints with a design shear strength of $15\sqrt{f'_c}$. The other joints in Fig. 4.2 and those in Fig. 4.3 are classified as corner joints with a design shear strength of $12\sqrt{f'_c}$. Although the recommendations of ACI 352 do not specify a method to design the joint biaxially, joints in moment-resisting space frames are likely to sustain biaxial shear forces during strong earthquake motions. Biaxial joint shear strength was analyzed using test data reported in Refs. 19 and 32 through 35. Specimens J2 and J3 were also included in the analysis. The results of the analysis are discussed in Section 4.4 for exterior and interior joints under biaxial loading.

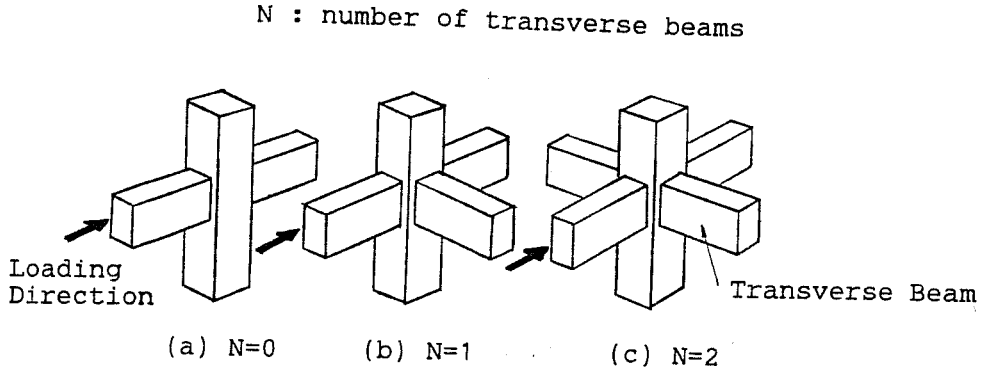

Figure 4.1 Interior-type Joints

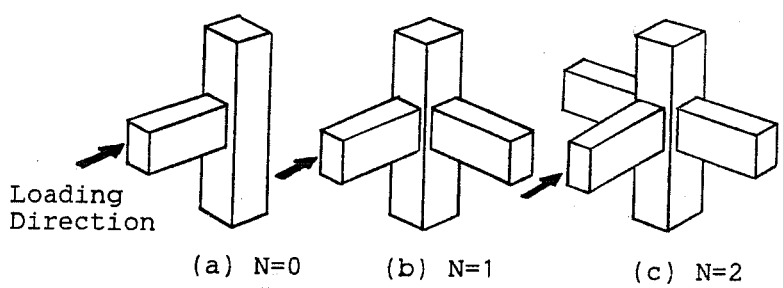

Figure 4.2 Exterior-type Joints

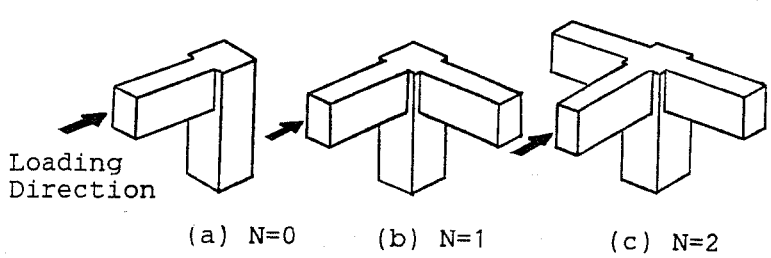

Figure 4.3 Corner-type Joints

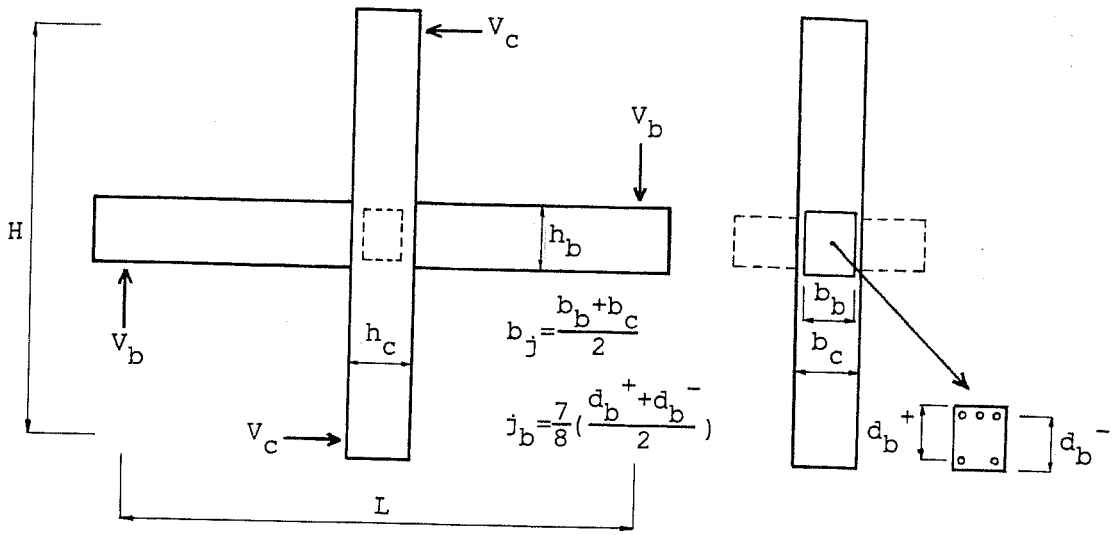

Joint Shear Stress : $v_j=M_j(1-\frac{h_c}{L}-\frac{j_b}{H})/(b_j h_c j_b)$, $M_j=V_b L=V_c H$

(a) Interior-type Joint

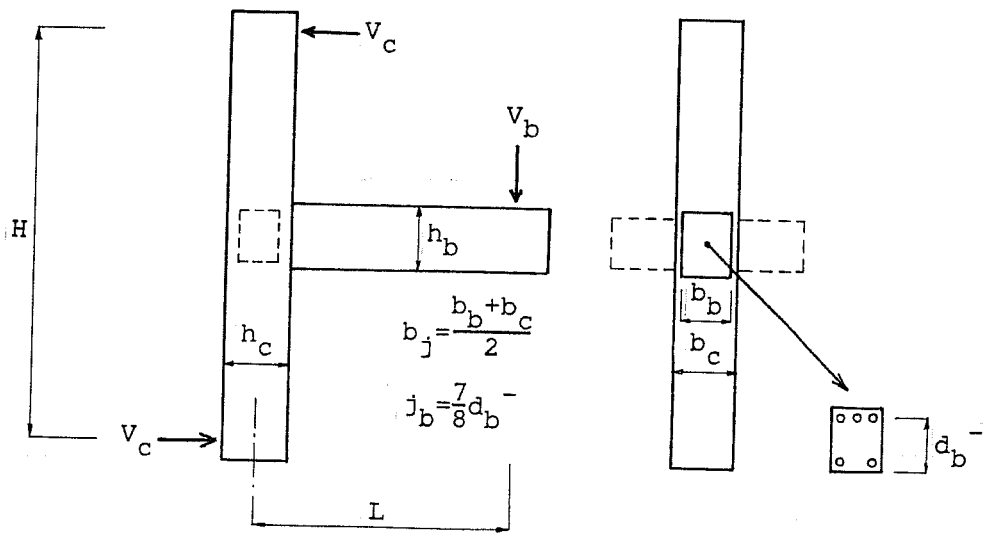

Joint Shear Stress : $v_j=M_j(1-\frac{h_c}{2L}-\frac{j_b}{H})/(b_j h_c j_b)$, $M_j=V_b L=V_c H$

(b) Exterior-type Joint

Figure 4.4 Calculation of Joint Shear Stress

4.2 Interior-Type Joints Under Uniaxial Loading

Shear Strength. Histograms for interior-type joints plotted against normalized joint shear strength are shown in Fig. 4.5. A total of 84 interior- type joints were analyzed; 57 without transverse beams, 13 with one transverse beam and 14 with two transverse beams. As shown in Fig. 4.5(a), the joints without transverse beams failed in shear; 38 before beam yielding and 19 after beam yielding. Specimens which failed in beam flexure were omitted. The histogram showed the largest number of tests with a joint shear strength of 15 to 20 times $\sqrt{f'_c}$. Twelve specimens did not reach the recommended strength of $15\sqrt{f'_c}$. As shown in Fig. 4.5(b), the histogram for the joints with one transverse beam was similar to the above-mentioned histogram. A transverse beam on one side of the joint did not appear to influence the joint shear strength. Among the 13 specimens in this category, however, only one specimen did not reach the recommended shear strength of $15\sqrt{f'_c}$. On the other hand, transverse beams on both sides of the joint enhanced the joint shear strength, as shown in Fig. 4.5(c). The mean value of the joint shear strength of this type was 23.2 times $\sqrt{f'_c}$ and approximately 30% higher than those for the other types.

Effect of Concrete Strength. The measured joint shear strength is plotted against concrete strength in Fig. 4.6. Solid and broken lines show the recommended values for joint shear strength. Various marks are used to distinguish failure mode and the number of transverse beams in this Figure and in the following Figures as well. Although the test data show considerable scatter, the measured joint shear strength had a tendency to increase with concrete strength. Use of the square root of concrete compressive strength resulted in better correlation with the measured joint shear strength than the concrete compressive strength itself. The coefficient of correlation was 0.58.

Effect of Beam to Column Width Ratio. Figure 4.7 shows the effect of the beam-to-column width ratio on joint shear strength. The solid line in this Figure shows the result of a linear regression analysis as do solid lines in the following Figures, unless otherwise noted. The joint shear strength (normalized with concrete strength) in this Figure is based on the gross area of the column section and is different from those in the other Figures. Beam width appeared to influence the joint shear strength because the measured strength had a high correlation with the beam-to-column width ratio. The results indicate that the joint effective width can be taken as the average of the beam and column widths, as recommended by ACI Committee 352.

Effect of Beam to Column Depth Ratio. Figure 4.8 shows the effect of the beam-to-column depth ratio on shear strength for the joints without transverse beams. The joint shear strength had a tendency to decrease with the beam-to-column depth ratio. The results indicate that oblong joints resulting from deep beams may have lower shear strength than square joints. The diagonal compressive strut in the joint probably becomes steeper and less effective in resisting horizontal joint shear, as the beam becomes deeper.

Effect of Transverse Beams. The affect of transverse beams on joint shear strength is shown in Fig. 4.9 where normalized joint shear strength is plotted against the ratio of sectional area of the transverse beam to the area of the joint (the masking ratio). The size of the transverse beam on only one side of the joint did not appear to influence the joint shear strength, as shown in Fig. 4.9(a). However, the masking ratio had a weak correlation with the joint shear strength when two transverse beams framed into the joint, as shown in Fig. 4.9(b). It should be noted that Specimen

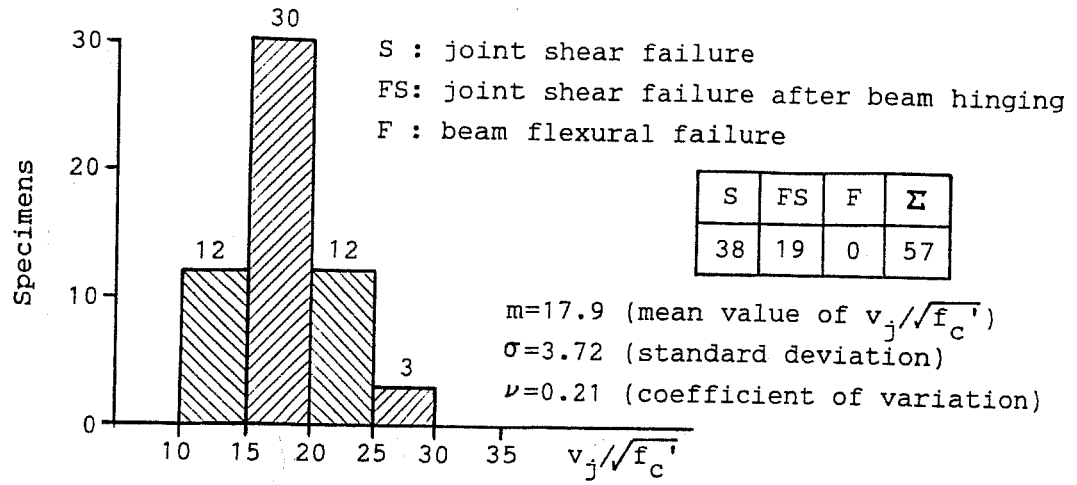

S	FS	F	Σ
38	19	0	57

(a) Joints without Transverse Beams (N=0)

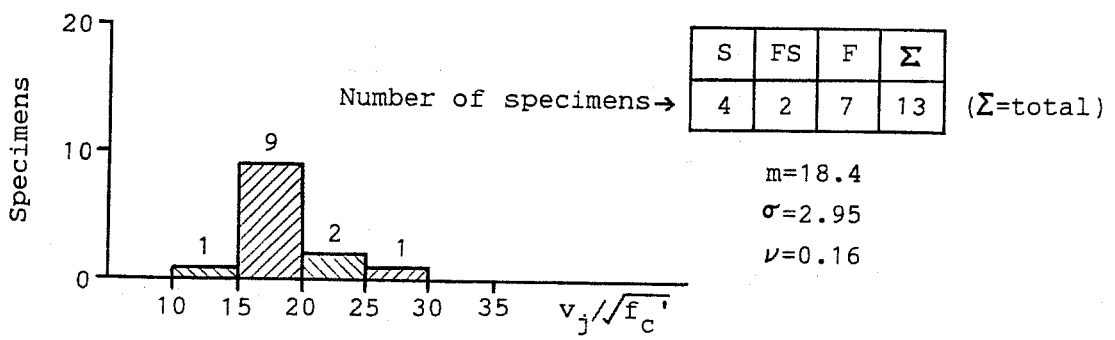

S	FS	F	Σ
4	2	7	13

(Σ=total)

(b) Joints with One Transverse Beam (N=1)

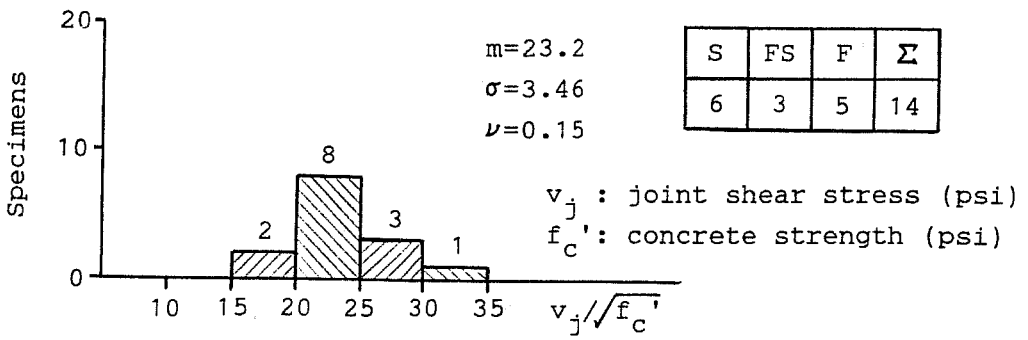

S	FS	F	Σ
6	3	5	14

(c) Joints with Two Transverse Beams (N=2)

Figure 4.5 Interior-type Joints Under Uniaxial Loading

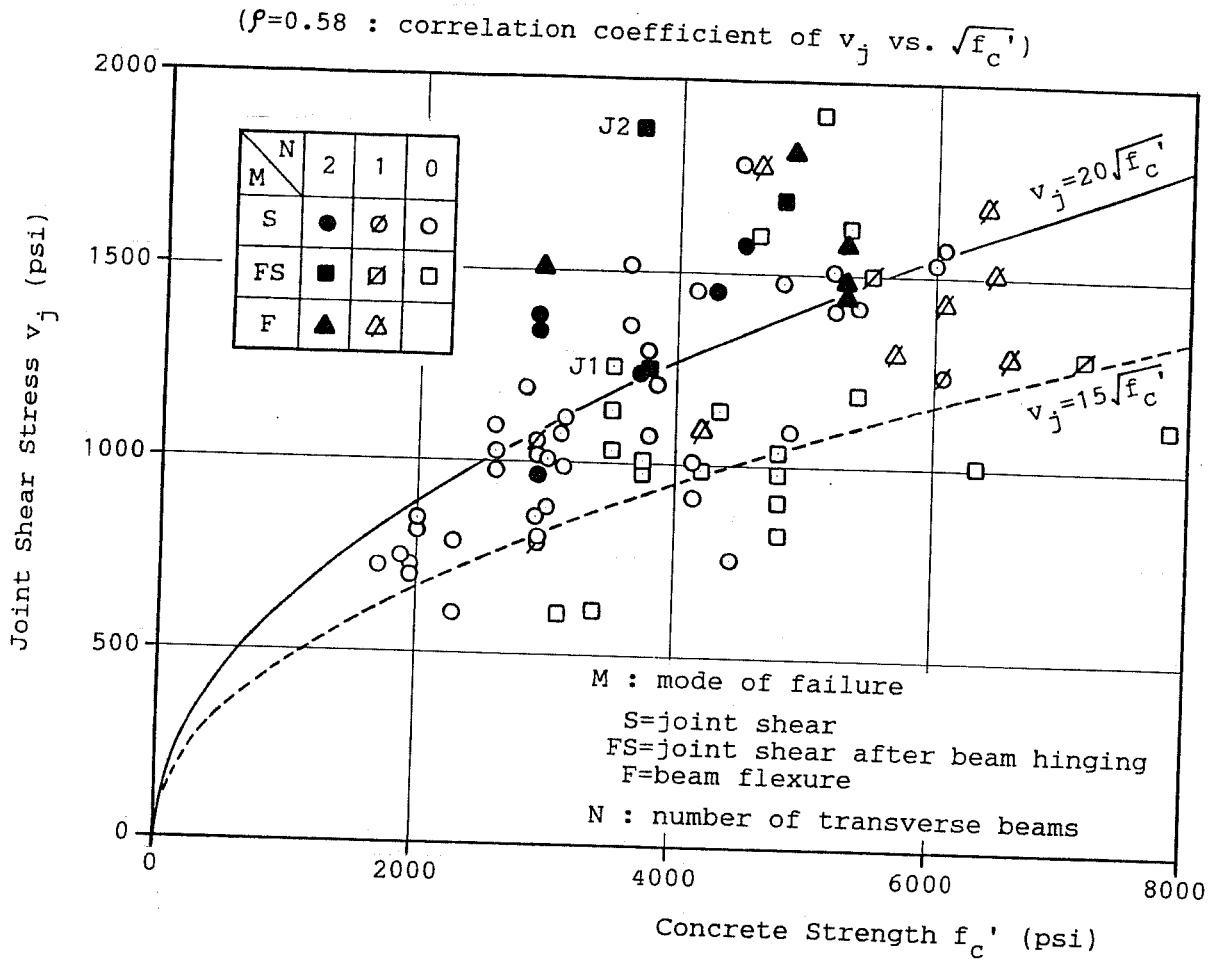

Figure 4.6 Maximum Joint Shear Stress vs. Concrete Strength

(Interior-type Joints)

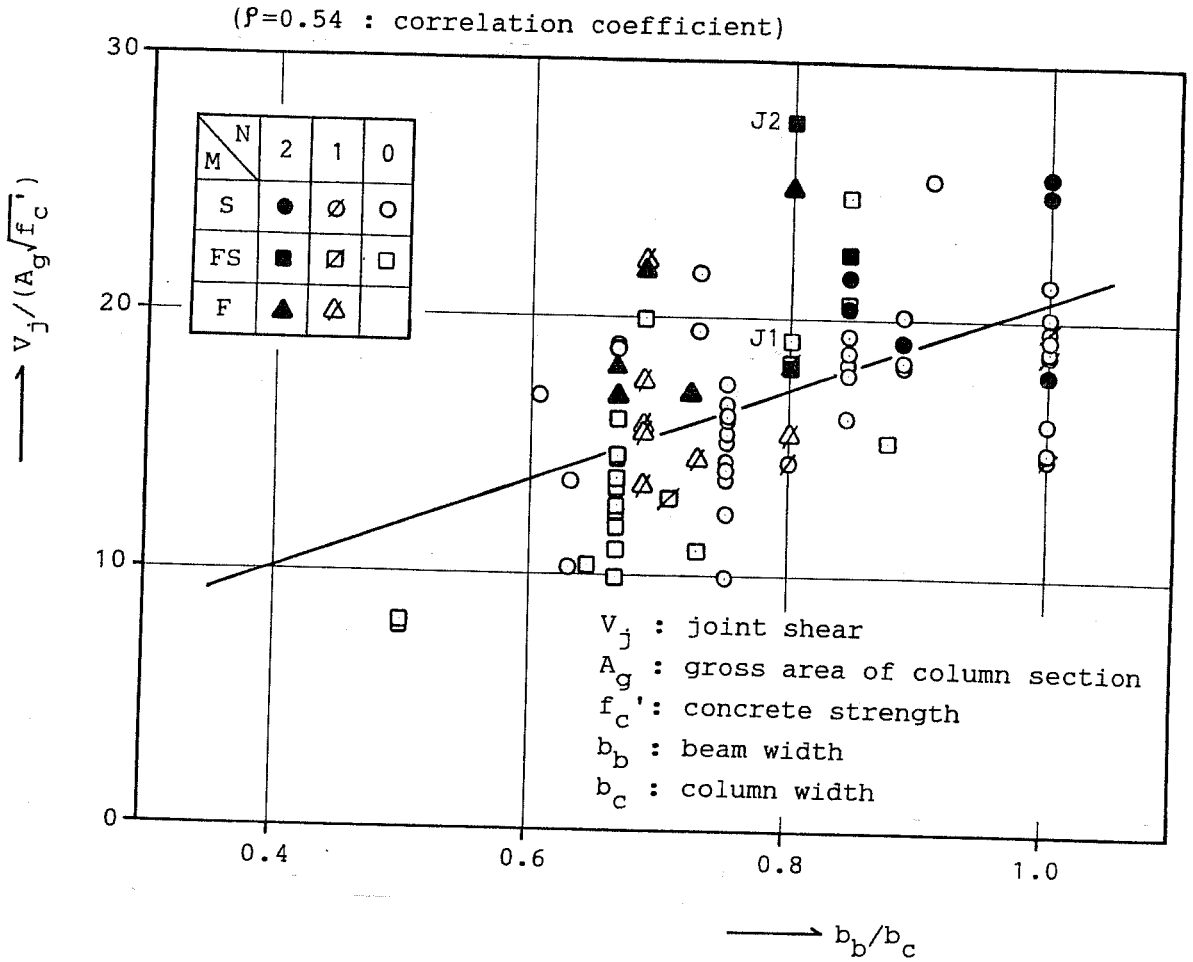

Figure 4.7 Effect of Beam-to-Column Width Ratio on Joint Shear Strength (Interior-type Joints)

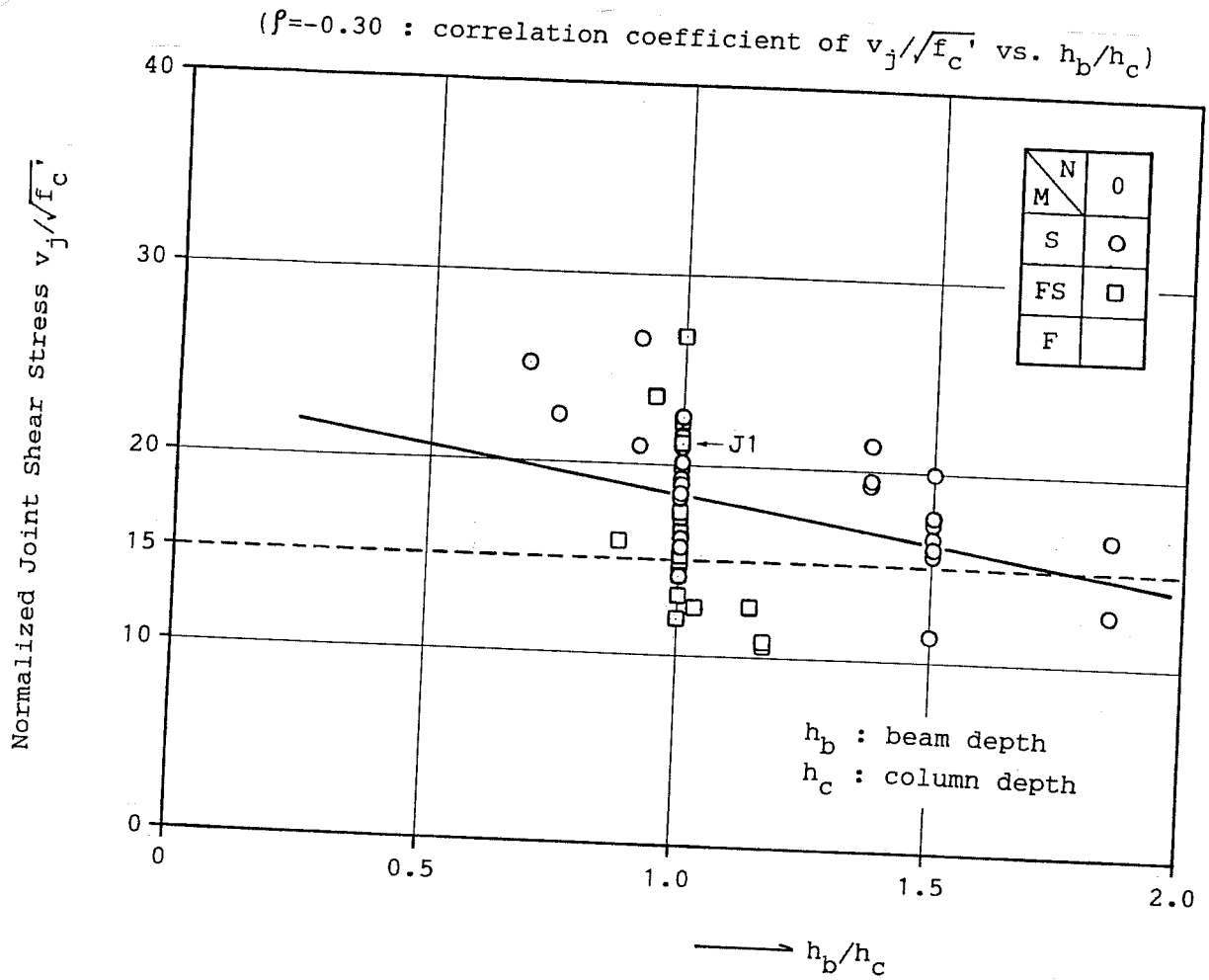

Figure 4.8 Effect of Beam-to-Column Depth Ratio on Joint Shear Strength (Interior-type Joints Without Transverse Beams)

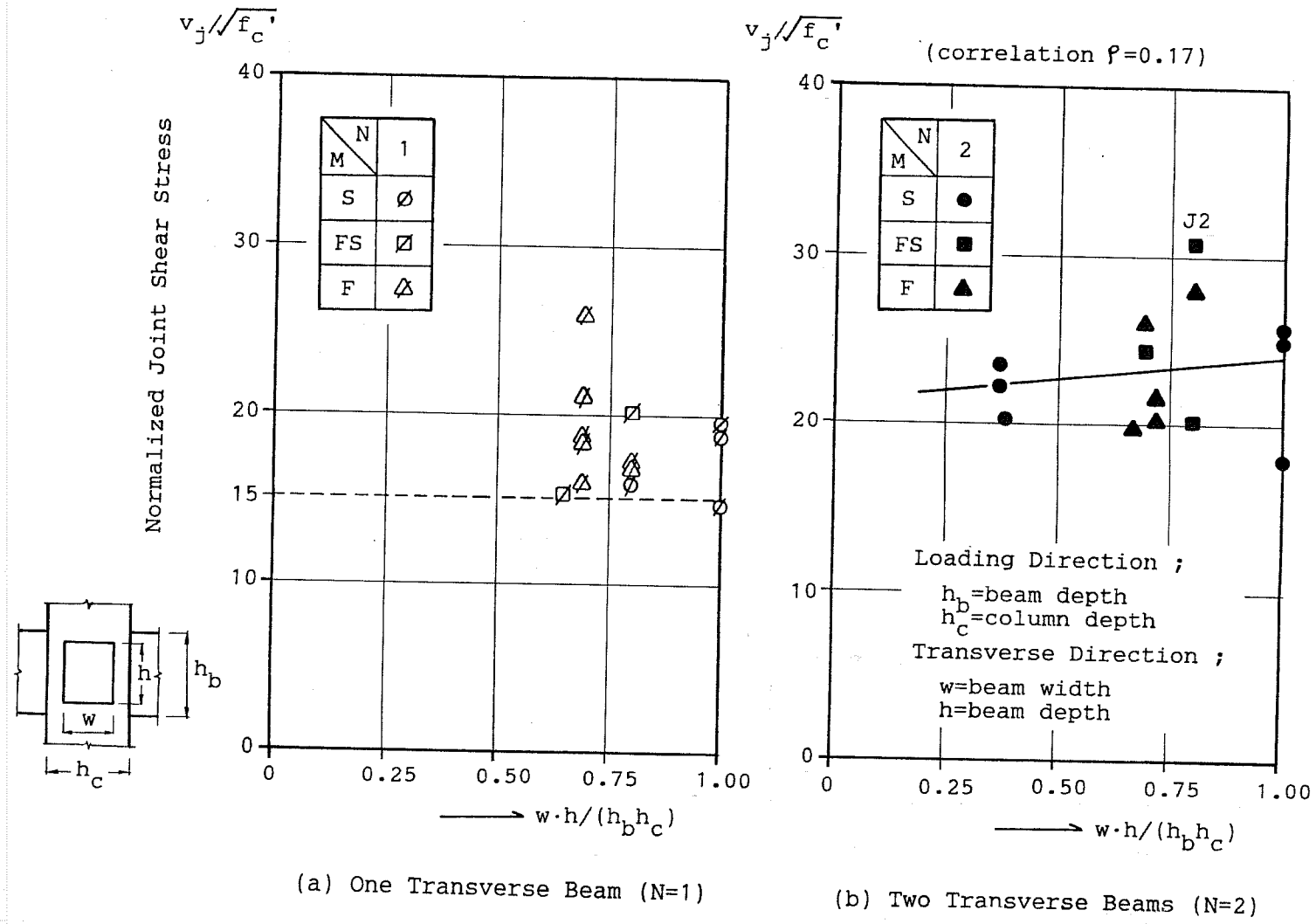

Figure 4.9 Effect of Transverse Beams on Joint Shear Strength

(Interior-type Joints)

J2 reached the highest strength among the joints with two transverse beams. The recommended values of $15\sqrt{f'_c}$ and $20\sqrt{f'_c}$ appeared to evaluate the joint shear strength somewhat conservatively.

Effect of Lateral Reinforcement. Figure 4.10(a) shows the effect of lateral reinforcement on joint shear strength. The broken line shows lateral reinforcement capacity, that is a joint shear stress considered to be carried by lateral reinforcement in a beam shear mechanism. The measured joint shear strength exceeded the lateral reinforcement capacity except for two specimens with an extraordinarily large amount of the reinforcement. Therefore, concrete in the joint was the primary source of shear strength. The amount of lateral reinforcement did not influence the shear strength for the joints with two transverse beams as shown with solid symbols in Fig. 4.10(a). However, joints with one or no transverse beam exhibited shear strength which increased with the amount of lateral reinforcement, as shown in Fig. 4.10(b). The results indicate that lateral reinforcement was effective in enhancing shear strength for joints which had at least one unconfined side.

Effect of Column Axial Load. Figure 4.11 shows the effect of column axial load on joint shear strength. The axial load did not appear to influence the joint shear strength.

Effect of Column Depth to Beam Bar Diameter Ratio. Figure 4.12 shows the effect of the column depth-to-beam bar diameter (h_c/D_b) ratio on joint shear strength. The h_c/D_b ratio is a measure of bond conditions along beam bars passing through the joint. The joint shear strength had a tendency to decrease with the h_c/D_b ratio. It is likely that poor bond along beam bars imposes large compressive forces on concrete in the beam end section and thus increases the force in the diagonal compressive strut in the joint.

Effect of Reinforcement Index (Beam Tensile, Top, Reinforcement). Figure 4.13 is a plot of joint shear strength versus reinforcement index of beam tensile bars. Specimens with the reinforcement index ranging from 0.06 to 0.2 showed a significant correlation between the joint shear strength and the reinforcement index. Most of the specimens in this range developed beam flexural yielding as shown in Figure 4.14(a). The strength for these specimens was controlled by beam moment capacities. On the contrary, specimens with the reinforcement index ranging from 0.2 to 0.5 exhibited considerable scatter in test data and showed no apparent correlation between the joint shear strength and the reinforcement index (Fig. 4.13). Most of the specimens in this range failed in joint shear as shown in Fig. 4.14(b). Therefore, the index value of 0.2 may provide an upper limit on the amount of beam tensile reinforcement to avoid premature shear failure in the joint.

Effect of Ratio Bottom to Top Reinforcement. Figure 4.15 shows the effect of the beam bottom-to-top reinforcement (As'/As) ratio on joint shear strength. Most of the specimens tested in Japan had the same amounts of beam reinforcement at the top and bottom (As'/As = 1). As shown in Fig. 4.15(a), the specimens reached average joint shear strength of 18.3 $\sqrt{f'_c}$ but twelve did not reach the recommended strength of $15\sqrt{f'_c}$. On the contrary, all of the specimens tested in the United States and some of those in Japan had heavier beam reinforcement at the top than at the bottom (As'/As < 1). As shown in Fig. 4.15(b), the specimens reached somewhat higher strength than those with the same amounts of reinforcement and all of them reached the recommended strength. The heavier top reinforcement forced the bottom concrete to carry compression in the beam section and probably enhanced the diagonal compressive strut in the joint.

Joint Shear Distortion. Figure 4.16 is a plot of joint shear strength versus joint shear distortion measured at the maximum load stage. Most of the distortion data were taken from the

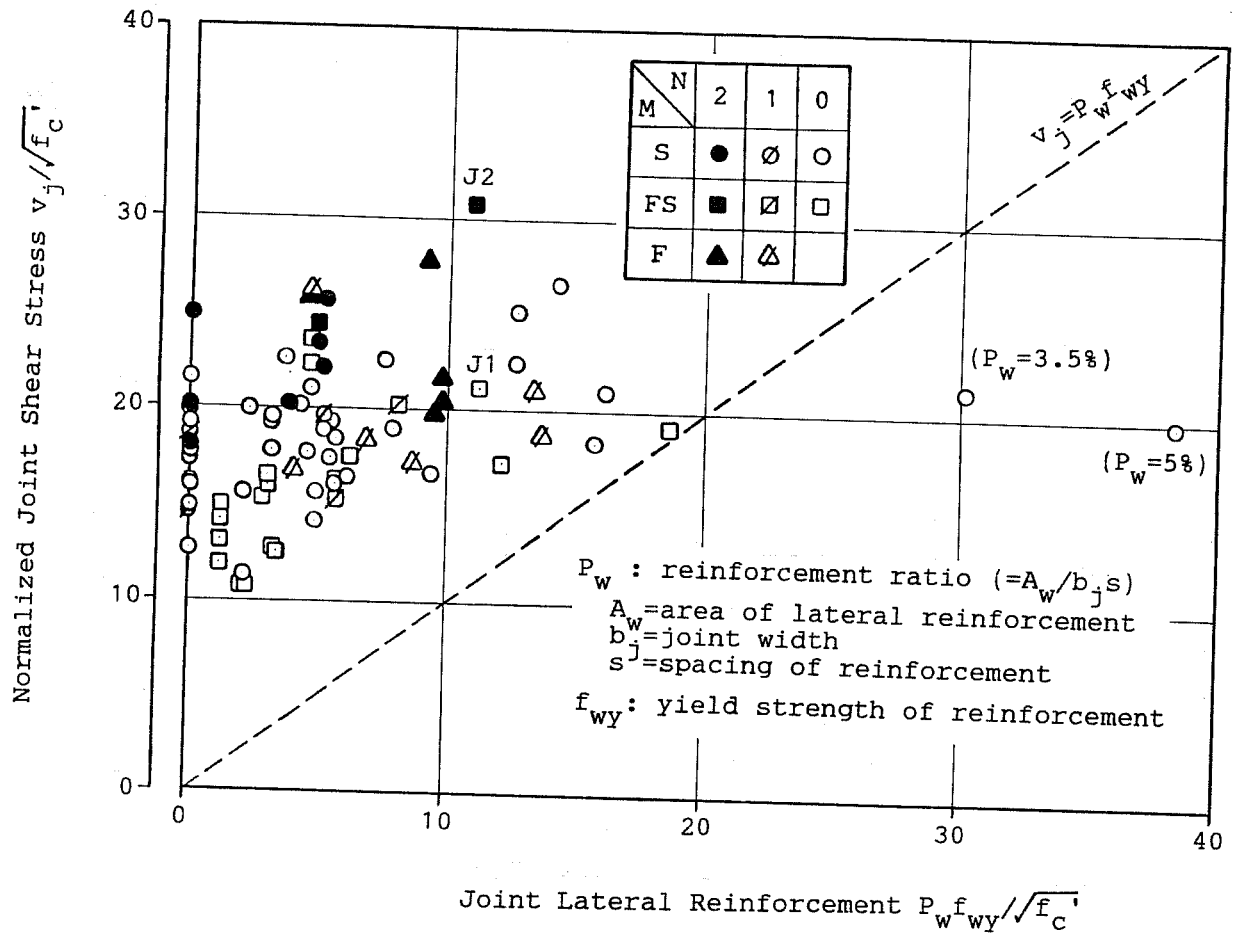

Figure 4.10(a) Effect of Joint Lateral Reinforcement on Joint Shear Strength (Interior-type Joints)

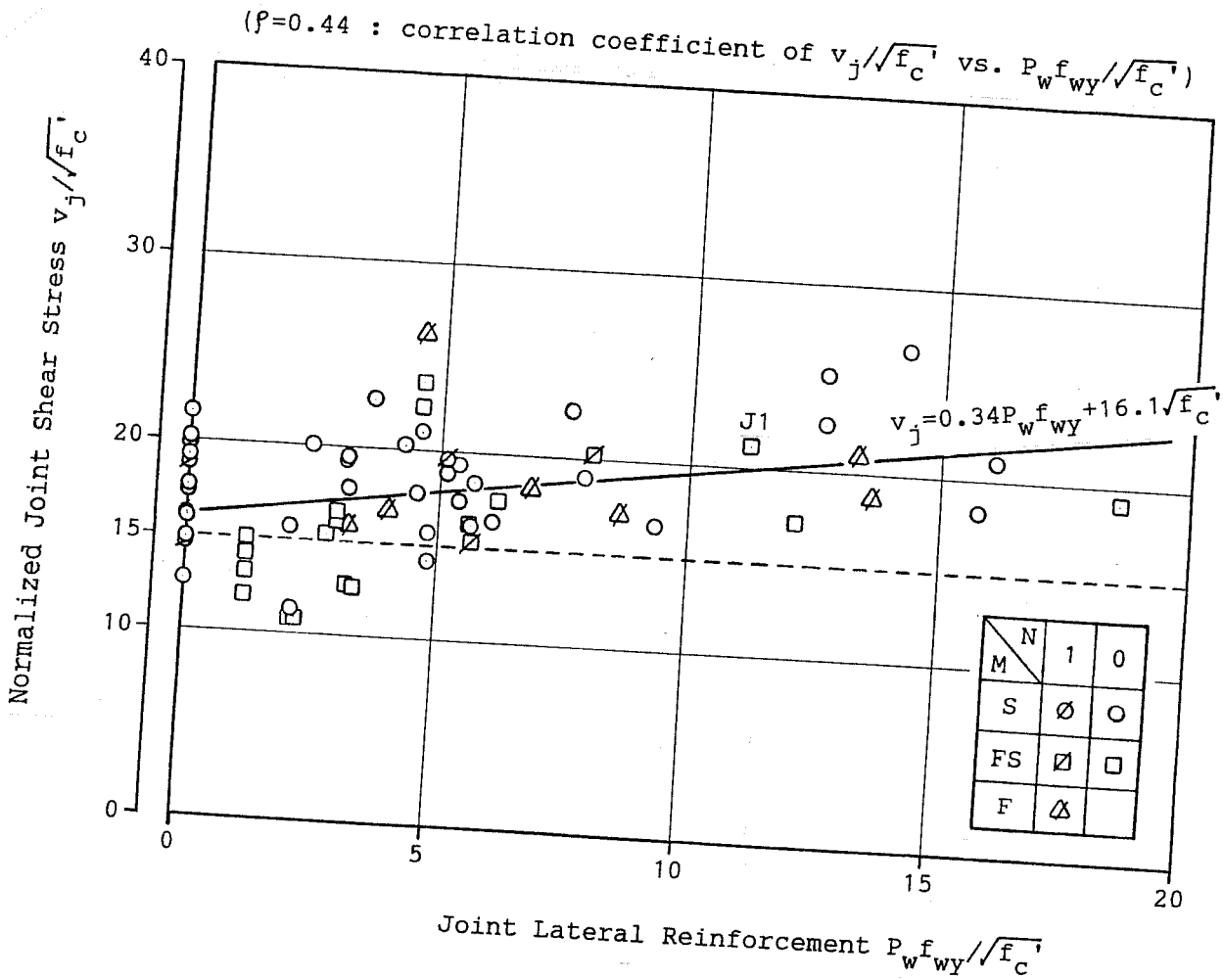

Figure 4.10(b) Effect of Joint Lateral Reinforcement on Joint Shear Strength

(Interior-type Joints With/Without One Transverse Beam)

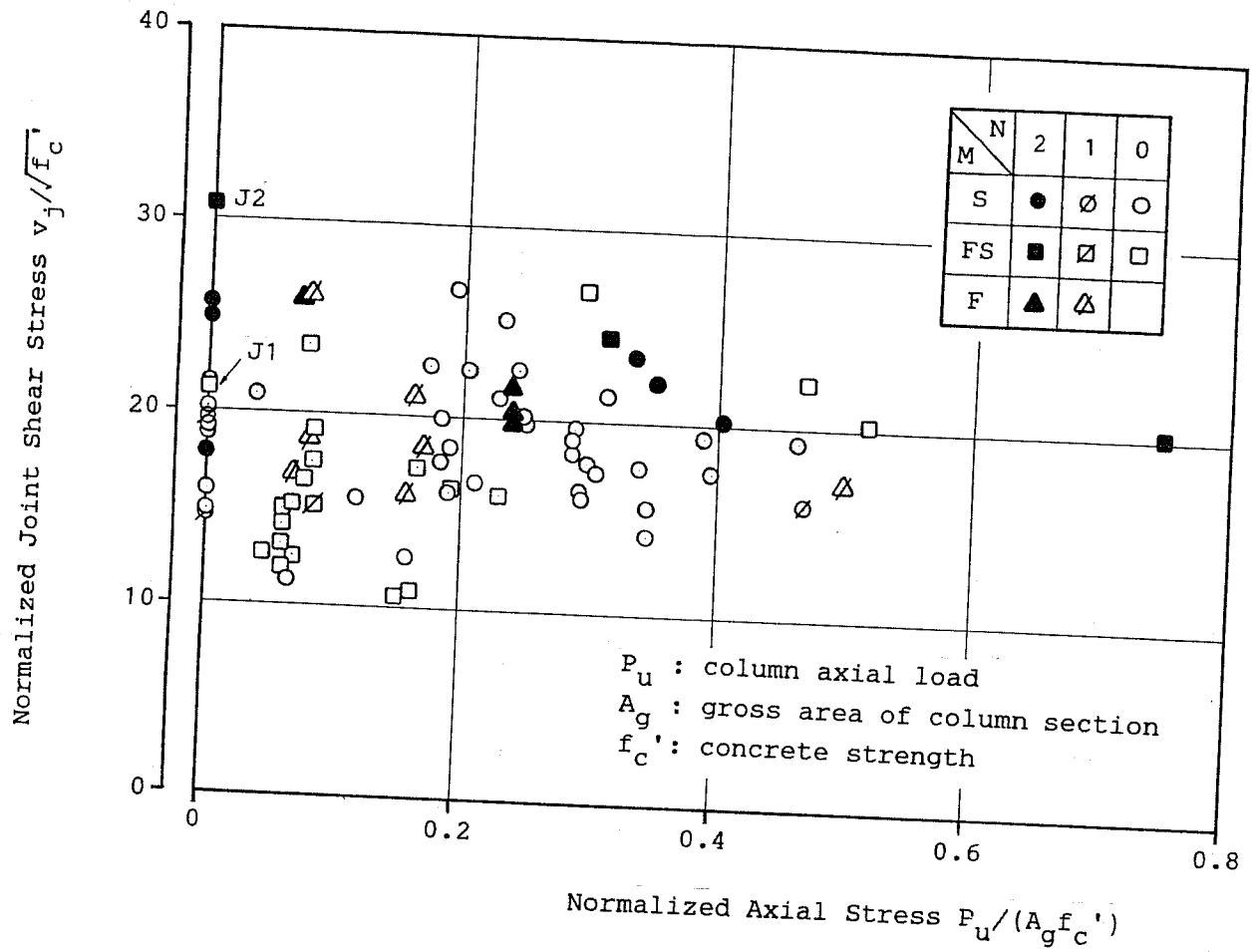

Figure 4.11 Effect of Column Axial Load on Joint Shear Strength (Interior-type Joints)

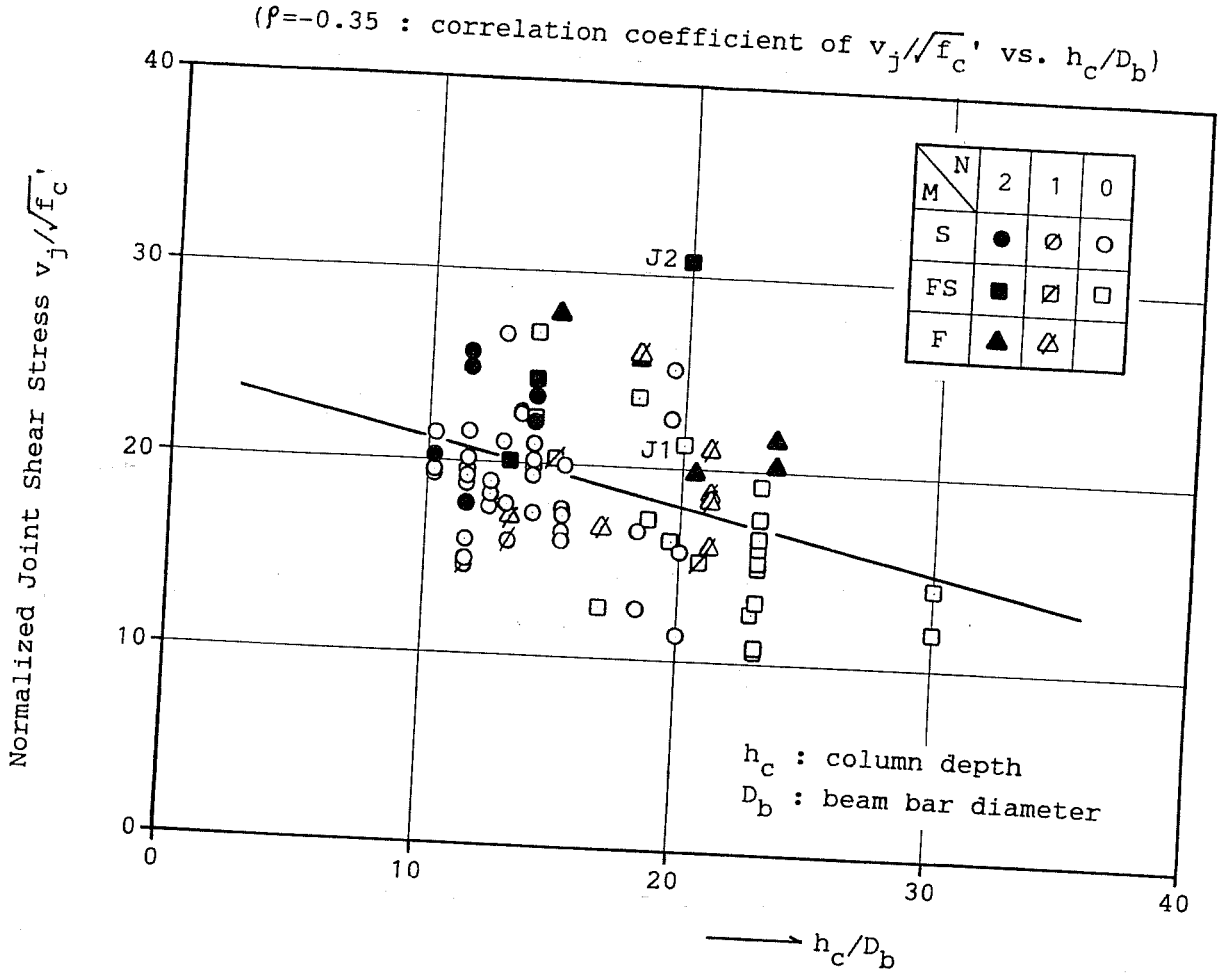

Figure 4.12 Effect of Column Depth-to-Beam Bar Diameter Ratio (Interior-type Joints)

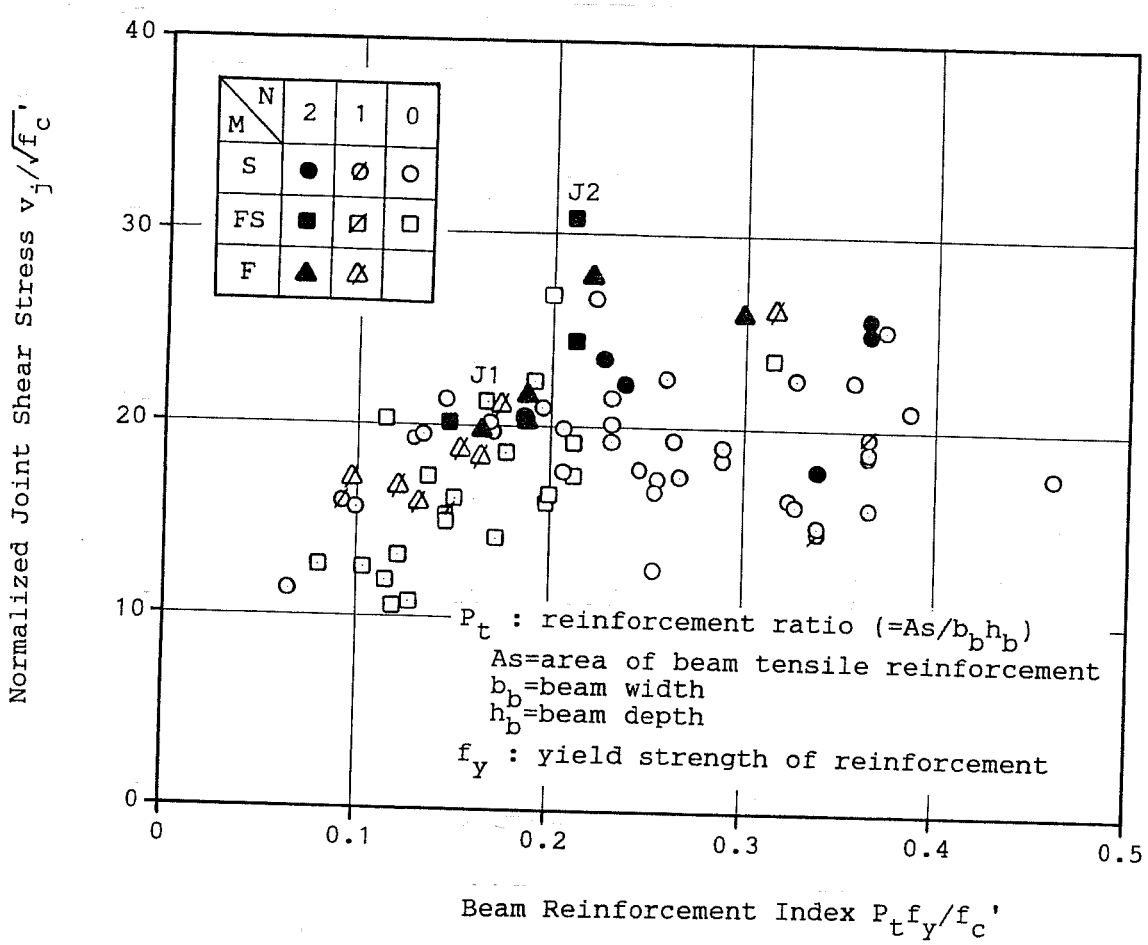

Figure 4.13 Effect of Beam Tensile Reinforcement on Joint Shear Strength

(Interior-type Joints)

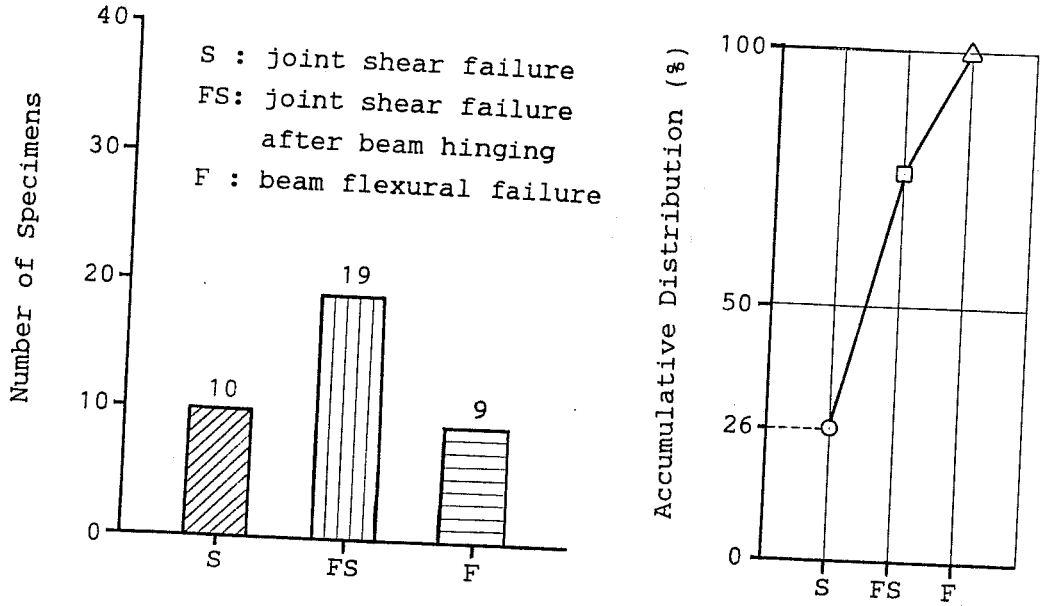

(a) Specimens with Beam Reinforcement Index of $P_t f_y / f_c' < 0.2$

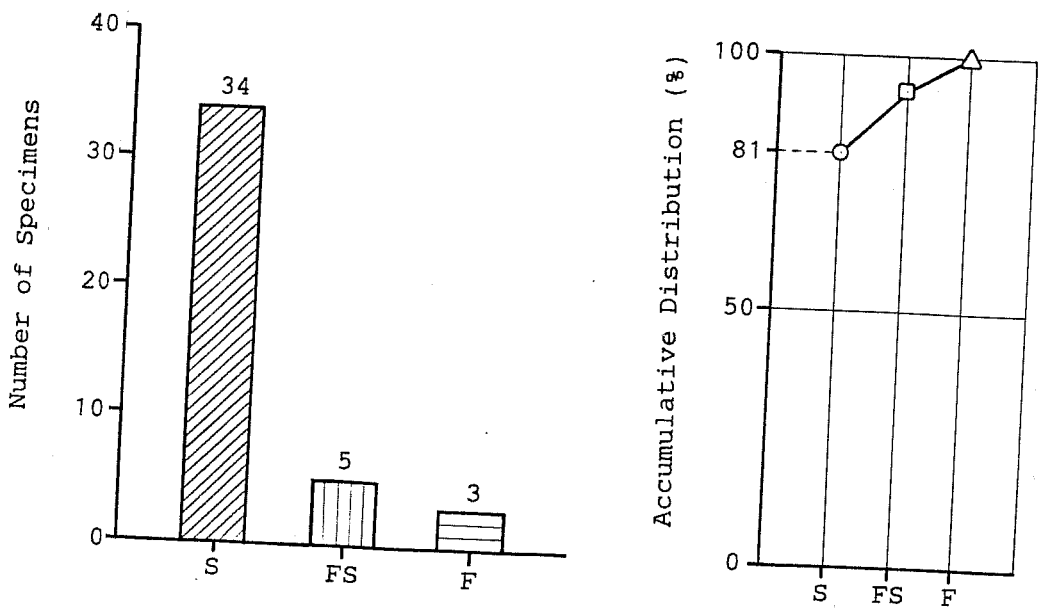

(b) Specimens with Beam Reinforcement Index of $P_t f_y / f_c' \geq 0.2$

Figure 4.14 Effect of Beam Tensile Reinforcement on Failure Mode

(Interior-type Joints)

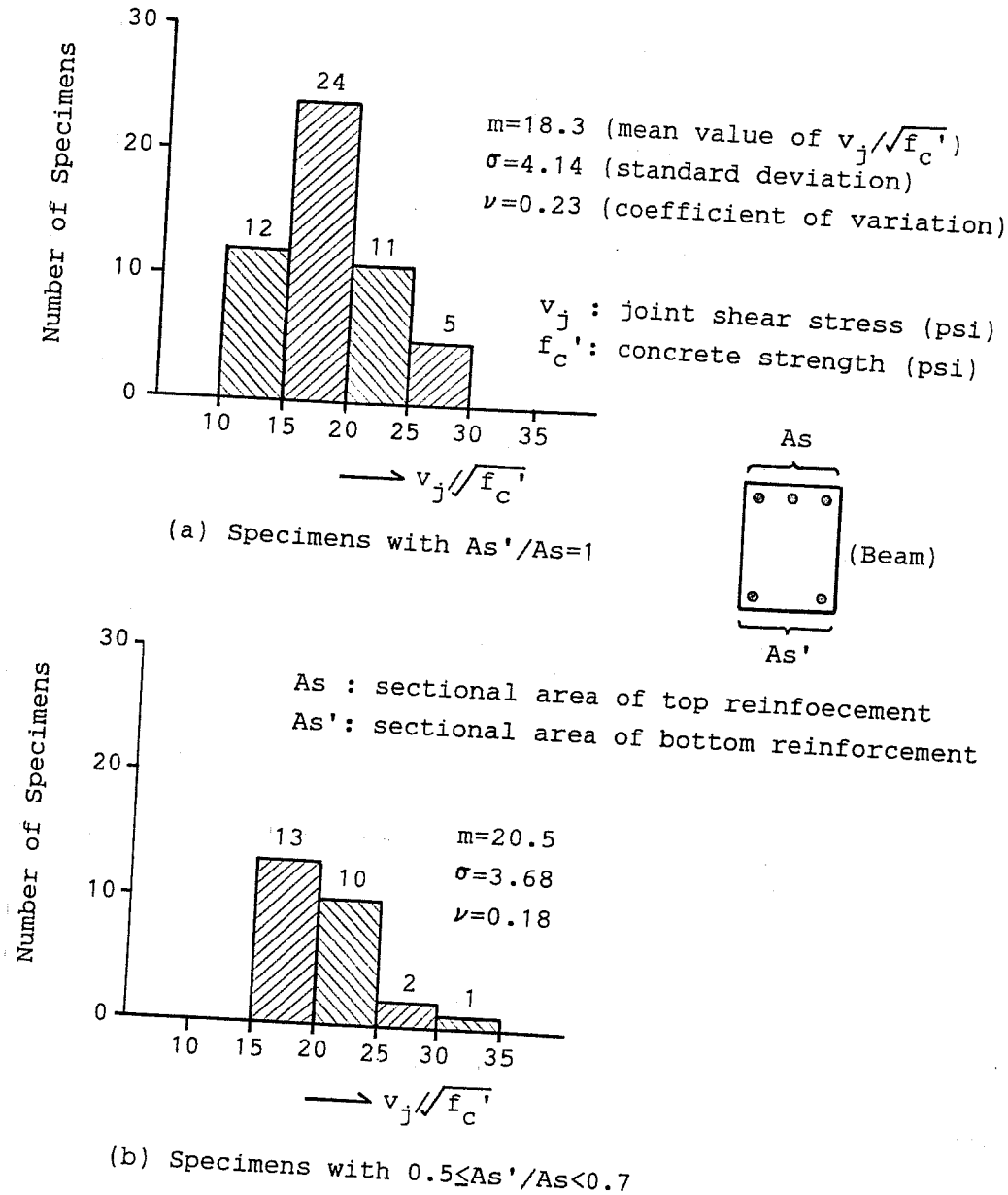

(a) Specimens with As'/As=1

(b) Specimens with 0.5≤As'/As<0.7

Figure 4.15 Effect of Beam Bottom-to-Top Reinforcement Ratio (Interior-type Joints)

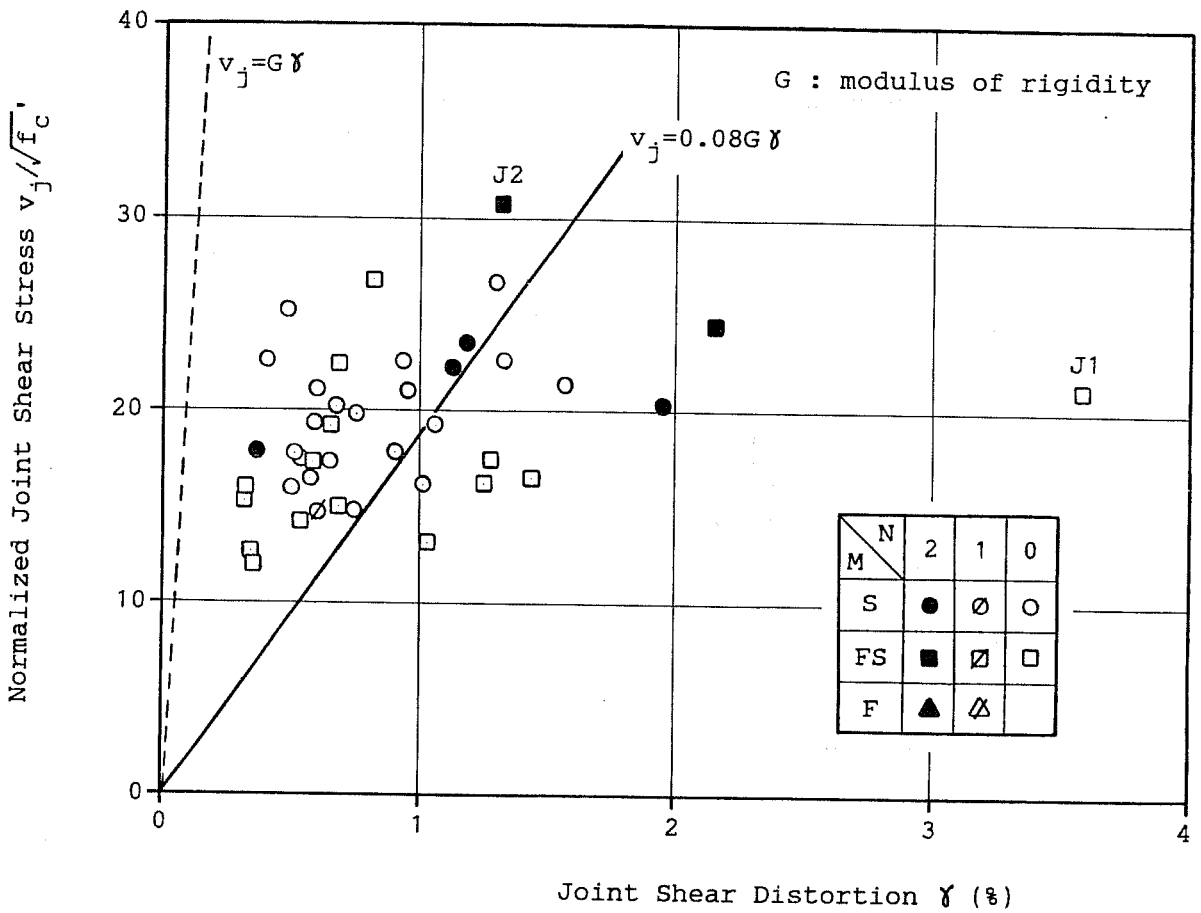

Figure 4.16 Joint Shear Distortion at Maximum Joint Shear Stress

(Interior-type Joints)

references. The broken line shows a shear stress-distortion relation for the joint in the elastic range. Although the test data scattered considerably, the result of a linear regression analysis (solid line) showed that the secant stiffness of the joint at the maximum shear stress levels was reduced to around 8% of the elastic stiffness. It should be noted that the joint in Specimen J1 underwent extremely large distortion when the maximum shear stress was reached.

4.3 Exterior-Type Joints Under Uniaxial Loading

Shear Strength. Histograms for exterior-type joints plotted against normalized joint shear strength are shown in Fig. 4.17. A total of 27 exterior- type joints were analyzed; 19 without transverse beams, 2 without transverse beam and 6 with two transverse beams. As shown in Fig. 4.17(a), the histogram for the joints without transverse beams showed most tests with joint shear strength of $10\sqrt{f_c'}$ or less. The mean value of the joint shear strength was lower than the recommended strength of $12\sqrt{f_c'}$. The specimens with one or two transverse beams, shown in Figs. 4.17(b) and 4.17(c), developed beam flexural yielding and reached a joint shear strength of $15\sqrt{f_c'}$ on the average.

Effect of Concrete Strength. The shear strength measured for the exterior-type joints is plotted against concrete strength in Fig. 4.18. In general, the measured joint shear strength increased with concrete strength. The coefficient of correlation between the joint shear strength and the square root of the concrete strength was 0.55. The shear strength measured for joints with two transverse beams (solid marks) showed good agreement with the recommended value of $15\sqrt{f_c'}$ (solid line). However, shear strength values measured for other joints were widely distributed and many were below the recommended strength of $12\sqrt{f_c'}$ (broken line).

Effect of Beam Bar Development. As shown in Fig. 4.19, beam bars were anchored with 90° hooks into the exterior-type joint. The effect of development length of the hooked beam bars on joints shear strength was examined using two different parameters. One is the ratio of the development length to column depth (ℓ_{dh}/h_c), a ratio of effective depth of the joint section to resist horizontal shear. The other is the ratio of the development length to beam depth (ℓ_{dh}/h_b), a measure of the inclination of the diagonal compressive strut in the joint. These two ratios are based on the assumption that the strut in the exterior-type joint forms between the compressive zone in the beam and section and the bend of the hooked beam bars. Test data and the result of a linear regression analysis are shown in the plot of joint shear strength versus the product of the two ratios. The joint shear strength increased with the product of the two ratios and verified the assumptions made above. The results indicate that joint shear strength is strongly influenced by development length of hooked beam bars. It should be noted that joints with a product of 0.5 or less did not reach the recommended shear strength of $12\sqrt{f_c'}$. The low shear strength for these joints biased correlations with various parameters in Figures 4.20 and 4.21.

Effect of Lateral Reinforcement. Figure 4.20 shows the effect of lateral reinforcement on joint shear strength. The joint shear strength had a tendency to increase with the amount of lateral reinforcement. However, the correlation was not as strong as for the interior-type joints described in the previous section. It should be noted also that the joint shear strength was higher than the reinforcement contribution expected in a beam shear mechanism (broken line).

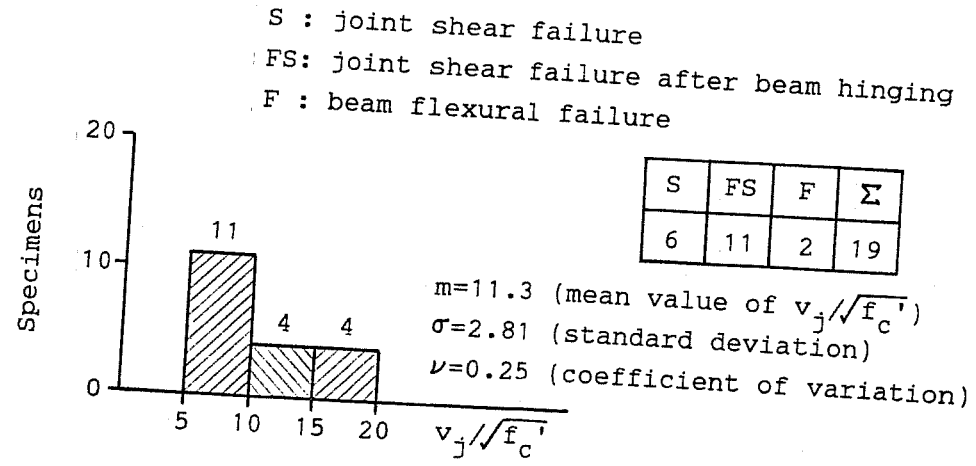

(a) Joints without Transverse Beams (N=0)

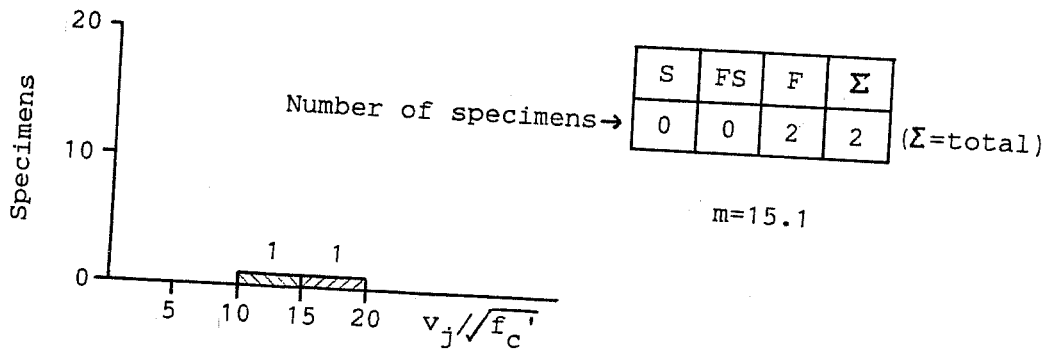

(b) Joints with One Transverse Beam (N=1)

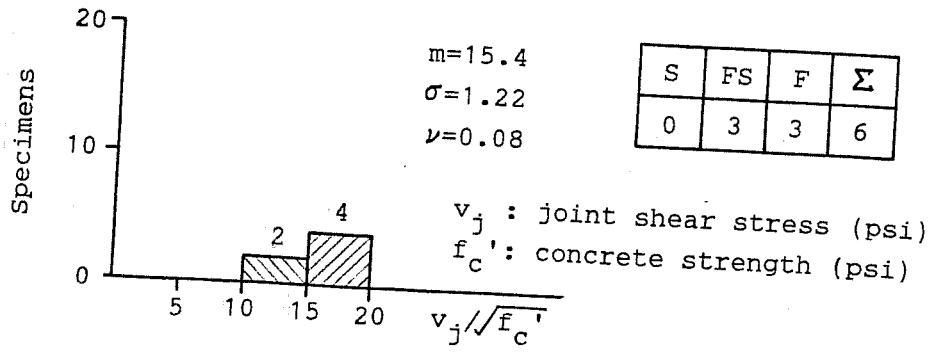

(c) Joints with Two Transverse Beams (N=2)

Figure 4.17 Exterior-type Joints Under Uniaxial Loading

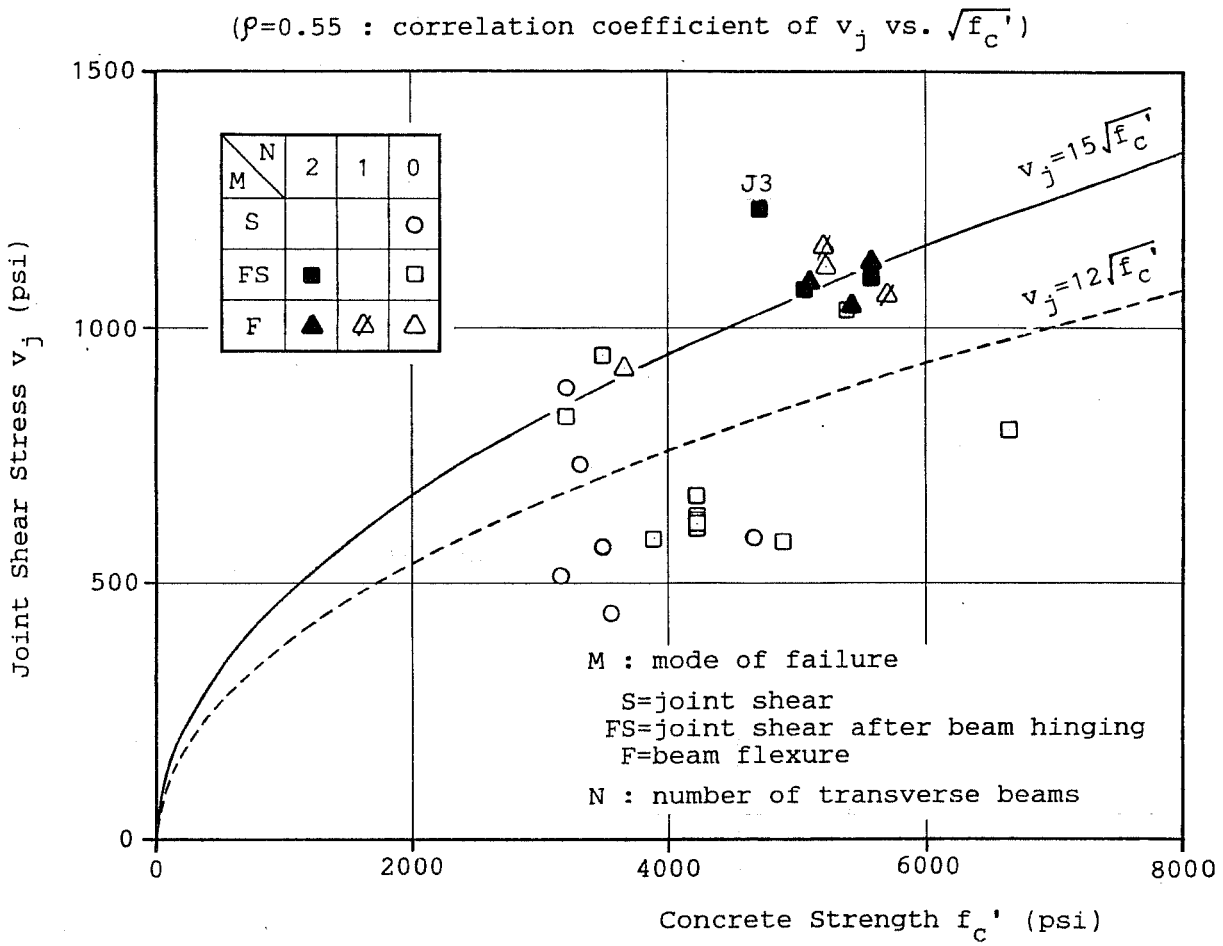

Figure 4.18 Maximum Joint Shear Stress vs. Concrete Strength

(Exterior-type Joints)

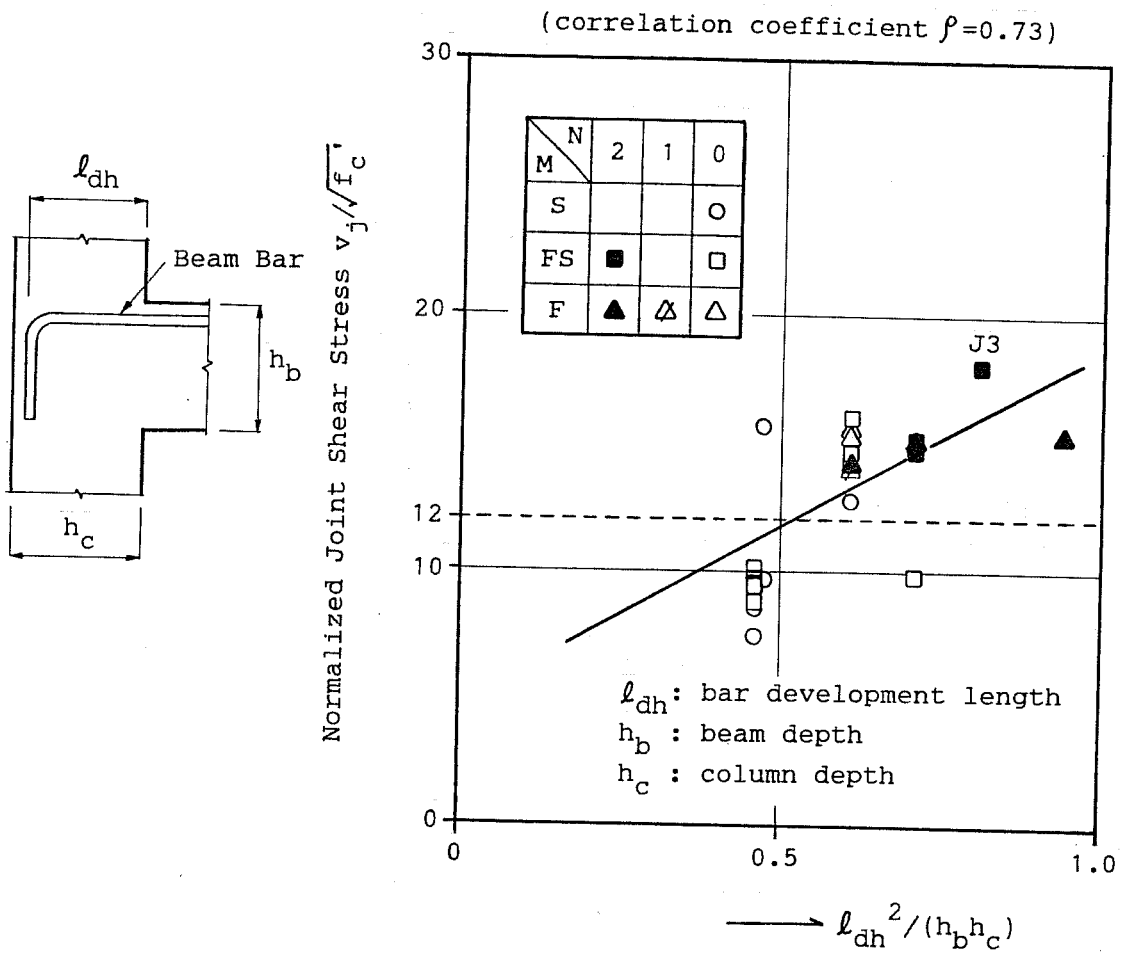

Figure 4.19 Effect of Beam Bar Development Length on Joint Shear Strength (Exterior-type Joints)

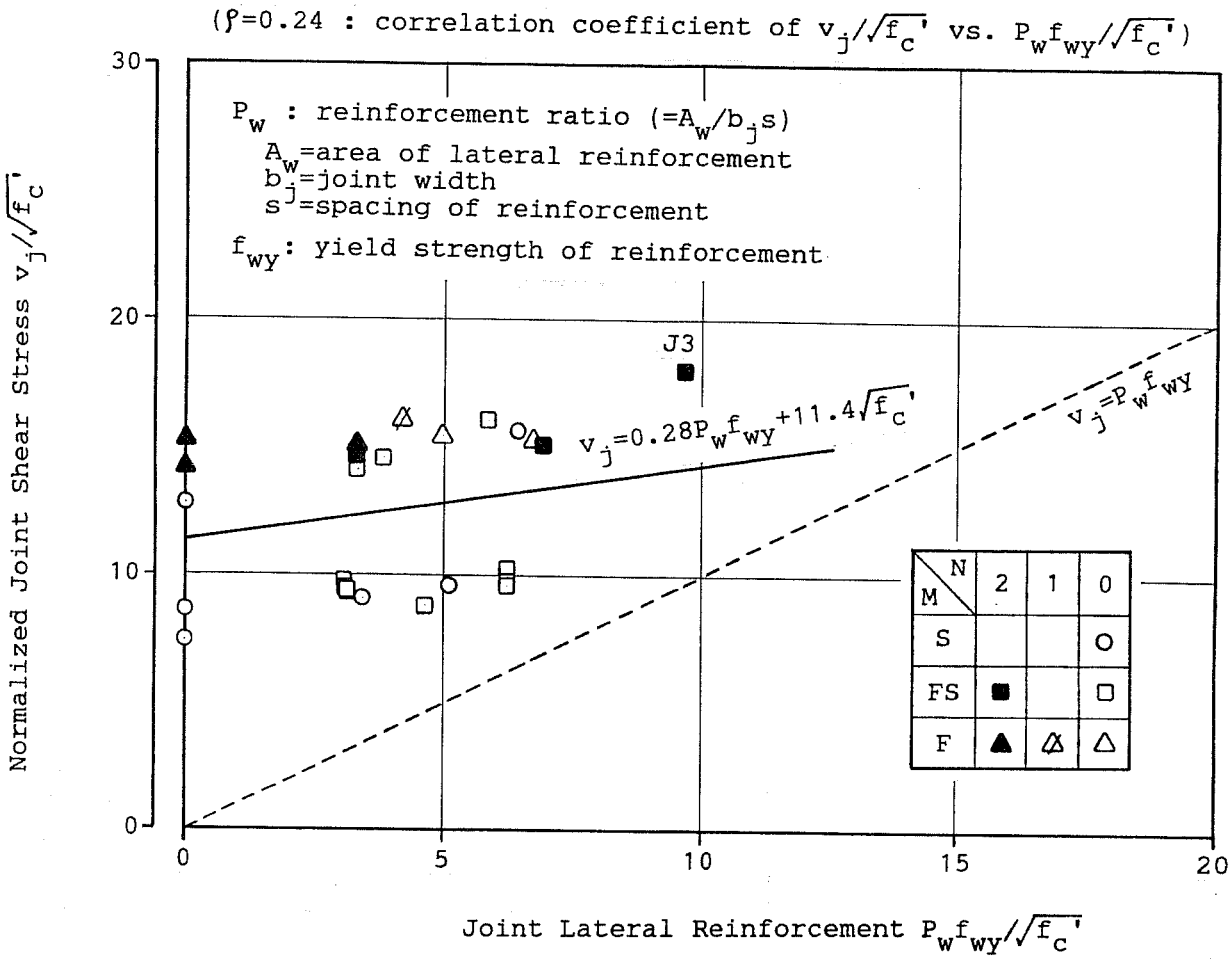

Figure 4.20 Effect of Joint Lateral Reinforcement on Joint Shear Strength (Exterior-type Joints)

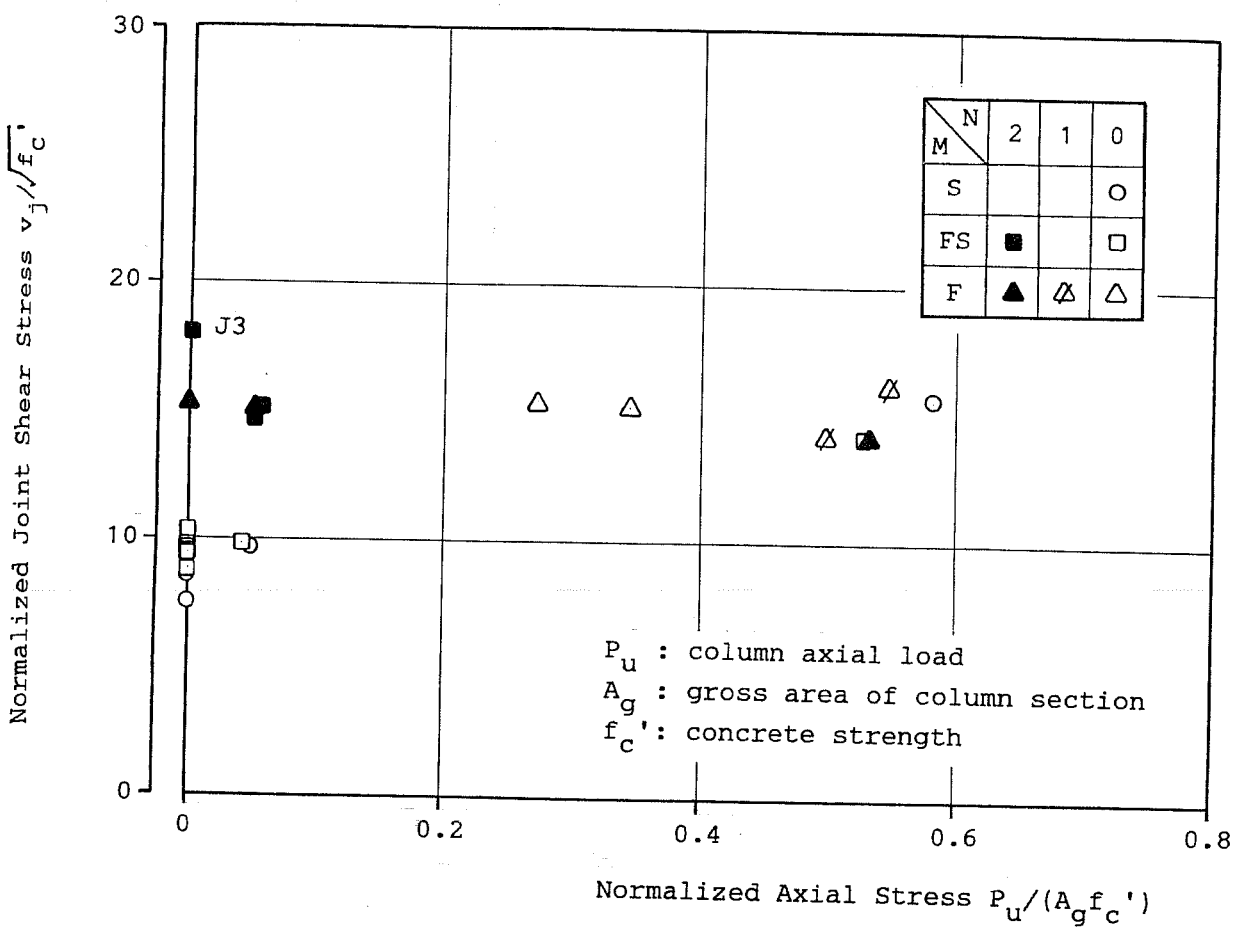

Figure 4.21 Effect of Column Axial Load on Joint Shear Strength

(Exterior-type Joints)

Effect of Axial Load. Figure 4.21 shows the effect of column axial load on joint shear strength. The column axial load did not appear to influence the shear strength for the exterior-type joints.

4.4 Interior and Exterior Joints Under Biaxial Loading

Several joint specimens which had beams in two directions were tasted under biaxial loading. The results of the interior joint tests in which specimens failed in beam flexure (except J2) are shown in terms of measured story shears in Fig. 4.22. Maximum biaxial shears are normalized with maximum uniaxial shears measured in the main loading direction and shown in two plots with the same ordinates and different abscissas. A circular curve (broken line) appeared to represent the biaxial interaction of shears in the two directions somewhat conservatively. It should be noted that the maximum biaxial shears did not reach the point corresponding to simultaneous yielding of the beams in the two directions, even under biaxial loading at an angle of 45° with the beam longitudinal axes.

Biaxial shear strength for interior and exterior joints is shown in Figs. 4.23 and 4.24, respectively. In each figure two plots are given with the same ordinates and different abscissas. The biaxial joint shear strength ranged from 22 to 31 times $\sqrt{f'_c}$ for the interior joints and 15 to 20 times $\sqrt{f'_c}$ for the exterior joints. Circular interaction curves with the recommended strength values of $20\sqrt{f'_c}$ and $15\sqrt{f'_c}$ in radius (broken lines) resulted in a somewhat conservative evaluation of the biaxial joint shear strength in the two cases. It should be noted that Specimen J2 reached much higher strength than any other test.

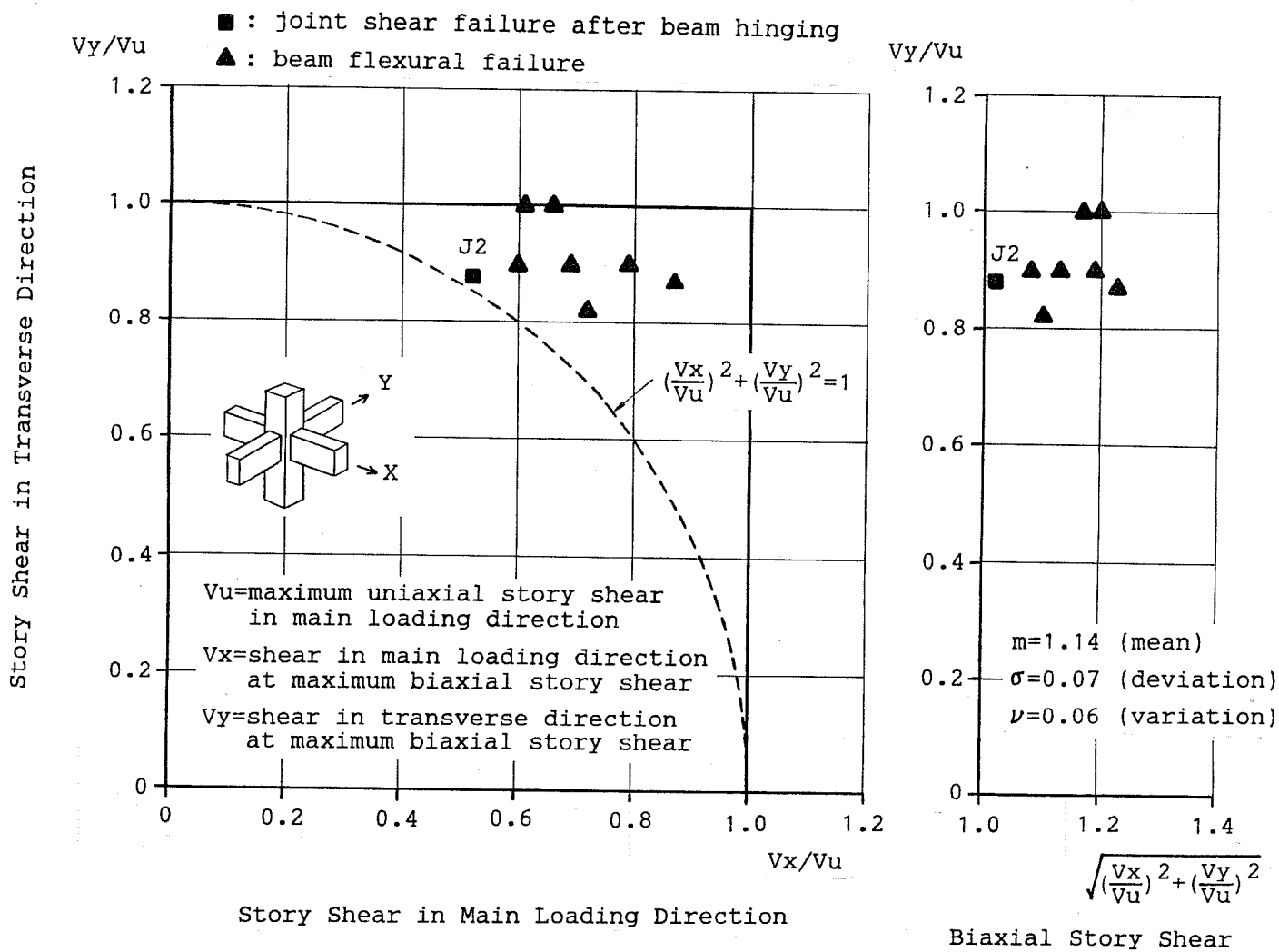

Figure 4.22 Maximum Story Shear for Interior Joints Under Biaxial Loading

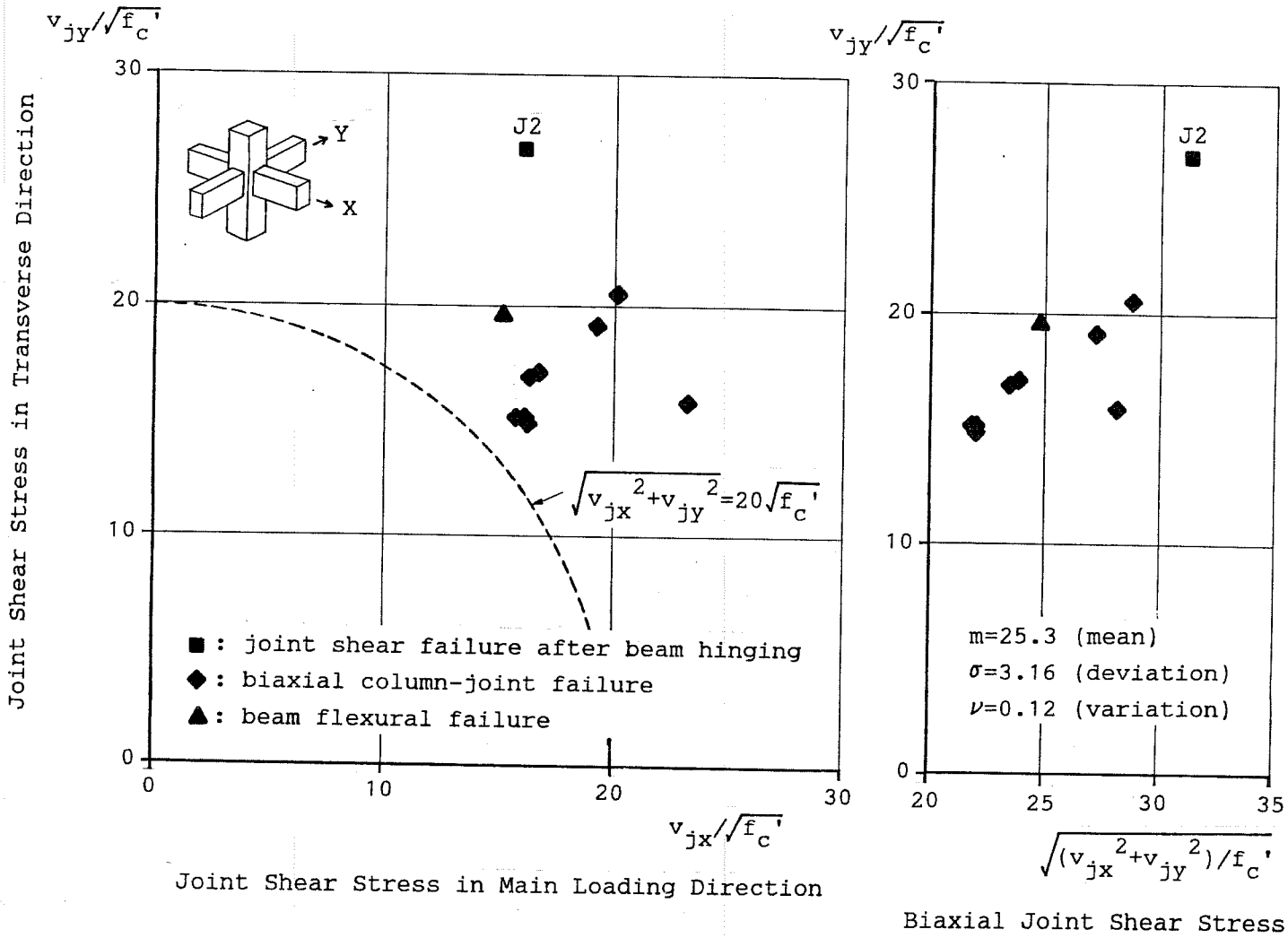

Figure 4.23 Biaxial Joint Shear Strength for Interior Joints

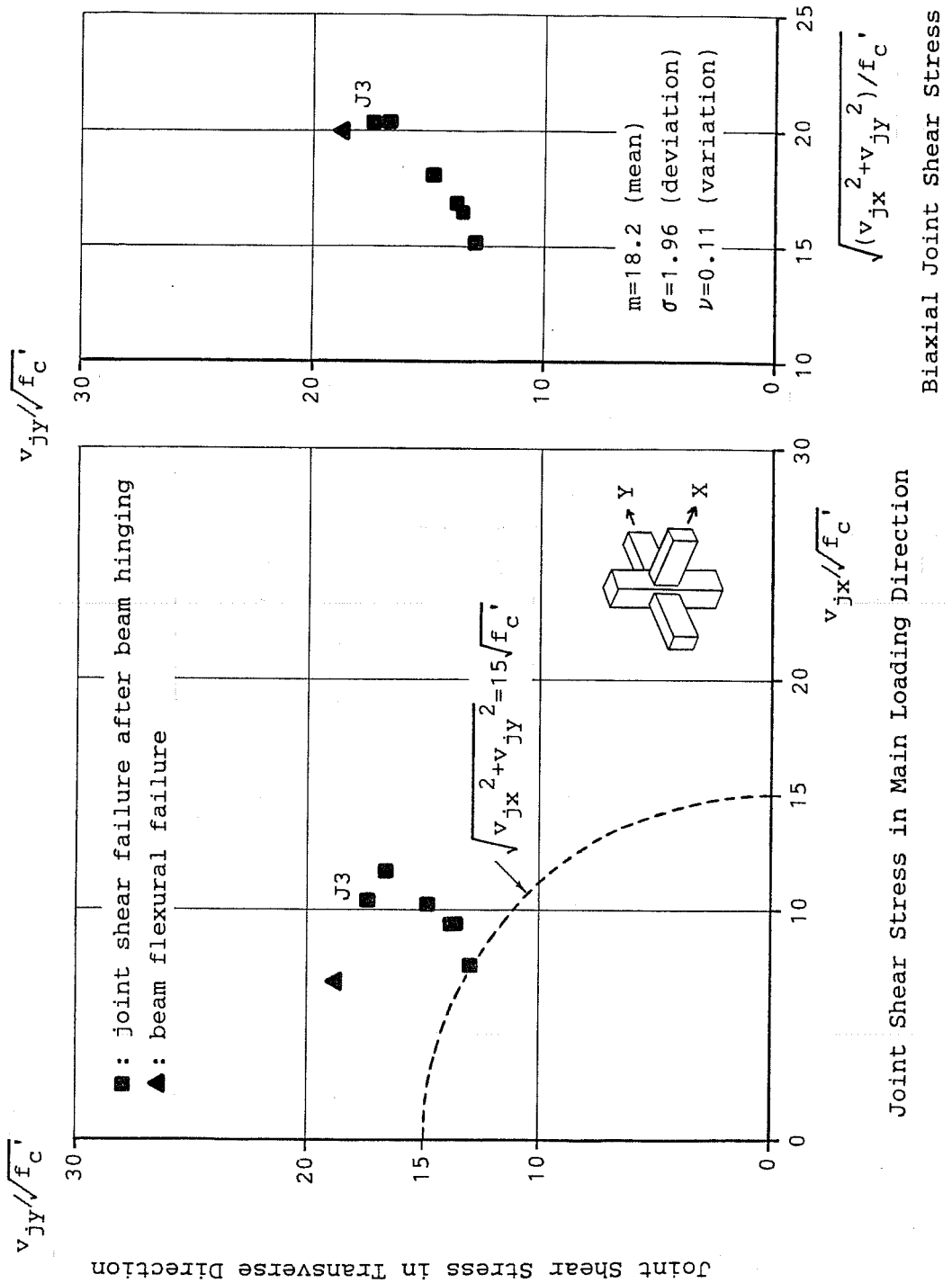

Figure 4.24 Biaxial Joint Shear Strength for Exterior Joints

5. DESIGN RECOMMENDATIONS

5.1 Scope

The recommendations in this chapter apply to cast-in-place reinforced concrete structures which consist of moment-resisting frames designed to resist earthquake motions. The structures should be designed so that the maximum sidesway response to strong ground motions is expected to remain smaller than 2% interstory drift. The recommendations address joints which connect members designed to develop a ductile beam-sidesway mechanism. Beams framing into the joint are expected to form plastic hinges at joint faces and dissipate seismic energy through inelastic deformation reversals during strong earthquake motions.

The recommendations are based on the results of the tests and analysis described in Chapter 4 and provide guidance only in cases where the beam width is less than or equal to the column width and the beam centerline passes through the column centroid. Connections which are structurally different from those described in Chapters 2 through 4 are excluded because of a lack of test data.

5.2 Design of Joints for Biaxial Shear

For joints with beams framing in from two perpendicular directions, the horizontal shear in the joint should be checked under biaxial force conditions. The following equation should be satisfied:

$$\phi V_n \geq V_u \tag{5.1}$$

where ϕ = strength reduction factor, V_n = nominal shear strength of the joint, and V_u = design biaxial shear stress in the joint. The strength reduction factor should be determined by accounting for uncertainties involved in material strength, anticipated forces and design formulas. The reduction factor of 0.85 may be used conforming to the recommendations of ACI 352[3].

5.2.1 Design shear stress in joint should be computed on a horizontal plane at the mid-height of the joint by considering the forces in two orthogonal directions. The design shear stress, V_u should be taken as the larger of V_{ux} or V_{uy}, horizontal joint shear stress generated by beam plastic hinges under unidirectional load conditions.

It should be noted that the joint shear is about 1.2 times the maximum unidirectional shear (See Fig. 4.22). However, no increase in design shear is specified because the strength under bidirectional loading was consistently 20% higher than the values suggested for joint shear strength. A more precise estimate of the design shear stress could be calculated using a correlation coefficient to express response between shear forces in two orthogonal directions. The correlation coefficient has to be determined from a three- dimensional dynamic response analysis using available ground motion records measured in two orthogonal directions. Such analyses are cumbersome and are not likely to substantially improve the design of the joint.

The uniaxial joint shear stress should be determined as follows:

$$V_{ux} \quad (or\ V_{uy}) \quad = \quad \frac{1}{b_j h_c}(\Sigma \frac{M_{bn}}{j_b} \quad - V_{col}) \tag{5.2}$$

where b_j = effective joint width, h_c = column depth in the direction of load being considered, Σ = summation for beams in the direction considered, M_{bn} = nominal beam moment capacity, j_b = internal moment arm in the beam section, and V_{col} = column shear force corresponding to development of beam hinge mechanism. The effective joint width should be the average of the beam and column widths. The internal moment arm may be calculated assuming a rectangular compressive stress block in the beam section but should not be greater than 7/8 times beam effective depth.

The beam moment capacity should be determined using the stress 1.25 fy, where fy is the specified yield strength of the reinforcing bars and 1.25 is a stress multiplier accounting for the difference between the specified yield and the actual bar stresses. The increase is made up of two components: the difference between specified and actual yield strength, and the increase due to strain hardening. The increase due to strain hardening varies with the interstory drift angle. The difference between actual and specified yield depends on the bar size. Since the values may not be known in the design phase, a factor of 1.25 reflects observed response reasonably well.

Slab reinforcement within at least one-third of the entire slab width on each side of the beam should be considered to participate in the beam negative moment capacity. Bottom slab reinforcement at the critical negative sections may be excluded if the reinforcement is not provided with sufficient anchorage into the beam. It should be noted that the column shear force is not constant as indicated by calculations using the beam hinge mechanism.

Column shear is variable and depends on the dynamic behavior of the structure during earthquake motions. After the beams framing into the column have formed plastic hinges at the column face on a number of stories, the column likely behaves as a cantilever. In this case, the inflection point of the column may be located somewhere in the upper stories in which case the column may develop smaller shear forces than those expected in a static analysis. Therefore, the column shear force may be appropriately reduced by referring to the results of a dynamic response analysis if cantilever action is expected to occur.

5.2.2 Nominal shear strength. An interior joint has beams framing into all four sides of the joint as shown in Fig. 4.1(c), and an exterior joint has beams framing into three sides of the joint as shown in Figs. 4.1(b) and 4.2(c). A corner joint has beams framing into one side or two orthogonal sides of the joint as shown in Fig. 4.2(b).

The nominal shear strength of the joint is given by the following equation:

$$V_n \quad = \quad \beta\, \gamma\, \sqrt{f'_c} \quad (psi) \tag{5.3}$$

where f'_c is the compressive strength of concrete in psi.

The constant β should be taken as unity unless the following conditions are satisfied:

a. The value of β may be taken as 1.2 for an interior joint confined by beams of a width at least three-quarters of the column width and by a floor slab with a thickness of at least one-fifth of the beam depth.

b. The value of β for exterior or corner joints should be taken as the product of β_1 and β_2.

$$\beta_1 = 0.9 \; if \; \frac{\ell_{dh}}{h_c} \leq \frac{3}{4}, \qquad \beta_1 = 1.0 \; if \; \frac{\ell_{dh}}{h_c} > \frac{3}{4} \tag{5.4}$$

$$\beta_2 = 0.9 \; if \; \frac{\ell_{dh}}{h_b} \leq \frac{3}{4}, \qquad \beta_2 = 1.0 \; if \; \frac{\ell_{dh}}{h_b} > \frac{3}{4} \tag{5.5}$$

where ℓ_{dh} = development length of hooked beam bars measured from column face (Fig. 4.19), h_c = column depth in the direction of the hooked beam bars, and h_b = beam depth.

The constant γ is given as follows:

$$\gamma = 20 \qquad for \; interior \; joints \tag{5.6}$$

$$\gamma = 15\left(1 + \frac{P_w f_{wy}}{45\sqrt{f'_c}}\right) \leq 20 \qquad for \; exterior \; joints \tag{5.7}$$

$$\gamma = 10\left(1 + \frac{P_w f_{wy}}{30\sqrt{f'_c}}\right) \leq 15 \qquad for \; corner \; joints \tag{5.8}$$

where P_w = lateral reinforcement ratio, and f_{wy} = yield strength of lateral reinforcement. The lateral reinforcement ratio may be calculated as follows:

$$P_w = \frac{A_w}{(sb_j)} \tag{5.9}$$

where A_w = area of lateral reinforcement, s = spacing of the reinforcement, and b_j = effective joint width. According to the results shown in Figs. 4.10(b) and 4.20, it is suggested that the amount of lateral reinforcement should satisfy the following equation:

$$P_w \geq \frac{5\sqrt{f'_c}}{f_{wy}} \tag{5.10}$$

An upper limit on the beam tensile reinforcement is given as a guideline for reducing the possibility for premature shear failure in the joint (Fig. 4.13). The amount of beam tensile (top) reinforcement (within the beam section) should be limited to the following value:

$$P_t \leq 0.2 \, \frac{f'_c}{fy} \tag{5.11}$$

where P_t = tensile reinforcement ratio, and fy = yield strength of beam reinforcement. The tensile reinforcement ratio is given as follows:

$$P_t = \frac{A_s}{b_b h_b} \tag{5.12}$$

where A_s = area of tensile reinforcement within the beam section (excluding steel in the slab considered in computing beam capacity), b_b = beam width, and h_b = beam depth.

5.3 Development of Reinforcement

The recommendations of ACI 352[3] provide an equation for determining development length of a bar terminating in a 90° standard hook. The recommended development length appears to be appropriate because hooked beam bars in Specimen J3 reached higher stresses than calculated using ACI 352. However, the top beam bars in J3 developed anchorage distress, probably because heavy congestion of vertical bars (column bars and extensions of hooked top bars) accelerated spalling of concrete on the exterior side and the cover over the bars was lost. Therefore, the bars should be carefully arranged by providing more clear space between bars in the joint.

The recommendations of ACI 352 also specify the minimum values of the joint depth to bar diameter ratio to limit slippage of the beam and column bars through the joint. The recommended value of 20 appeared appropriate because top beam bars in Specimen J2 (column depth / beam bar diameter = 20) showed good bond behavior under cyclic loading at large deflection levels. The influence of bond deterioration on member response was discussed in Section 3.3. It is particularly important to note that for joints with slabs, the neutral axis is very high in the section, and the top reinforcement may be below the vertical axis under positive bending in the beam. As a result the beam bars will not be subjected to large stress reversals across the joint.

Bond deterioration along longitudinal reinforcement is considered to cause the following undesirable phenomena:

a. loss of moment capacity

b. premature crushing of concrete

c. slip deformation

d. pinching in hystersis curves

Among these, slip deformation and pinching in hysteresis curves are particularly important for frame structures designed to resist earthquake motions through inelastic deformation reversals because they reduce energy-dissipating capacity and may result in excessive deformations. Therefore, the effect of bond deterioration on performance of the structure should be examined by using hysteresis curves which include the effects of bond deterioration in a dynamic response analysis. It should be noted that pinching in hysteresis curves is possibly caused by various sources as discussed in Section 3.1. For example, heavy top reinforcement in the beam section likely causes flexural pinching by closing cracks in the bottom concrete under downward loading. Attention should be paid to flexural and shear pinching as well as pinching caused by bond deterioration.

6. CONCLUSIONS

6.1 Summary of Test Results

Three full-scale reinforced concrete specimens were tested uniaxially and biaxially to study the behavior of slab-beam-column connections under seismic load conditions. The results of the tests are summarized as follows:

1. All specimens developed beam flexural yielding at 2% drift cycles and then failed in joint shear at 4% drift cycles.
2. All specimens showed considerable pinching in story shear-drift angle relations. Pinching is likely due to shear distress in the joint, flexural distress in the slab, beam and column, and bond or anchorage deterioration along beam bars.
3. Biaxial interaction was evident in the measured story shears in which loading in one direction lowered the story shear in the other direction.
4. All joints developed yielding of lateral reinforcement and exhibited shear distortions which contributed to an increasing amount of story drift. Among the three specimens, the joint with beams in only one direction exhibited the largest shear distortion and it dominated the overall response of the specimen.
5. The measured strength of all specimens was higher than that calculated for joint shear failure. The interior joint with beams in two directions reached the highest strength of the three specimens.
6. The measured biaxial strength exceeded the measured uniaxial strength. The biaxial interaction curve for joint shear strength can be represented conservatively by a circle or an ellipse constructed between the calculated uniaxial strength values in the two orthogonal directions.
7. In the exterior joint, the top beam hooked bars whose tail extensions lined up with column bars on the exterior side developed anchorage distress at 4% drift levels due to spalling of cover concrete over the extensions, and caused large rotations at the column face.
8. Top straight beam bars with a column depth to bar diameter ratio of 20 showed good bond behavior under large deflection reversals. Bottom straight beam bars with a column depth to bar diameter ratio of 27 exhibited a loss of bond stress likely due to redistribution of compressive stresses from bars to concrete at the level of the bottom bars.
9. The column developed concrete crushing at 2% drift levels under a biaxial load less than the calculated capacity. As a result, there was pinching of the hysteresis curves with further loading.

10. Column bars developed saddle-shaped hysteresis in story shear- strain relations probably due to the effect of joint shear.

11. The slab width acting with the beam in negative bending increased with drift angle. The slab supported on transverse beams was more effective than a slab with no transverse beams.

6.2 Joint Shear Strength

The effect of various factors on joint shear strength was analyzed using test results reported here and those reported elsewhere in Japan and in the United States. The results of the analysis are summarized as follows:

1. A transverse beam on only one side of the joint did not appear to influence joint shear strength. However, transverse beams on both sides of the joint enhanced the joint shear strength.

2. Joint shear strength is directly related to concrete compressive strength.

3. Beam width appeared to influence joint shear strength.

4. Column axial load had no influence on joint shear strength.

5. The amount of lateral reinforcement influenced shear strength for the joint in cases with only one or no transverse beam framing into the joint.

6. The development length of hooked beam bars influenced the shear strength of exterior-type joints.

7. The shear strength for interior-type joints had a tendency to decrease with the beam-to-column depth ratio and with the column depth to beam bar diameter ratio.

8. Most interior-type joints with a beam reinforcement index of 0.2 or more failed in shear prior to developing beam flexural yielding.

9. The maximum biaxial story shear for specimens which failed in beam flexure did not reach the point corresponding to simultaneous yielding of the beams in the two directions.

10. The recommended values of $10\sqrt{f'_c}$ and $15\sqrt{f'_c}$ for interior and exterior joints appear to be a conservative estimate of the biaxial joint shear strength.

6.3 Design Recommendations

A method to design the joint for biaxial shear was recommended based on the results of the tests and analysis reported here. The method is summarized as follows:

1. The design shear stress in the joint should be the larger of uniaxial shear stresses in two orthogonal directions.

2. The uniaxial shear stress in the joint should be calculated from a beam hinge mechanism where the beam moment capacity accounts for increased stresses (due to strain loading) in longitudinal bars and for participation of slab reinforcement.

3. The nominal shear strength for an interior joint should be taken entirely by concrete. The shear strength for exterior and corner joints should be provided mainly by concrete but the contribution may be enhanced by lateral reinforcement.

REFERENCES

1. "Summary of Meeting," The U.S.-N.Z.-Japan Seminar on Design of Reinforced Concrete Beam-Column Joints, Monterey, California, July 30-August 1, 1984.

2. "Summary of Meeting," The U.S.-N.Z.-Japan Seminar on Design of Reinforced Concrete Beam-Column Joints, Tokyo, Japan, May 29-30, 1985.

3. ACI-ASCE Committee 352, "Recommendations for Design of Beam- Column Joints in Monolithic Reinforced Concrete Structures," (ACI 352 R-85), American Concrete Institute, Detroit, 1985.

4. ACI Committee 318, "Building Code Requirements for Reinforced Concrete (ACI 318-83)," American Concrete Institute, Detroit, 1983.

5. "Code of Practice for the Design of Concrete Structures," (NZS 3101, Part 1:1982), Standards Association of New Zealand, Wellington, 1982.

6. "Standard for Structural Calculation of Steel Reinforced Concrete Structures," Architectural Institute of Japan, 1975.

7. Otani, S., Kitayama, K., and Aoyama, H., "Beam Bar Bond Stress and Behavior of Reinforced Concrete Interior Beam-Column Connections," The U.S.- N.Z.-Japan Seminar on Design of Reinforced Concrete Beam-Column Joints, Tokyo, Japan, May 29-30, 1985.

8. Kamimura, T., "Ultimate Shear Strength of Reinforced Concrete Beam-Column Joints," (In Japanese), Transactions of the Architectural Institute of Japan, Extra, October, 1975.

9. Sonobe, Y., and Ishibashi, K., "Experimental Study on Beam-Column Joints with D51 Reinforcing Bars," (In Japanese), Quarterly "Column", No. 69, July 1978.

10. Shibata, T., and Joh, O., "Behavior of R/C Interior Beam-Column Joints with Various Details under Cyclic Lateral Loads," The U.S.-N.Z.-Japan Seminar on Design of Reinforced Concrete Beam-Column Joints, Monterey, California, July 30-August 1, 1984.

11. Otani, S., Kobayashi, Y., and Aoyama, H., "Reinforced Concrete Interior Beam-Column Joints under Simulated Earthquake Loading," The U.S.-N.Z.- Japan Seminar on Design of Reinforced Concrete Beam-Column Joints, Monterey, California, July 30-August 1, 1984.

12. Noguchi, H., and Kurusu, K., "The Effect of Beam Bar Bond and Joint Shear on the Behavior of Reinforced Concrete Interior Beam-Column Joints," The U.S.-N.Z.-China Seminar on Design of Reinforced Concrete Beam-Column Joints, Christchurch, New Zealand, August 10-12, 1987.

13. Kamimura, T., et al., "Experimental Study on Reinforced Concrete Beam-Column Joints," (In Japanese) Transactions of the Architectural Institute of Japan, Extra, September 1978 and 1979.

14. Owada, Y., "Experimental Study on Effect of Transverse Beams on Reinforced Concrete Beam-Column Joints," (In Japanese), Transactions of the Architectural Institute of Japan, Extra, October 1976 and 1977.

15. Owada, Y., "Experimental study on Effect of Transverse Beams on Reinforced Concrete Beam-Column Joints," (In Japanese), Proceedings of the Kanto District Symposium, Architectural Institute of Japan, July 1977.

16. Bessho, S., et al., "Experimental Study on Beam-Column Joints in reinforced Concrete High-Rise Buildings," (In Japanese), Transactions of the Architectural Institute of Japan, Extra, September 1979.

17. Yamada, T., et al., "test of Structural Members and Frames in Tall Buildings Utilizing the Reinforced Concrete Layered Construction System," (In Japanese), Taisei Technical Research Report, No. 18, March 1986.

18. Sugano, S., et al., "Report on Full-Scale Test of Reinforced Concrete Beam-Column Joints," (In Japanese), Takenaka Technical Research Institute, January, 1986.

19. Fujii, S., and Morita, S., "Behavior of Exterior Reinforced Concrete Beam-Column-Slab Sub-assemblages under Bi-Directional Loading," The U.S.-N.Z.-Japan-China Seminar on Design of Reinforced Concrete Beam-Column Joints, Christchurch, New Zealand, August 10-12, 1987.

20. Tada, T., Takeda, T., and Takemoto, Y., "Experimental Study on Reinforcing Method for Reinforced Concrete Beam-Column Joints," (In Japanese), Proceedings of the Kanto District Symposium, architectural Institute of Japan, July 1976.

21. Tada, T., and Takeda, T., "Experimental Study on Reinforcing Method for Reinforced Concrete Beam-Column Joints," (In Japanese), Transactions of the architectural Institute of Japan, Extra, September 1981.

22. Wakabayashi, M., Et al., "Experimental Study on Force Transfer Mechanism and Strength of Reinforced Concrete Beam-Column Joints," (In Japanese), Transactions of the Architectural Institute of Japan, Extra, October 1977.

23. Sugano, S., Et al., "Experimental Study on Columns and Frames in High-Rise Reinforced Concrete Buildings," (In Japanese), Transactions of the architectural Institute of Japan, Extra, August 1986.

24. Yamanobe, K., et al., "Study on structural Characteristics of Reinforced concrete High-Rise Residential Buildings," (In Japanese), Transactions of the Architectural Institute of Japan, Extra, October 1985.

25. Meinheit, D.F., and Jirsa, J.O., "Shear Strength of R/C Beam- Column Connections," Journal of the Structural Division, Proceedings of the American Society of Civil Engineers, Vol. 107, ST 11, November 1981.

26. Hanson, N.W., "Seismic Resistance of Concrete Frames with Grade 60 Reinforcement," Journal of the structural Division, Proceedings of the american Society of Civil Engineers, Vol. 97, ST6, June 1971.

27. Hanson, N.W., and Conner, H.W., "tests of Reinforced Concrete Beam-Column Joints under Simulated Seismic Loading," Research and Development Bulletin RD012, Portland Cement Association, Skokie, Illinois, 1972.

28. Morita, S., and Fujii, S., "Interactive Decay of Bent-Bar Anchorage and Joint-Shear Capacity at Exterior Beam-Column Joints under Reversed Cyclic Loadings," The U.S.-N.Z.-Japan Seminar on Design of Reinforced Concrete Beam-Column Joints, Monterey, California, July 30-August 1, 1984.

29. Kanada, K., Fujii, S., and Morita, S., "Effect of Joint Shear Reinforcement on Behaviors of Exterior Beam-Column Joints Under Reversed Cyclic Loadings," The U.S.-N.Z.-Japan Seminar on Design of Reinforced Concrete Beam- Column Joints, Tokyo, Japan, May 29-30, 1985.

30. Bessho, S., et al., "Full-scale Test of Exterior Beam-Column Joint with U-Shaped Beam Bar Anchorage," (In Japanese), Kajima Technical Research Report, No. 25, June 1977.

31. Hanson, N.W., and Conner, H.W., "Seismic Resistance of Reinforced Concrete Beam-Column Joints," Journal of the Structural Division, Proceedings of the american Society of Civil Engineers, Vol. 93, ST5, October 1967.

32. Kitayama, K., Otani, S., and Aoyama, H., "Behavior of Reinforced Concrete Beam-Column Connections," The U.S.-N.Z.-Japan-China Seminar on Design of Reinforced Concrete Beam-Column Joints, Christchurch, New Zealand, August 10- 12, 1987.

33. Suzuki, N., Halim, J.K., Otani, S., and Aoyama, H., "Behavior of Reinforced Concrete Beam-Column Subassemblages With and Without Slab," Department of Architecture, Faculty of Engineering, The University of Tokyo, March 1984.

34. Leon, R.T., "The Influence of Floor Members on the Behavior of RC Beam-Column Joints Subjected to Severe Bidirectional Cyclic Loads," Ph.D. Thesis, The University of Texas at Austin, December 1983.

35. Shibata, T., and Joh, O., "Behavior of Three-Dimensional R/C Beam-Column Subassemblages with Slab," The U.S.-N.Z-Japan Seminar on Design of reinforced Concrete Beam-Column Joints, Tokyo, Japan, May 29-30, 1985.

APPENDIX A: LONGITUDINAL BAR POSITIONS

A.1 Specimen J1

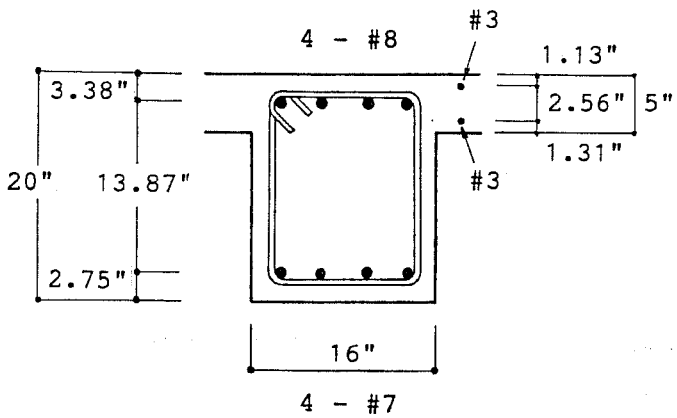

Figure A.1(a) Beam Bars

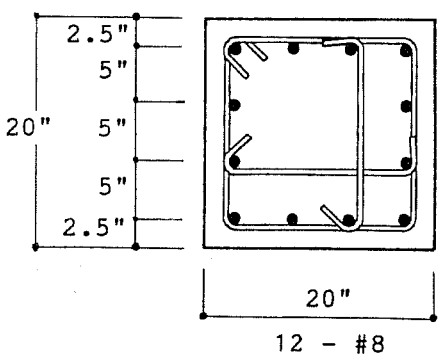

Figure A.1(b) Column Bars

A.2 Specimen J2

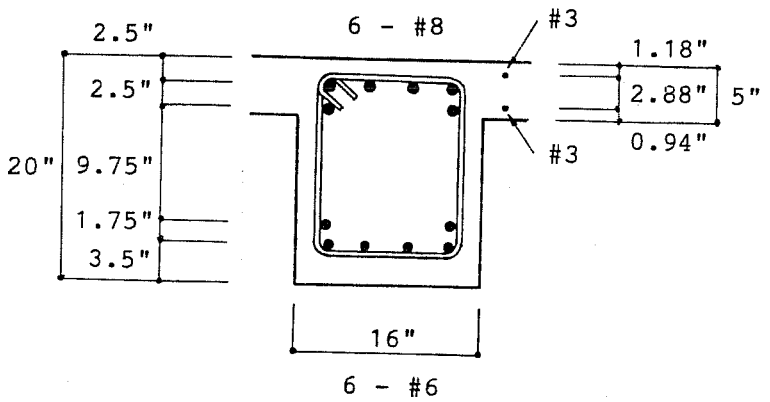

Figure A.2(a) East-West Beam Bars

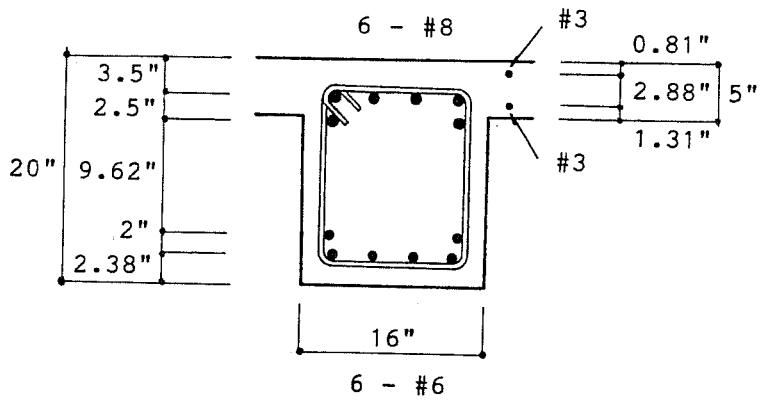

Figure A.2(b) North-South Beam Bars

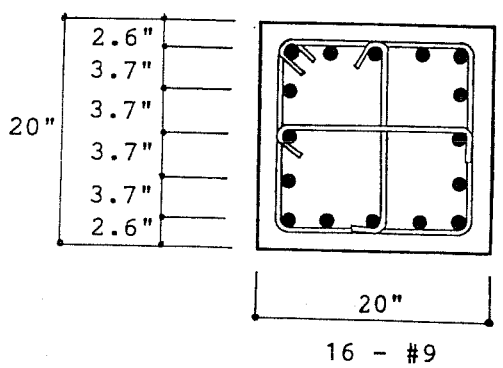

Figure A.2(c) Column Bars

A.3 Specimen J3

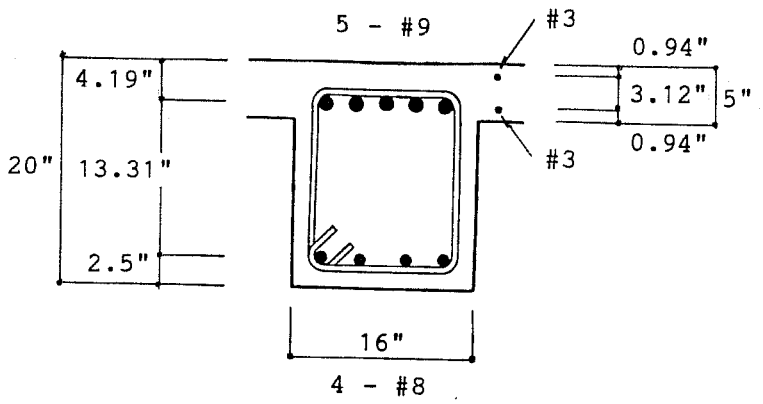

Figure A.3(a) West Beam Bars

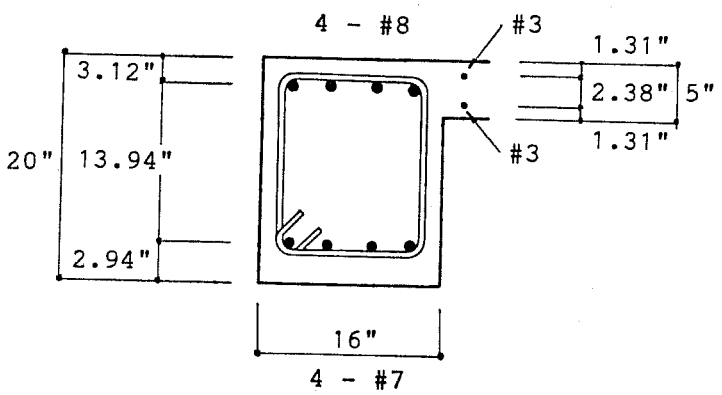

Figure A.3(b) North-South Beam Bars

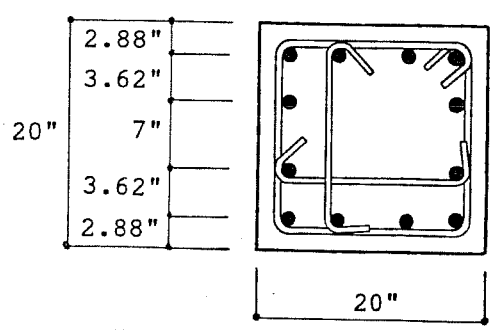

Figure A.3(c) Column Bars

APPENDIX B:
LOADS AND DISPLACEMENTS AT LOADING PEAKS

Notation

P_E : east beam load (kips)

P_W : west beam load (kips)

P_N : north beam load (kips)

P_S : south beam load (kips)

V_{EW} : story shear in east-west direction (kips)

V_{NS} : story shear in north-south direction (kips)

D_E : east ram displacement (in.)

D_W : west ram displacement (in.)

D_N : north ram displacement (in.)

D_S : south ram displacement (in.)

R_{EW} : corrected drift angle in east-west direction (%)

R_{NS} : correct drift angle in north-south direction (%)

Table B.1 Loads and Displacements at Load Cycle Peaks, Specimen J1

Load Cycle	P_E	P_W	V_{EW}	D_E	D_W	R_{EW}
1	11.9	-22.1	19.8	-0.3	0.42	0.4
	-22.7	11.9	-20.1	0.4	-0.3	-0.4
2	15.6	-18.5	19.8	-0.4	0.5	0.4
	-18.6	15.6	-19.9	0.4	-0.4	-0.4
3	28.6	-33.2	36.0	-1.1	1.1	1.2
	-36.0	28.0	-37.3	1.2	-1.2	-1.2
4	35.0	-46.2	47.3	-1.9	1.9	1.9
	-47.9	33.9	-47.6	1.9	-1.9	-1.9
5	31.9	-40.2	42.0	-1.9	1.9	1.9
	-41.3	31.0	-42.1	1.9	-1.9	-1.9
6	34.0	-52.6	50.3	-3.9	3.9	3.9
	50.0	30.9	-47.0	3.9	-3.9	-3.8
7	25.7	-38.2	37.2	-3.8	3.9	3.8

Table B.2
Loads and Displacements at Load Cycle Peaks, Specimen J2

Load Cycle	P_E	P_W	V_{EW}	D_E	D_W	R_{EW}
1	-20.2	25.0	26.2	0.4	-0.4	0.4
	26.2	-18.7	-26.0	-0.4	0.4	-0.4
2	-18.7	24.6	25.1	0.4	-0.4	0.4
	25.	-18.6	-25.8	-0.5	0.4	-0.4
3	-31.1	42.3	42.8	1,0	-1.0	1.0
	41.4	-30.8	-42.0	-1.0	1.0	-1.0
5	-44.1	66.5	64.3	2.0	-2.0	2.1
	63.3	-43.6	-62.2	-2.0	2.0	-2.0
6	-41.4	61.6	60.0	2.0	-2.0	2.0
	59.3	-41.1	-58.4	-2.0	2.0	2.0
7	-39.8	58.4	57.2	1.9	-1.9	2.0
	54.1	-39.0	-54.1	-2.0	2.0	-2.0
8	-34.2	51.0	49.6	1.9	-1.9	2.0
	45.4	-32.3	-45.1	-2.0	2.0	-2.0
9	-48.4	75.3	72.0	3.9	-3.9	4.0
	71.6	-46.1	-68.4	-3.9	3.9	-4.0
10	-47.5	66.2	66.1	3.9	-3.9	4.1
	64.2	-43.0	-62.4	-3.9	3.9	-4.0
11	-44.8	62.4	62.4	3.9	-3.9	4.1
	57.1	-38.6	-55.6	-3.9	3.9	-4.0
12	-34.7	41.9	44.5	3.9	-3.9	4.0
	41.6	-29.7	-41.5	-3.9	3.9	-4.0

Load Cycle	P_N	P_S	V_{NS}	D_N	D_S	R_{NS}
4	-33.4	39.2	42.2	1.3	-1.3	1.0
	40.9	-32.3	-42.6	-1.2	1.2	-1.0
7	-44.0	55.9	58.1	2.4	-2.4	2.0
	58.9	-43.0	-59.3	-2.3	2.3	-2.0
8	-39.0	48.6	51.0	2.2	-2.2	2.0
	51.0	-38.1	-51.8	-2.3	2.3	-2.0
11	64.3	-44.0	-63.0	-4.2	4.2	-4.0
	-41.5	57.4	57.5	4.2	-4.2	4.0
12	50.6	-34.0	-49.2	-4.1	4.1	-4.0
	-33.9	45.3	46.1	4.1	-4.1	4.0

Table B.3
Loads and Displacements at Load Cycle Peaks, Specimen J3

Load Cycle	P_W	V_{EW}	D_W	R_{EW}
1	29.4	17.1	-0.5	0.5
	-29.0	-16.9	0.5	-0.5
3	44.7	-26.0	-0.9	1.0
	-47.1	-24.3	0.9	-0.9
5	72.7	42.3	-1.9	2.0
	-56.9	-33.1	2.12	-2.0
6	69.3	40.3	-2.0	2.1
	-56.0	-32.6	2.2	-2.1
7	66.6	38.7	-1.9	2.1
	-53.1	-30.9	2.1	-2.0
8	52.0	30.2	-1.9	2.1
	-46.3	-26.9	2.0	-2.0
9	78.7	45.8	-3.9	4.1
	-57.4	-33.4	3.9	-3.9
10	73.8	42.9	-3.9	4.1
	-55.2	-32.1	3.8	-3.9
11	70.6	41.1	-3.9	4.1
	-52.4	-30.5	3.9	-3.9
12	47.0	27.3	-3.9	4.2
	-42.4	-24.7	3.9	-4.0

Load Cycle	P_N	P_S	V_{NS}	D_N	D_S	R_{NS}
2	-18.9	17.1	21.0	0.6	-0.7	0.4
	19.0	-17.4	-21.2	-0.5	0.5	-0.5
4	-27.9	30.2	33.8	1.2	-1.2	1.0
	31.3	-26.5	-33.7	-1.1	1.1	-1.0
7	-35.5	44.1	46.3	2.2	-2.2	2.1
	46.0	-32.7	-45.7	-2.2	2.2	-2.0
8	-31.0	38.8	40.6	2.1	-2.1	2.1
	39.1	-27.8	-38.9	-2.1	2.0	-1.9
11	-35.9	-46.6	48.0	4.1	-4.2	4.1
	46.6	-30.9	-45.1	-4.1	4.1	-4.0
12	33.0	-27.0	-34.9	-4.0	4.0	-4.9
	-25.6	33.3	34.3	4.1	-4,1	4.1

APPENDIX C: CALCULATIONS

C.1 Initial Stiffness (see Fig. C.1)

$$K = 1 \,/\, (1 \,/\, K_b + 1 \,/\, K_c + 1 \,/\, K_j) \qquad \text{(initial stiffness)}$$

$$K_b = 12EI_b \,/\, (1-u)^3 L^2 [1 + 12EI_b k \,/\, (1-u)^2 GA_b L] \qquad \text{(beam stiffness)}$$

$$K_c = 12EI_c \,/\, (1-v)^3 H^2 [1 + 12EI_c k \,/\, (1-v)^2 GA_c H] \qquad \text{(column stiffness)}$$

$$K_j = GB_j h_b h_c \,/\, H(1-u-v)^2 \qquad \text{(joint stiffness)}$$

where

$$I_b = \gamma b_b h_b^3 \,/\, 12 \,,\; A_b = b_b h_b$$

$$\gamma = 1 + 2rs^3 + 6rs(1-2)^2 \,/\, (1+2rs)$$

$$I_c = b_c h_c^3 \,/\, 12 \,,\; A_c = b_c h_c$$

$$k = 1.5 \qquad \text{(shape factor for shear distortion)}$$

$$E = 57\sqrt{f_c'} \qquad \text{(modulus of elasticity)}$$

$$G = E \,/\, 2(1+P) \qquad \text{(modulus of rigidity)}$$

$$p = 1/6 \qquad \text{(Poisson's ratio)}$$

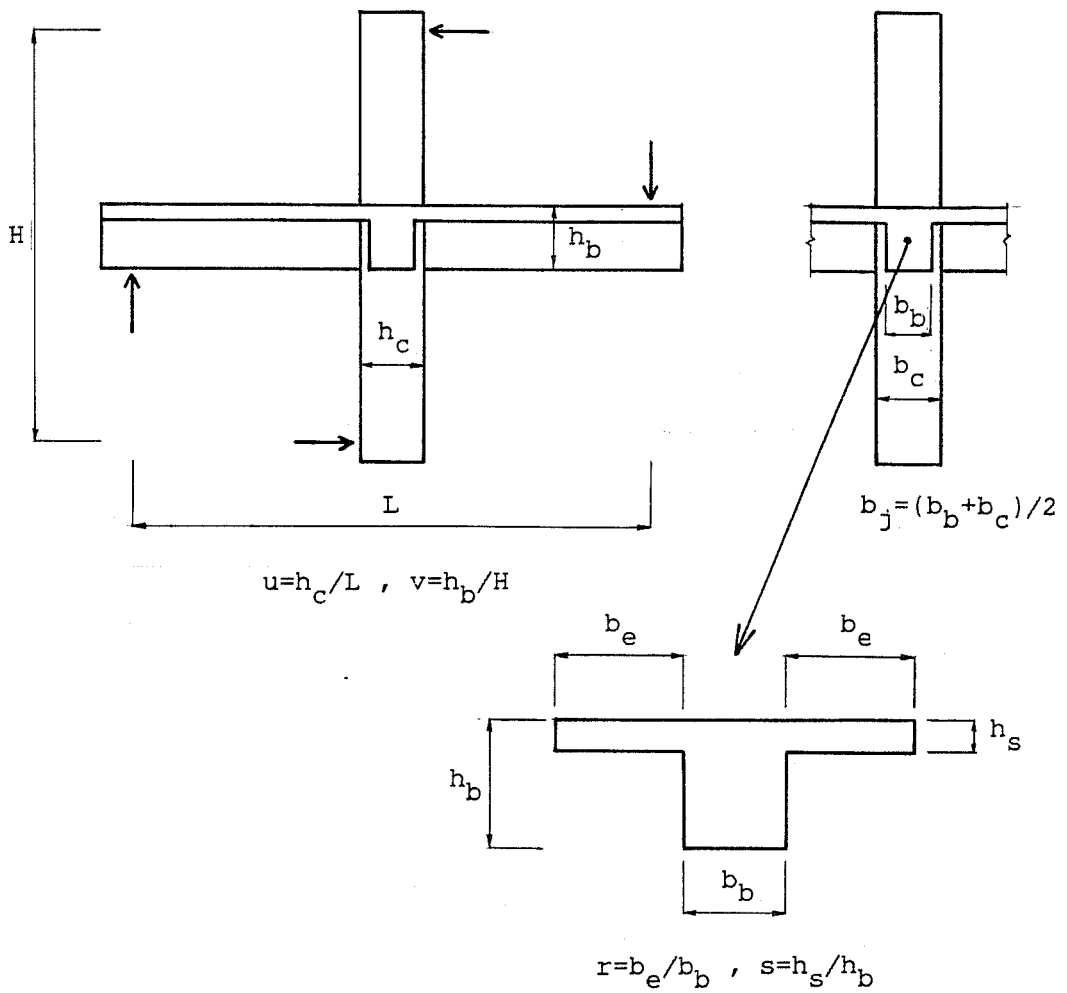

Figure C.1 Parameters in Stiffness Calculation

C.2 Moment Capacity

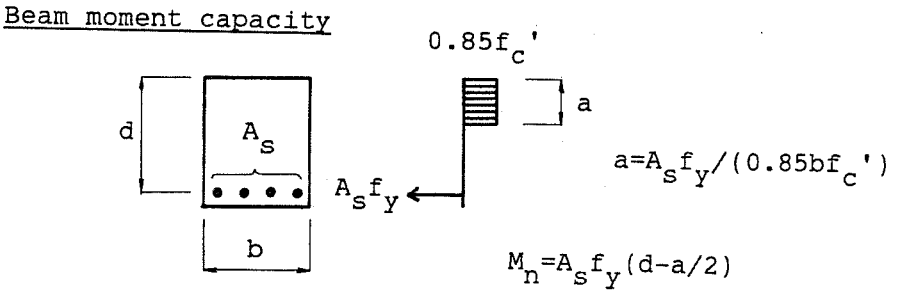

Figure C.2(a) Beam Moment Capacity

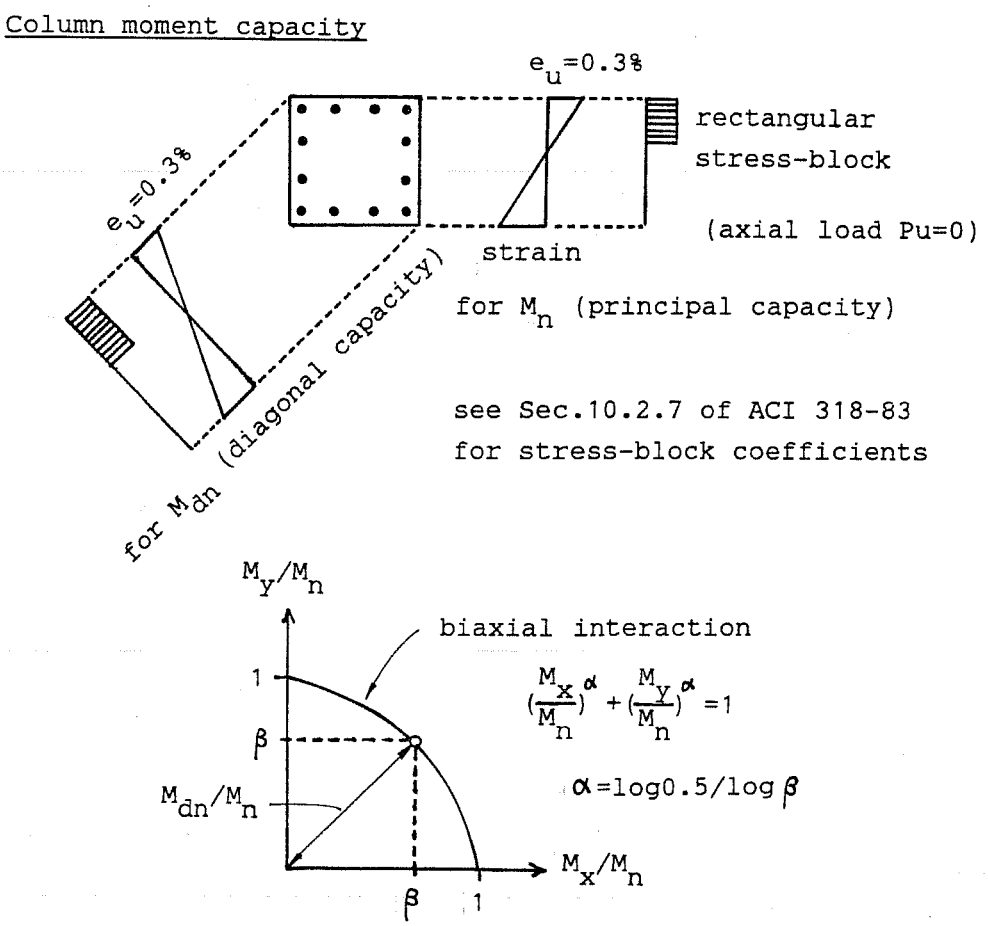

Figure C.2(b) Column Moment Capacity

C.3 Joint Shear Strength

$$V_{jn} = \gamma\sqrt{f'_c}b_j h_c \qquad (ACI\ 352)$$

where:

$\gamma =$ 15 for Specimens J1 and J3

$\gamma =$ 20 for Specimen J2

$f'_c =$ concrete strength

$b_j =$ $b_b + b_c)/2$

$h_c =$ column depth

$$V_{jn} = (2\phi f_s + P_w f_{wy})b_j j_c \qquad (AIJ - SRC)$$

where:

$\phi =$ 2 for Specimen J3 (EW)

$\phi =$ 3 for Specimens J1, J2 and J3 (NS)

$f_s =$ $1.5(f'_c/100 + 71.4)$

$P_w =$ $A_w/(b_c s)$

$A_w =$ area of lateral reinforcement

$b_c =$ column width

$s =$ spacing of lateral reinforcement

$j_c =$ $0.875d_c$

$d_c =$ column effective depth

$f_{wy} =$ yield strength of reinforcement

$$V_{jn} = V_{ch} + A_{jh} f_{wy} \qquad (NZS3101)$$

where:

V_{ch} = 0 for Specimens J1, J2 and J3 (NS)

V_{ch} = $\phi 0.5(As'/As)V_{jh}$ for Specimen J3 (EW)

ϕ = 3/4

V_{jh} = total horizontal joint shear

As = area of beam tensile reinforcement

As' = area of beam compressive reinforcement

A_{jh} = = total area of joint lateral reinforcement

C.4 Rebar Stress

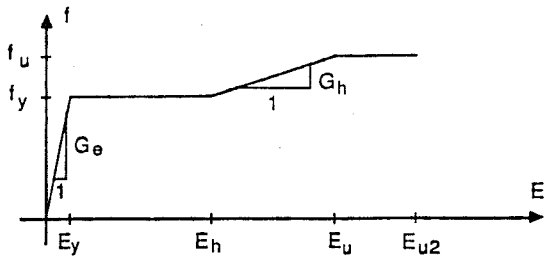

Subjected to Monotonic Loading

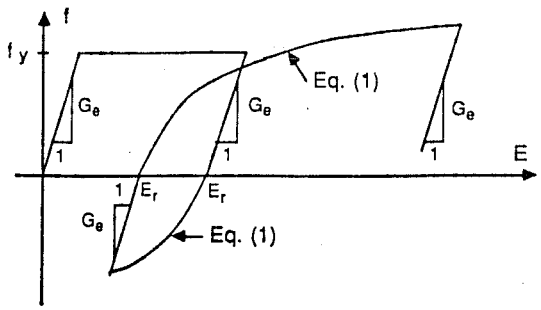

Subjected to Reversed Loading

where f = stress
E = strain
f_y = the yield stress
E_y = the yield strain
G_e = the modulus of elasticity
E_h = the strain where hardening begins
f_u = the ultimate stress
E_u = the strain corresponding to f_u
G_h = the modulus of strain hardening
E_{u2} = the failure strain

$$f = f_u (E - E_r) / (|E - E_r| + C) \qquad \text{Eq. (1)}$$

where f = stress
E = strain
f_y = the yield stress
f_u = the ultimate stress
G_e = the modulus of elasticity
E_r = the residual strain
C = 0.0025, parameter

Figure C.3 Analytical Model for Stress vs. Strain Relation

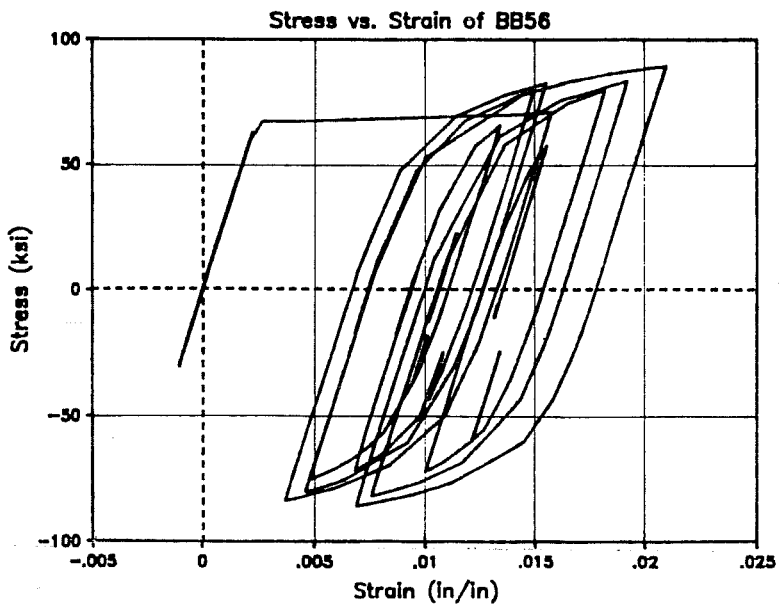

Figure C.4 Example of Stress-Strain Curve